

2m11.2772. 2

Université de Montréal

The Catalytic Mechanism of Purified Guinea Pig Liver Transglutaminase:
Substrate Synthesis and Kinetic Investigation of the Deacylation Step

par

Anouk Leblanc

Département de chimie

Faculté des arts et des sciences

Mémoire présenté à la Faculté des études supérieures

en vue de l'obtention du grade de

Maître ès science (M.Sc.)

en chimie

(Juillet 1999)

© Anouk Leblanc, 1999



2 1000 1000

QD
3
U54
2000
V.006

Université de Montréal

The Catalytic Mechanism of Purified Sulfoxide Oxidase from *Candida utilis*
Substrate Specificity and Kinetic Investigation of the Active Site

Thèse de doctorat
Département de chimie
Localité de la thèse et des recherches

Mémoire présenté à la Faculté des études supérieures
en vue de l'obtention du grade de
Maîtrise en sciences (M.Sc.)
en chimie
Juillet 1991



Année (année) 1991

Université de Montréal
Faculté des études supérieures

Ce mémoire intitulé:

The Catalytic Mechanism of Purified Guinea Pig Liver Transglutaminase:
Substrate Synthesis and Kinetic Investigation of the Deacylation Step

Présenté par
Anouk Leblanc

a été évalué par un jury composé des personnes suivantes:

Hermann Dugas	président-rapporteur
Jeffrey Keillor	directeur de recherche
James D. Wuest	membre du jury

Mémoire accepté le: 00-01-13

Résumé

La transglutaminase (TGase) est une enzyme de plus en plus impliquée dans plusieurs phénomènes de désordres physiologiques, tels la thrombose et l'artériosclérose (1), la formation de plaques d'amyloïdes insolubles dans le cerveau, ce qui entraîne le début de la maladie d'Alzheimer (2), l'inflammation intestinale induite par un excès d'albumine végétale provenant du blé, autrement connue sous le nom de maladies céliaques (3), et le développement de cataractes dans l'oeil humain causé par le dépôt de cristaux sur la lentille de l'oeil (4). La réaction catalysée par cette enzyme est de type ping-pong modifié, ce qui consiste en une étape d'acylation suivie par une désacylation. Le rôle biologique de la transglutaminase est de catalyser la formation de liens ϵ -(γ -glutamyl)lysine entre l'amide des résidues glutamine et l'amine primaire de la chaîne latérale des résidus lysine (5). Cette réaction est classifiée comme un transfert d'un groupe acyle d'un donneur (Gln) à un accepteur (Lys). Un lien commun entre chacune des maladies mentionnées est un dépôt excessif de protéines réticulées. Dans le but ultime de pouvoir concevoir des drogues inhibitrices comme sources d'interventions thérapeutiques, nous désirons avoir une meilleure compréhension du mécanisme enzymatique.

La transglutaminase a été purifiée à partir de foies de cobayes. Cette source de TGase est très avantageuse en ce qui concerne nos études cinétiques, car elle démontre une basse spécificité pour ses substrats par rapport aux autres membres de la même famille. Donc, ceci nous permet d'utiliser une plus grosse gamme d'analogues de substrats nécessaires pour bien étudier le mécanisme de cette enzyme. Les modifications que nous avons apportées au protocole de purification classique publié par Folk et Chung (6) nous a permis d'augmenter de 28 % l'activité spécifique de l'enzyme et d'améliorer le rendement global de la purification de 55 %, tout en diminuant le nombre d'étapes. Nous sommes donc heureux d'avoir réalisé les meilleurs résultats publiés jusqu'à ce jour en ce qui concerne le rendement et l'activité spécifique pour la TGase, ainsi que d'avoir résolu le problème d'entreposage de cette

enzyme en la lyophilisant, permettant ainsi de la conserver avec jusqu'à 90% de son activité originale (6b).

Nous avons synthétisé un substrat, le *N*-Cbz-L-Glu(γ -*p*-nitrophényl ester)Gly (**5**, $K_M = 0,02$ mM), qui a une bonne affinité dans le site actif de la TGase (**7**) ainsi que la capacité d'effectuer l'acylation rapide de l'enzyme pour assurer que la désacylation soit l'étape limitante (**8**). Ceci nous permet d'étudier spécifiquement l'étape de désacylation. De plus, pendant la réaction, un chromophore est libéré, soit le *p*-nitrophénol, ce qui nous permet de suivre directement le progrès de la désacylation. Nous avons effectué plusieurs synthèses du substrat *N*-Cbz-L-Glu(γ -*p*-nitrophényl ester)Gly, pour essayer d'optimiser le rendement et minimiser le degré de racémisation, puisque l'isomère D est un inhibiteur compétitif (**8**) de la TGase.

La TGase réagit avec **5** dans une étape d'acylation rapide qui est suivie par spectrophotométrie à 400 nm (pH 7,0, 25 °C). La désacylation se produit lorsqu'un nucléophile attaque le thioester intermédiaire pour régénérer le thiol au site actif de l'enzyme. Donc, pour étudier la désacylation, plusieurs amines primaires, dont la basicité varie largement ($pK_{NH^+} = 5,6 - 10,5$), ont été étudiées en tant que nucléophile et un graphique de type Brønsted a été construit pour déterminer si la nucléophilie de l'amine est importante pour la désacylation. Des études cinétiques pendant la phase stationnaire ont permis d'obtenir le V_{max} et le K_M pour chacune de ces amines primaires, et le graphique de type Brønsted démontrant la relation entre le $\log(V_{max}/K_M)$ et la basicité de ces amines (pK_{NH^+}). Ce graphique démontre une relation d'énergie libre linéaire entre la basicité des amines et la vitesse de l'étape de désacylation ($\beta_{nuc} = -0,37 \pm 0,07$). Cela est en accord avec un mécanisme de désacylation de type base générale, caractérisé par le transfert d'un proton entre l'amine et l'enzyme durant l'attaque nucléophile sur le thioester. Pour confirmer ces résultats, des études de l'effet isotope ont été faites pour trois substrats (aminoacétonitrile, $K_{ie} = 4,3 \pm 0,8$; glycine méthyl ester, $K_{ie} = 3,4 \pm 0,7$ et *N*-acétyl-L-lysine méthyl ester, $K_{ie} = 1,2 \pm 0,2$) et les résultats démontrent qu'il y a en effet un transfert de proton lors de

l'état de transition de l'étape limitante de la désacylation. Le pH peut affecter les paramètres cinétiques de la réaction enzymatique. Il peut modifier la stabilité du complexe enzyme-substrat (K_M), la vitesse de la réaction enzymatique (V_{max}), ou aussi intervenir en même temps sur les deux processus de la réaction (liaison et catalyse). Donc, en faisant des études de pH en fonction de la vitesse de la réaction enzymatique, des renseignements importants peuvent être déterminés quant à la formation et au bris de certains liens lors de cette réaction. Les effets de pH sur les valeurs de V_{max} , K_M et V_{max}/K_M pour l'eau, l'aminocétonitrile et la glycine méthyl ester comme accepteurs ont été déterminés. Nous avons découvert la présence d'un résidu, autre que le résidu impliqué dans la catalyse de type base générale, qui joue un rôle dans la liaison des substrats. Ces études de pH nous ont aussi permis de confirmer que la désacylation est l'étape limitante au cours des cinétiques et qu'elle n'est pas affectée par des variations de pH. Nous n'avons pas pu déterminer le pK_a du résidu dans le site actif responsable de la catalyse de type base générale, car il y a de très grandes erreurs expérimentales associées avec les valeurs de pH très hautes et très basses ($< 6,5$ et $> 7,5$). Ceci introduit quelques limites à l'application de notre méthodologie adaptée à l'étude de l'étape de désacylation pour la TGase.

Néanmoins, ces résultats cinétiques ont permis pour la première fois de mettre en évidence l'implication d'une base générale lors de l'étape limitante de la désacylation de la TGase.

Summary

In general, transglutaminase (TGase) has been implicated in recent years in many physiological disorders including thrombosis and atherosclerosis (1), Alzheimer's disease (2), celiac disease (3) and cataract development (4). Belonging to a class of enzymes which catalyze calcium-dependent acyl transfer reactions, transglutaminases effect catalysis *via* a modified "ping-pong" mechanism. Catalytic activity is exhibited towards γ -carboxamide groups of peptide bound glutamine residues which serve as acyl donors (acylation) to ϵ -amino groups of peptide-bound lysine residues (deacylation), resulting in new intermolecular ϵ -(γ -glutamyl)lysine crosslinks (5). Common to all TGase-associated disorders is superfluous protein deposition due to excessive crosslinking. Consequently, the design of mechanistic-based inhibitors for therapeutic intervention of TGase-mediated diseases necessitates a detailed mechanistic study.

Tissue transglutaminase was first purified from guinea pig liver. The broad substrate specificity with this source of TGase, in comparison with other members of the transglutaminase family, proved extremely advantageous for our substrate analogue kinetic studies. Modifications made in our laboratory to a standard purification protocol (6) have yielded a 28 % increase in specific activity and 55 % increase in yield, while reducing the number of steps to the purification. We are therefore pleased to report the highest yields and specific activities in the literature for the purification of guinea pig liver TGase, as well as the use of lyophilization as a solution to our longstanding enzyme stability storage problem (6a).

In order to selectively study the deacylation step, an active ester substrate analogue, *N*-Cbz-L-Glu(γ -*p*-nitrophenyl ester)Gly (**5**, prepared herein, $K_M = 0.02$ mM), was synthesized. This substrate satisfied certain essential criteria, namely that the peptide framework was known to confer good affinity for the TGase binding site (7), the active ester moiety was capable of rapidly acylating the enzyme making deacylation rate-limiting (8), and the reaction product released upon acylation (*p*-nitrophenol) is an excellent chromophore, providing a rapid, direct and sensitive

mode for following the deacylation step. Several different synthetic routes were developed in this laboratory in order to optimize the yield and practicality of the synthesis, while minimizing the degree of possible racemization, given that the D-isomer is a competitive inhibitor of the native substrate (8).

TGase reacts with **5** to undergo rapid acylation that can be followed spectrophotometrically at 400 nm (pH 7.0, 25 °C). Deacylation of the transiently formed thiolester acyl-enzyme intermediate *via* catalytic aminolysis was studied in the presence of eight primary amines of widely varying basicity ($pK_{\text{NH}^+} = 5.6 - 10.5$). Steady-state kinetic studies were performed to measure V_{max} and K_{M} values for each amine substrate. A Brønsted plot constructed through the correlation of $\log(V_{\text{max}}/K_{\text{M}})$ and pK_{NH^+} for each amine substrate displays a linear free-energy relationship with a slope $\beta_{\text{nuc}} = -0.37 \pm 0.07$. The shallow negative slope is consistent with a general-base catalyzed deacylation mechanism in which a proton is removed from the amine substrate during its rate-limiting nucleophilic attack on the thiolester carbonyl. Kinetic isotope effects were measured for three substrates (aminoacetonitrile, $K_{\text{ie}} = 4.3 \pm 0.8$; glycine methyl ester, $K_{\text{ie}} = 3.4 \pm 0.7$; *N*-acetyl-L-lysine methyl ester, $K_{\text{ie}} = 1.2 \pm 0.2$) and are consistent with a proton in flight at the rate-limiting transition state. The active site general base implicated by these kinetic results on the guinea pig liver TGase is believed to be His-334, of the highly conserved TGase Cys-His-Asp catalytic triad identified through primary sequence analysis of different members of the TGase family (5) and X-ray crystallography of FXIIIa (9). To identify the effect of different ionization states of the catalytically competent active site residues on the efficiency of the deacylation step, pH-rate studies were conducted. The effect of pH on K_{M} , V_{max} , and $V_{\text{max}}/K_{\text{M}}$ was determined for water, aminoacetonitrile, and glycine methyl ester. The pH- K_{M} profiles have revealed a residue, other than the catalytic general-base, involved in improved binding affinity. Also conclusive from the pH-rate studies is that deacylation is rate-limiting over the broad range of pH values and that deacylation (V_{max}) is not influenced by pH. Determination of the pK_{a} of the general base involved

in deacylation was difficult due to high experimental error associated with kinetics conducted at the necessary extremes in pH (< 6.5 and > 7.5). This introduces some limitations to the kinetic methodology.

Nonetheless, application of this methodology for the kinetic study of the TGase-catalyzed deacylation step has resulted in the first *kinetic* evidence for the involvement of a general base during the deacylation step of guinea pig liver TGase-catalyzed reaction.

Table of Contents

Résumé	I
Summary	IV
Table of Contents	VII
List of Figures	XII
List of Schemes	XVI
List of Tables	XVII
List of Equations	XIX
List of Abbreviations	XX
Dedication	XXII
Acknowledgements	XXIII

Chapter 1:

INTRODUCTION

1.1 Enzymology is the Study of Enzymes	24
1.2 Members of the Transglutaminase Family	
1.2.1 Introduction.....	25
1.2.2 Physiological Roles.....	26
1.3 Tissue Transglutaminase.....	27
1.3.1 Guinea Pig Liver Transglutaminase.....	28
1.3.2 Catalytic Mechanism	29
1.4 Evidence for an Essential Catalytic Histidine Residue.....	30
1.4.1 Enzyme Model Studies Involving Thiolester Chemistry	30
1.4.2 Papain is a Protease with a Catalytic Cysteine Residue.....	32
1.4.3 High Sequence Homology within the Transglutaminase Family	33
1.4.4 Conclusion	36

1.5	Research Methodology	
1.5.1	Study of the Deacylation Step Catalyzed by Tissue TGase.....	36
1.5.2	Enzyme Purification	37
1.5.3	Substrate Synthesis	37
1.5.4	Kinetic Studies on Deacylation.....	38

Chapter 2:

PURIFICATION OF GUINEA PIG LIVER TRANSGLUTAMINASE

2.1	Overview	40
2.2	Protocol Modifications	
2.2.1	The Time Course	41
2.2.2	Ion Exchange Resin	41
2.2.3	TGase Precipitation.....	42
2.2.4	An Alternative Concentration Step.....	43
2.2.5	Storage of Lyophilized TGase	43
2.2.6	Storage of Lyophilized TGase	44
2.2.7	Assessment of TGase Purity	45
2.3	Conclusion	48

Chapter 3

SYNTHESIS OF SUBSTRATE ANALOGUE

3.1	Overview.....	49
3.2	Synthesis of <i>N</i> -Cbz- <i>L</i> -glutamyl(γ - <i>p</i> -nitrophenyl ester)glycine	
3.2.1	<i>L</i> -Glutamic Acid Cyclic Anhydride Formation: Use of Glycine <i>tert</i> -Butyl Ester and <i>p</i> -Nitrophenyl Chloroformate in the Synthetic Route	52

3.2.2	L-Glutamic Acid Cyclic Anhydride Formation: Use of Glycine Allyl Ester and EDC/HOBt Coupling of <i>p</i> -Nitrophenol in the Synthetic Route	56
3.3	Synthesis of <i>N</i> -Cbz- <i>D</i> -glutamyl(γ - <i>p</i> -nitrophenyl ester)glycine	
3.3.1	Sequential Protection/Deprotection Synthesis	58
3.3.2	Formation of 5-Oxazolidinone Derivative of <i>N</i> -Cbz- <i>D</i> -Glutamate	61
3.4	Conclusion	62

Chapter 4

KINETIC STUDIES ON THE DEACYLATION STEP

4.1	Overview	64
4.2	General Considerations for the Kinetic Studies on Enzymes	64
4.3	Specific Considerations for Kinetic Studies on TGase	65
4.3.1	Calcium Requirements	65
4.3.2	Microscopic Reversibility.....	66
4.3.3	Extinction Coefficient.....	67
4.3.4	Background Hydrolysis and Enzyme Stability	68
4.3.5	Corroboration that Deacylation is Truly Rate-Limiting	69
4.3.6	Data Acquisition for TGase-Catalyzed Hydrolysis and Aminolysis	70
4.4	Structure-Activity Relationship (Brønsted Plot)	72
4.5	Isotope Effect Studies (Kie)	84
4.6	pH-Rate Studies	89
4.7	Conclusion	93
	Conclusion	94
	Appendices	96

Appendix A: Materials & Methods for the Purification

Materials.....	97
Methods:	
A-1: <i>Protein concentration</i>	97
A-2: <i>Transglutaminase Activity</i>	98
A-3: <i>Enzyme Purification</i>	98
STEP 1 - Preparation of liver supernatant solution.....	98
STEP 2 - Ion-exchange chromatography	98
STEP 3 - Protamine sulfate precipitation and extraction	99
STEP 4 - Size exclusion chromatography.....	100
A-4: <i>Electrophoresis</i>	100
A-5: <i>Enzyme Purity Analysis</i>	101

Appendix B: Materials & Methods for Synthesis

Materials	102
Methods:	
B-1: <i>General</i>	102
B-2: <i>Synthesis of N-Cbz-L-Glutamyl(γ-p-nitrophenyl)glycine via glutamic acid anhydride formation method and glycine t-butyl ester</i>	103
B-3: <i>Synthesis of N-Cbz-L-Glutamyl(γ-p-nitrophenyl)glycine via glutamic acid anhydride formation method and glycine allyl ester</i>	109
B-4: <i>Synthesis of N-Cbz-D-Glutamyl(γ-p-nitrophenyl)glycine via complete sequential protection/deprotection synthesis</i>	112
B-5: <i>Synthesis of N-Cbz-D-Glutamyl(γ-p-nitrophenyl)glycine via formation of the 5-oxazolidinone derivative</i>	118

Appendix C: Materials, Methods & Results for Kinetics

Materials 124

Methods & Results:

C-1: *General Kinetics* 124

C-2: *Extinction Coefficient*

 C-2.1: 4-Nitrophenol 125

 C-2.2: 2,4-Dinitrophenol (2,4-DNP) 127

C-3: *Titration of Primary Amines (pK_{NH^+})* 129

C-4: *Steady-State Kinetics*

 C-4.1: The Catalyzed Hydrolysis Reaction 129

 C-4.1.1 *Background Hydrolysis* 132

 C-4.2: The Transpeptidation Reaction (Brønsted plot) 134

C-5: *Isotope Effect Studies* 135

C-6: *pH-Rate Profile Experiments* 135

C-7: *Data Analysis* 140

Appendix D: Definitions and Equations

D-1: *Briggs-Haldane Steady-State Kinetics* 141

D-2: *The Michaelis-Menton Kinetic Parameters* 142

D-3: *The Modified Ping-Pong Mechanism* 143

D-4: *The Rate Equations for the Modified Ping-Pong Mechanism* 144

Bibliography 145

3.2.2	L-Glutamic Acid Cyclic Anhydride Formation: Use of Glycine Allyl Ester and EDC/HOBt Coupling of <i>p</i> -Nitrophenol in the Synthetic Route	56
3.3	Synthesis of <i>N</i> -Cbz- <i>D</i> -glutamyl(γ - <i>p</i> -nitrophenyl ester)glycine	
3.3.1	Sequential Protection/Deprotection Synthesis	58
3.3.2	Formation of 5-Oxazolidinone Derivative of <i>N</i> -Cbz- <i>D</i> -Glutamate	61
3.4	Conclusion	62

Chapter 4

KINETIC STUDIES ON THE DEACYLATION STEP

4.1	Overview	64
4.2	General Considerations for the Kinetic Studies on Enzymes	64
4.3	Specific Considerations for Kinetic Studies on TGase	65
4.3.1	Calcium Requirements	65
4.3.2	Microscopic Reversibility	66
4.3.3	Extinction Coefficient	67
4.3.4	Background Hydrolysis and Enzyme Stability	68
4.3.5	Corroboration that Deacylation is Truly Rate-Limiting	69
4.3.6	Data Acquisition for TGase-Catalyzed Hydrolysis and Aminolysis	70
4.4	Structure-Activity Relationship (Brønsted Plot)	72
4.5	Isotope Effect Studies (Kie)	84
4.6	pH-Rate Studies	89
4.7	Conclusion	93
	Conclusion	94
	Appendices	96

List of Figures

Figure 1	25
A free energy of reaction profile for a hypothetical single-substrate enzymatic reaction and corresponding non-enzymatic reaction. ΔG^\ddagger (Gibbs free energy) represents the activation energy for the uncatalyzed reaction. Catalysts lower the activation barrier of a reaction by $\Delta\Delta G_{\text{cat}}^\ddagger$, because they generate a stabilized transition state, ES^\ddagger .	
Figure 2	29
The transglutaminases effect catalysis <i>via</i> a modified “ping-pong” mechanism.	
Figure 3	31
Enzyme modeling studies reveal that lone thiol groups are insufficient to accommodate thiolester formation (<i>acylation</i>) (A) and that amines alone are incapable of accommodating S_N2 reactions on thiolesters (<i>deacylation</i>) (B), without the aid of a general catalyst.	
Figure 4	32
The “ping-pong” mechanism utilized by cysteine proteases is very similar to that of the transglutaminases, and both enzymes initiate the catalytic reaction with an active site thiol.	
Figure 5	34
A highly conserved active site is present in <i>all</i> members of the TGase family, as revealed by primary amino acid sequence analysis. For illustration, below is the sequence alignment surrounding that active site thiol of Factor XIIIa and guinea pig liver tissue TGase (GP _{tissue}).	
Figure 6	35
A three-dimensional X-ray crystallography structure of the active site of Factor XIIIa. The structure was downloaded from the PDB and modified in Rasmol.	
Figure 7	36
The thiolate-imidazolium ion pair. When in close proximity to an imidazole group, the thiol group of cysteine will generally predominate in its deprotonated form, thereby becoming a more efficient nucleophile.	
Figure 8	37
Despite our multidisciplinary approach to research, kinetic studies are at the heart of our research interests.	

Figure 9	42
Chromatogram of the ion exchange column showing specific activity and protein concentrations of collected fractions as a function of gradient eluant composition.	
Figure 10	44
Chromatogram of the size exclusion column showing specific activity and protein concentrations of collected fractions as a function of column volume eluted.	
Figure 11	46
Peak histogram of the purified TGase fraction developed by Coomassie staining as generated by Scion Image for Windows.	
Figure 12	47
SDS-PAGE gel analysis of the final purified TGase solution.	
Figure 13	52
Two electrophilic centers are available for nucleophilic ring opening of <i>N</i> -Cbz-L-glutamic acid cyclic anhydride.	
Figure 14	68
A graphical representation of the pH-dependence of the molar extinction coefficient of <i>p</i> -nitrophenolate.	
Figure 15	70
Rate of TGase-catalyzed hydrolysis as a function of leaving group capabilities. Effect of leaving group on the rate of acylation.	
Figure 16	71
(a) Plot of absorbance vs time as a consequence of varying substrate concentration. (b) Michaelis-Menton saturation curve generating kinetic parameters V_{\max} and K_M .	
Figure 17	74
Acid-base equilibrium for a primary amine in aqueous solution. Determination of the pK_{NH^+} for an amine.	
Figure 18	78
The Brønsted slope β was obtained according to Equation 5 for the aminolysis reaction involving the thiolester acyl-enzyme intermediate of TGase and various primary amines ranging in basicity (closed circles). The same reaction in D_2O for several of the amines is shown as open circles.	

Figure 19	80
A general trend revealed by the Brønsted plot is the increased reaction velocity with increasing primary amine acidity, which is explained schematically by application of the Hammond postulate.	
Figure 20	82
There are two plausible mechanisms involving nucleophilic attack during the TGase-catalyzed deacylation step: A. the <i>concerted</i> and B. <i>stepwise</i> mechanisms.	
Figure 21	84
Solvent kinetic isotope effects result from the greater strength of the nitrogen-deuteron bond in comparison to the nitrogen-hydrogen bond.	
Figure 22	86
The Linear correlation observed between the solvent kinetic isotope effect and the pK_{NH^+} of the primary amine is significantly linear.	
Figure 23	88
Diagrammatic representation of the speculative degree of proton transfer realized at the transition state of the general-base catalyzed deacylation reaction in D_2O according to the relative acidity of the primary amine.	
Figure 24	90
The effect of pH on $\log(K_M)$, obtained according to Equations 3 and 4, for the TGase-catalyzed hydrolysis reaction and the aminolysis reactions involving aminoacetonitrile and glycine methyl ester as primary amine nucleophiles.	
Figure 25	91
The effect of pH on $\log(V_{max})$, obtained according to Equations 3 and 4, for the TGase-catalyzed hydrolysis reaction and the aminolysis reactions involving aminoacetonitrile and glycine methyl ester as primary amine nucleophiles.	
Figure 26	92
The effect of pH on $\log(V_{max}/K_M)$, obtained according to Equations 3 and 4, for the TGase-catalyzed hydrolysis reaction and the aminolysis reactions involving aminoacetonitrile and glycine methyl ester as primary amine nucleophiles.	

Figure 27	128
A graphical representation of the pH-dependence of the molar extinction coefficient of 2,4-dinitrophenolate, at pH 6.0 – 9.0 as measured at 400 nm.	
Figure 28	131
The Michaelis-Menton saturation curve for the TGase catalyzed hydrolysis of <i>p</i> -nitrophenyl acetate as observed at pH 7.0 (0.1 M MOPS) and 25 °C, using Equation 3 to obtain V_{\max} and K_M .	
Figure 29	131
Saturation kinetics for the TGase catalyzed hydrolysis of 2,4-dinitrophenyl acetate as observed at pH 7.0 (0.1 M MOPS) and 25 °C, using Equation 3 to obtain V_{\max} and K_M .	
Figure 30	132
The Michaelis-Menton saturation curve for the TGase-catalyzed hydrolysis of substrate analogue 5 as observed at pH 7.0 (0.1 M MOPS) and 25 °C, using Equation 3 to obtain V_{\max} and K_M .	
Figure 31	133
Observed reaction rates for the hydroxide-ion catalyzed background hydrolysis of 0.1 mM <i>N</i> -Cbz-L-glutamyl(γ - <i>p</i> -nitrophenyl ester)glycine at various pH values.	
Figure 32	141
Simple one substrate/one product mechanism and related rate expression.	
Figure 33	143
The transglutaminase modified ping-pong mechanism with the various rate constants.	

List of Schemes

Scheme 1	26
Physiologically, transglutaminases are crosslinking enzymes which form new γ -glutamyl isopeptide bonds between different proteins.	
Scheme 2	51
Synthesis of <i>N</i> -Cbz-L-glutamyl(γ - <i>p</i> -nitrophenyl ester)glycine via glutamic acid anhydride formation and ring opening with glycine <i>tert</i> -butyl ester.	
Scheme 3	55
Synthesis of <i>N</i> -Cbz-L-glutamyl(γ - <i>p</i> -nitrophenyl ester)glycine via L-glutamic acid cyclic anhydride formation and ring opening with glycine allyl ester and EDC/HOBt coupling of <i>p</i> -nitrophenol.	
Scheme 4	57
Synthesis of <i>N</i> -Cbz-D-glutamyl(γ - <i>p</i> -nitrophenyl ester)glycine via a complete and sequential protection/deprotection synthetic route.	
Scheme 5	60
Synthesis of <i>N</i> -Cbz-D-glutamyl(γ - <i>p</i> -nitrophenyl ester)glycine via formation of 5-oxazolidinone derivative of <i>N</i> -Cbz-D-glutamic acid and nucleophilic ring opening with glycine <i>tert</i> -butyl ester.	

List of Tables

Table I	40
Summary of results from the purification (herein) of tissue transglutaminase from guinea pig liver, and comparison with results previously reported by Folk and Chung (18).	
Table II	54
Regioselectivities observed upon varying the polarity of the solvent, or by using different ester protective groups of glycine (nucleophile), on the <i>N</i> -Cbz- <i>L</i> -glutamic acid cyclic anhydride ring opening reaction.	
Table III	63
Summary of results for the proposed synthetic schemes in the synthesis of <i>N</i> -Cbz-(<i>L</i> or <i>D</i>)-glutamyl(γ - <i>p</i> -nitrophenyl ester) glycine.	
Table IV	75
Summary of the primary amines chosen for construction of the Brønsted plot, their pK_{NH^+} values determined herein, and an illustration of their comparative structures.	
Table V	77
Kinetic parameters (V_{max} , K_M and $\log(V_{max}/K_M)$) obtained according to Equation 4 for the TGase catalyzed transamidation reaction in the presence of 0.1 mM substrate 5 and a series of primary amine acceptor substrates at 25 °C and pH 7.0 (0.1 M MOPS), and the respective pK_{NH^+} values determined under kinetic experimental conditions.	
Table VI	85
Kinetic parameters (V_{max} and K_M) obtained according to Equation 4 and kinetic isotope effects ($(V_{max}/K_M)^{H_2O} / (V_{max}/K_M)^{D_2O}$) for the reaction of TGase in D_2O , at 25 °C at pD 7.0 (0.1 M MOPS), with 0.1 mM of substrate analogue 5 in the presence of three different primary amine acceptor substrates.	
Table VII	126
The results from the determination of the <i>p</i> -nitrophenol molar extinction coefficient (ϵ) as a function of the pH at 400 nm.	
Table VIII	127
Results for the determination of the extinction coefficients 2,4-dinitrophenol at various pH values, as observed at 400 nm.	

Table IX	130
Kinetic parameters (V_{\max} , K_M and V_{\max}/K_M) obtained according to Equation 3 for the TGase catalyzed hydrolysis reaction involving various active ester substrate at 25 °C and pH 7.0 (0.1 M MOPS).	
Table X	133
Observed reaction rates for the enzyme-catalyzed and hydroxide-ion catalyzed hydrolysis of 0.1 mM <i>N</i> -Cbz-L-glutamyl-(γ - <i>p</i> -nitrophenyl ester)glycine at various pH values.	
Table XI	136
Results for the control experiments relating loss of TGase activity to pH environment effects.	
Table XII	137
Kinetic results for the pH-rate experiment involving the TGase catalyzed <i>hydrolysis</i> of the active ester <i>N</i> -Cbz-L-glutamyl(γ - <i>p</i> -nitrophenyl ester)glycine at various pH values and 25 °C, where V_{\max} and K_M values were determined using Equation 3.	
Table XIII	138
Kinetic parameters (V_{\max} and K_M) obtained using Equation 4 for the TGase catalyzed <i>transamidation</i> reaction between 0.2 mM <i>N</i> -Cbz-L-glutamyl(γ - <i>p</i> -nitrophenyl ester)glycine and varying concentrations of glycine methyl ester at various pH values and 25 °C.	
Table XIV	139
Kinetic parameters (V_{\max} and K_M) obtained using Equation 4 for the TGase catalyzed <i>transamidation</i> reaction between 0.2 mM <i>N</i> -Cbz-L-glutamyl(γ - <i>p</i> -nitrophenyl ester)glycine and varying concentrations of aminoacetonitrile at various pH values and 25 °C.	

List of Equations

Equation 1	67
The Beer-Lambert equation serves to convert absorbance values into concentration by use of the extinction coefficients.	
Equation 2	129
Determination of the ionic strength (μ) of a solution.	
Equation 3	130
The kinetic equation for the construction the hyperbolic Michaelis-Menton saturation curve and acquisition of the kinetic parameters K_M and V_{max} for the TGase-catalyzed hydrolysis reaction.	
Equation 4	134
The kinetic equation for the construction the hyperbolic Michaelis-Menton saturation curve and acquisition of the kinetic parameters K_M and V_{max} for the TGase-catalyzed transamidation reaction.	
Equation 5	134
The equation used to obtain the slope of the Brønsted plot (β_{nuc})	

List of Abbreviations

[]	concentration
2,4-DNPA	2,4-dinitrophenyl acetate
aa	amino acid
ACN	acetonitrile
Ala	alanine
Ar	aryl
Asp	aspartic acid
β_{nuc}	beta nucleophile parameter; slope of Brønsted plot
br s	broad singlet
Cbz	benzyloxycarbonyl
Cys	cysteine
d	doublet
δ	chemical displacement
DCM	dichloromethane
DMF	N,N-dimethylformamide
DNPA	2,4-dinitrophenol acetate
DTT	dithiothreitol
ϵ	epsilon - nomenclature for defining the fourth carbon from the chiral carbon of an amino acid along the side chain
EDTA	ethylenediaminetetraacetic acid
eq	equivalent
FXIII	factor XIII
γ	gamma - nomenclature for the third carbon from the α carbon on the amino acid side chain
Gln	glutamine
Glu	glutamic acid
His	histidine
HOBt	1-hydroxybenzotriazole
hr	hour
Im	imidazole
kDa	kilo dalton
kie	kinetic isotope effect
K_M	binding constant
LG	leaving group

To my parents, Pierrette and Michel, for their
constant moral and financial support
throughout this long journey
called my *education*.

To my friend
and my companion,
Laurent, for sharing with me his
knowledge of chemistry...and beyond.

Lys	lysine
m	multiplet
MES	2-[N-Morpholino]ethanesulfonic acid
MOPS	3-[N-Morpholino]propanesulfonic acid
mp	melting point
NMR	nuclear magnetic resonance
PDB	Protein data bank
pK_{NH^+}	pK_a of the conjugate acid of the amine
<i>p</i> NP	<i>p</i> -nitrophenol
<i>p</i> -NPA	<i>p</i> -nitrophenyl acetate
ppm	parts per million
s	singlet
sat.	saturated
t	triplet
T	temperature
TGase	transglutaminase
TLC	thin layer chromatography
Tris	Tris[hydroxymethyl]aminomethane
TS [‡]	transition state
UV	ultra violet
V_{max}	maximum velocity

Acknowledgements

I would like to thank Professor J.W. Keillor for his encouragement, confidence, patience and a marvelous sense of humor, but first and foremost for giving me the opportunity to learn about chemistry and enzymology. I wish him a fulfilling and prosperous career. I would like to thank my colleagues Nicholas Day, Annie Ménard, and Roselyne Castonguay for their insightful discussions and camaraderie. A note of gratitude to Nicholas Day for his helpful involvement in the enzyme purification project. Finally, a very special thanks to Laurent Bélec for ‘showing me the ropes’!

Chapter 1

1. INTRODUCTION:

1.1: ENZYMOLGY IS THE STUDY OF ENZYMES

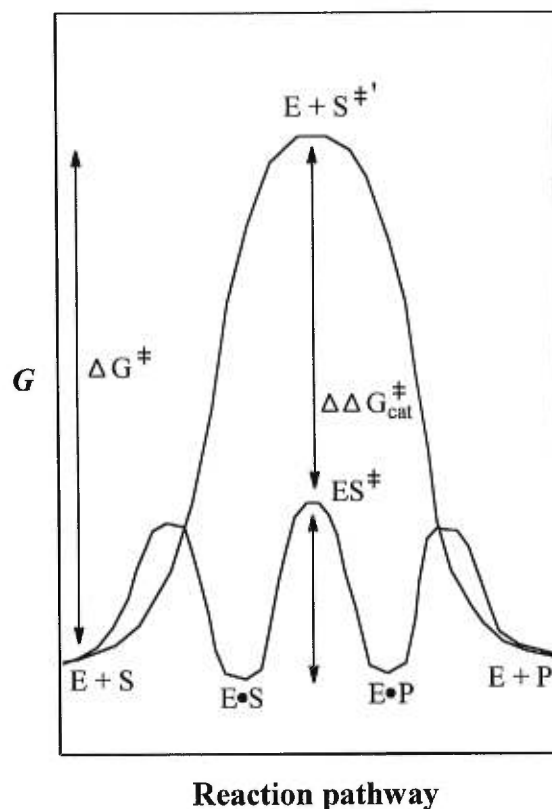
The chemical reactions of life are mediated by enzymes, which are the most versatile and specific catalysts known. It is through the comparison of an enzyme-catalyzed reaction with its non-enzymatic organic equivalent that we can reach a deeper level of appreciation for their catalytic proficiency. Amide bond hydrolysis is an excellent example which illustrates the impressive rate accelerations observed in the presence of enzymes. For instance, the rate constant for the hydroxide-ion (OH^-) catalyzed hydrolysis of the *N*-acetyl-L-tryptophan amide bond (pH 8.0) is in the vicinity $3 \times 10^{-10} \text{ sec}^{-1}$ (10). In the presence of α -chymotrypsin, however, the pseudo first order rate constant increases to $4.4 \times 10^{-2} \text{ sec}^{-1}$. This represents an astounding 1.5×10^8 fold increase in reaction rate afforded by α -chymotrypsin!

Enzymes, like all catalysts, lower the activation energy of a reaction without affecting the equilibrium (see **Figure 1**, page 25)(11). The catalytic efficiency of any given enzyme is the composite of a variety of factors. Currently, there are numerous conjectures regarding the driving force in enzymatic reactions, or in more specific terms how enzymes achieve large reductions in free energy of activation. These provide only an attempt at defining chemically how enzymes work. It is agreed that many contributive events lead to enzymatic including steric compression and strain of the substrate, proximity and orientation effects of reacting species, substrate-active site complementarity, acid-base catalysis, electrostatic effects, catalytic deployment of binding energy and transition state stabilization (10,11).

Through the past century, a whole new area of research has evolved into what is known as enzymology, or the study of enzymes. An integral part of enzymology is the study of enzymatic catalysis, and the work presented in this thesis is a perpetuation of the research on enzyme catalytic mechanisms. The enzyme under investigation is a member of the transglutaminase family. Our research on the transglutaminases is

focused mainly on delineating the catalytic events leading to product formation, and the catalytic residues involved in this process.

Figure 1: A free energy of reaction profile for a hypothetical single-substrate enzymatic reaction and corresponding non-enzymatic reaction. ΔG^\ddagger (Gibbs free energy) represents the activation energy for the uncatalyzed reaction. Catalysts lower the activation barrier of a reaction by $\Delta\Delta G_{\text{cat}}^\ddagger$, because they generate a stabilized transition state, ES^\ddagger .



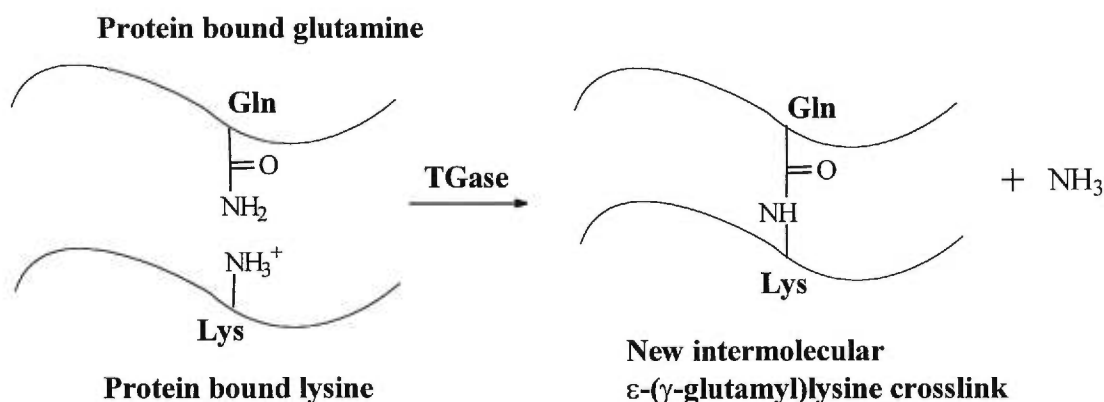
1.2: THE MEMBERS OF THE TRANSGLUTAMINASE FAMILY

1.2.1 Introduction

Transglutaminases (EC 2.3.2.13) are found in all vertebrates. They belong to a class of calcium-dependent enzymes known as aminoacyltransferases (EC 2.3.2), which modify peptides and proteins by catalyzing the formation of isopeptide

crosslinks *via* acyl transfer reactions. Catalytic activity is exhibited towards γ -carboxamide groups of peptide-bound glutamine residues, which serve as acyl donors to ϵ -amino groups of peptide-bound lysine acceptor residues, resulting in new intermolecular ϵ -(γ -glutamyl)lysine crosslinks (see **Scheme 1** below)(12). These resulting covalent amidic bonds are stable and resistant to chemical, enzymatic, and physical degradation. There are presently fifteen known members of the aminoacyltransferases.

Scheme 1: Physiologically, transglutaminases are crosslinking enzymes which form new γ -glutamyl isopeptide bonds between different proteins.



1.2.2 Physiological Roles

In mammals, TGases form a large family of proteins which are distributed throughout the plasma, tissues and extracellular fluids. They are distinguishable from each other on the basis of their physical properties as well as their distribution in the body. There are six distinct TGases which have been isolated and characterized in mammals: a membrane-associated enzyme of 92 kDa first discovered in keratinocytes (TGase1) but now recognized to be widely expressed in epithelial tissues; a ubiquitous "soluble" or "tissue" protein (TGase2) of 90 kDa; a soluble zymogen of 77 kDa known as "epidermal" or "hair follicle" due to its expression in these tissues (TGase3); the catalytic 'a' subunit of the blood clotting proenzyme Factor XIII of 77 kDa; a catalytically inactive TGase-like protein of 75 kDa, erythrocyte band 4.2, found as a

component of the subplasma membrane of eukaryotic cells; and a most recently discovered protein with TGase activity originating from the prostate (TGase4) (13,14).

Due to such widespread occurrence of TGase activity in mammals, there are numerous examples of proteins modified by this ubiquitous enzyme. For instance the plasma TGase, Factor XIIIa, impedes blood loss by stabilizing the fibrin clot at sites of blood coagulation due to hemostasis and wound healing. The squamous epithelium, which constitutes the protective callus layer of skin, is formed by the action of keratinocyte TGase and epidermal TGase. The erythrocyte band 4.2, although lacking catalytic activity, is an important component of the cytoskeletal network underlying the erythrocyte plasma membrane. Clearly, the TGase family plays an important physiological role in structural integrity and homeostasis in the mammalian system. When the balance is upset, however, this enzyme can become a promoting agent for disease. The focal point of the following body of work is a single member of the TGase family, the tissue transglutaminase (TGase2).

1.3: TISSUE TRANSGLUTAMINASE

Tissue transglutaminase is a monomeric protein containing 690 amino acid residues, has a molecular weight of 90 kDa, and is neither glycosylated or disulfide bonded despite the presence of 17 cysteine residues and 6 potential sites for N-linked glycosylation (5). Various cell types express tissue TGase, and through immunohistochemical studies these tissues have been identified as liver, kidney, lung, intestine, spleen, brain, endothelial and smooth muscle cells of arteries, veins and capillaries (5). The enzyme is situated in large majority intracellularly, but may also be localized in the interstitial fluids. There is no consensus yet regarding its precise physiological role; however, tissue TGase has been ascribed to several processes including stabilization of extracellular matrices, formation of crosslinked cell envelopes in programmed cell death (apoptosis), modulation of cell-matrix interactions which facilitate the assembly of the matrix, wound healing and excessive tissue repair, and cellular adhesive processes modulated by the interactions between cells and the extracellular matrix (5).

Tissue TGase has been implicated in many physiological disorders which share the hallmark of increased protein crosslinking and deposition. These include the onset of thrombosis and atherosclerosis (1), deposition of insoluble amyloid plaques in the brain leading to Alzheimer's disease (2), a wheat gliadin-induced intestinal inflammatory disease known as celiac disease (3), cataract development due to β A3-crystallin deposition on the eye lens (4), premature red blood cell aging and elimination from circulation known as Hb-Koln disease (15), and neurodegenerative diseases (such as Huntington's disease) associated with an increase in polyglutamine-containing peptides in the brain (16). Due to its broad involvement in disease, tissue TGase is a compelling candidate for therapeutic intervention. A viable approach to treatment is the use of mechanism-based inhibitors, which provides incentive for a detailed mechanistic study of the enzyme.

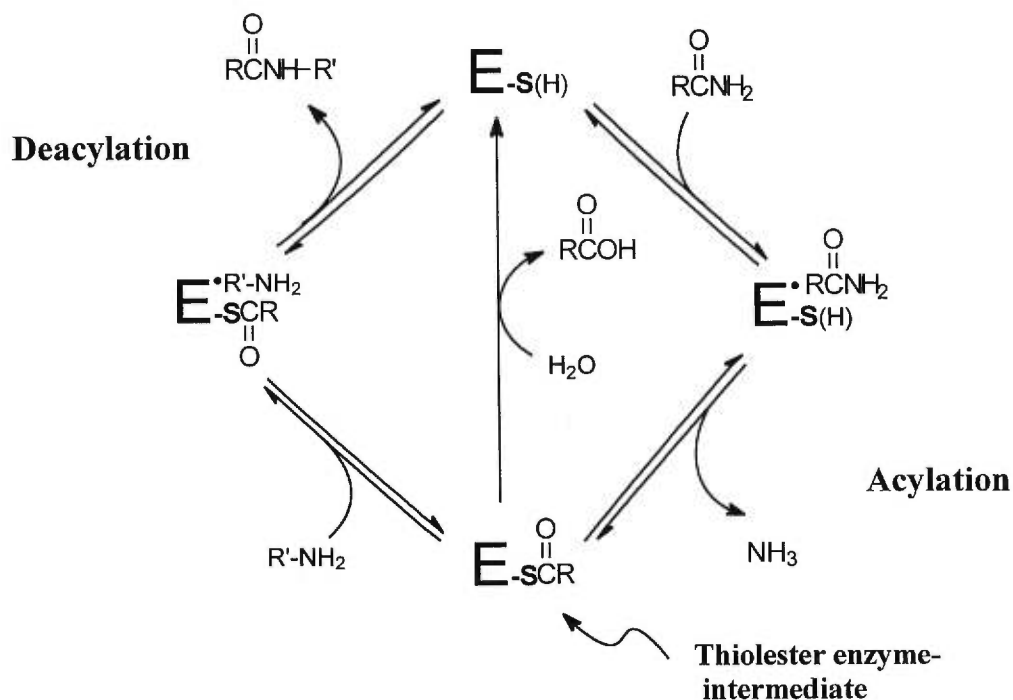
1.3.1 Guinea Pig Liver Transglutaminase

Guinea pig liver, because of its endogenous rich abundance of TGase in comparison to rat, mouse, rabbit and calf liver, has become the mostly widely cited source of TGase for research (17), and several protocols have been published for its purification (18,19,20). Furthermore, guinea pig liver TGase shows 80 % homology with human tissue TGase thereby validating its use as a human model (5). Finally, guinea pig liver TGase has a much broader substrate specificity making it suitable for the proposed substrate analogue kinetic studies involving a wide range of primary amines as second substrate described herein.

1.3.2 Catalytic Mechanism

Although members of the transglutaminase family vary in structure, location and even substrate specificity, they all share the ability to form ϵ -(γ -glutamyl)lysine crosslinks. This supports an underlying premise that all transglutaminases share a common catalytic mechanism.

Figure 2: Transglutaminases operate *via* a modified “ping-pong” mechanism.



The enzyme is known to proceed by the modified “ping-pong” mechanism shown above in **Figure 2** (21). An active site thiol (cysteine residue) is transiently acylated by the γ -carboxamide group of peptide-bound glutamine (acyl donor) with the release of ammonia. This acylation step is an energetically uphill reaction, which results in the formation of a thiolester acyl-enzyme intermediate. A partial driving force for the reaction is supplied by the release of ammonia and its subsequent protonation to ammonium occurring readily at physiological pH (5). The deacylation step is accomplished by either hydrolysis or aminolysis of the thiolester intermediate, and is characterized by the regeneration of free enzyme. The acyl acceptor during this process is either the ϵ -amino group of peptide-bound lysine or the primary amino group of some naturally occurring polyamine (such as spermidine, spermine or

putrescine) (22). In the absence of a primary amine acceptor, water is capable of regenerating free enzyme, giving rise to the term 'modified' of the ping-pong mechanism, albeit the reaction is much slower than with primary amine nucleophiles.

1.4: EVIDENCE FOR AN ESSENTIAL CATALYTIC HISTIDINE RESIDUE

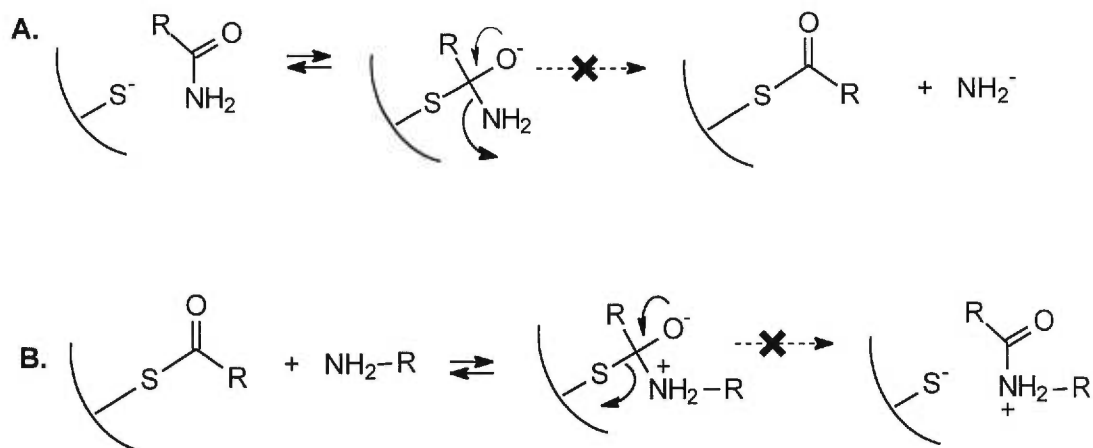
Some insight can be gained from a survey of enzyme mechanistic studies described in the literature, and predictions made, as to the components required for catalytic activity in TGases. Certainly, the evidence is compelling for the necessity of a general base in the acylation and deacylation steps of the TGase catalyzed reaction. To be more explicit, the literature has reaffirmed repeatedly that enzyme catalysis is accommodated by the combined action of several residues, and that rarely is one residue in the active site alone responsible for the observed rate accelerations. There is convincing evidence for the presence of a putative histidine residue in the TGase active site, which serves as a general acid/base catalyst during the course of the enzyme reaction. This hypothesis is based on several lines of evidence: a three-dimensional crystallographic structure of Factor XIIIa, the comparative primary amino acid sequence analysis of the TGase family, an enzyme model study for thiolate chemistry and kinetic data accumulated from studies involving cysteine proteases. Each of these will be addressed in more detail in the ensuing sections.

1.4.1 Enzyme Model Studies Involving Thiolester Chemistry

All enzymatic reactions have close if not identical organic reaction analogues for each discrete step. The study of enzymes can be approached by a parallel understanding of enzyme model systems, to serve as an aid in the appraisal of active site requirements. Thus the catalytic contribution of certain functional groups in a proposed enzyme mechanism can be assessed through the application of these specific model systems. One such enzyme model investigates thiolester formation via thiolate attack on the carbonyl of an amide bond (23,24). These small molecule biomimics provide evidence for the formation of a tetrahedral intermediate resulting from the attack of a lone thiolate. However, the reaction is easily reversible and was shown to

be unproductive unless the tetrahedral intermediate could be “trapped”. The model, as depicted below in **Figure 3A**, showed that the thiolate was expelled upon decomposition of the tetrahedral intermediate, and not NH_2^- , because the latter is a much poorer leaving group. We can therefore deduce the need for a general-acid catalyst to accommodate formation of the thiolester intermediate. The general-acid would participate in the reaction by donating a proton to NH_2^- thereby generating its protonated form, *ammonia* (NH_3), which is now rendered the better leaving group. Likewise, for the deacylation step we can envision the involvement of a general base which acts to remove a proton from the attacking amine in order to render the *thiolate* the better leaving group (see **Figure 3B** below) upon tetrahedral decomposition. In both situations described above, “trapping” the intermediate simply means that the intermediate is committed follow a specific reaction pathway because the alternate route, that is the expulsion of the *attacking* nucleophile, is obstructed. This model suggests the need for general-acid/base assistance in any such analogous enzymatic reaction, such as that catalyzed by TGase, and helps map out the active site requirements for effective catalysis.

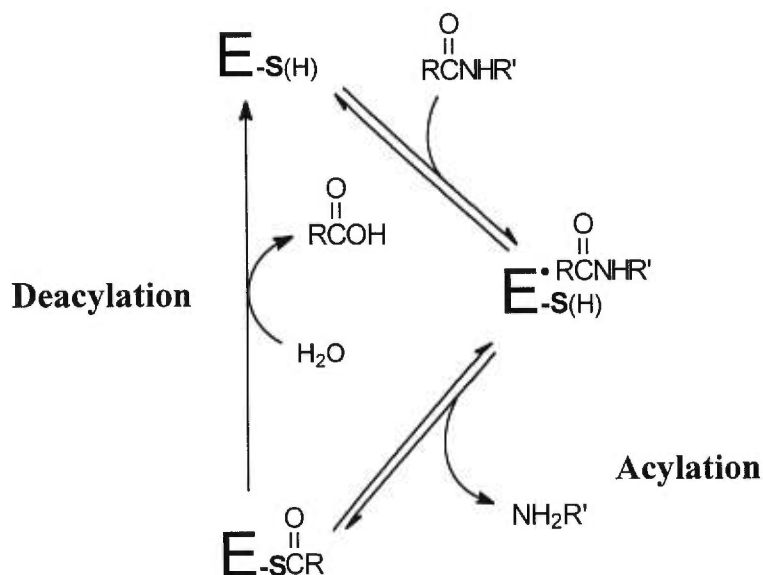
Figure 3: Enzyme modeling studies reveal that lone thiol groups are insufficient to accommodate thiolester formation (*acylation*) (**A**) and that amines alone are incapable of accommodating $\text{S}_{\text{N}}2$ reactions on thiolesters (*deacylation*) (**B**), without the aid of a general catalyst.



1.4.2 Papain is a Protease with a Catalytic Cysteine Residue

Since nature has a limited number of catalytically competent amino acid combinations at its disposal, we were interested in investigating any known enzyme mechanisms involving an active site thiol, in order to perhaps ascertain relevant information regarding the transglutaminase. Papain, an enzyme of plant origin, is a well studied member of the cysteine proteases. Interestingly, the mechanisms of papain and TGase have similarities, as is showcased below in **Figure 4**; both enzymes proceed by a “ping-pong” type mechanism featuring the formation of an acyl-enzyme intermediate and both enzymes rely on a nucleophilic thiol to catalyze the cleavage of an amidic bond (25). In papain, however, it has been established that catalytic activity involves a thiolate-imidazolium ion pair. The emerging question is whether or not this requirement is intrinsic to enzymes possessing a catalytic thiol involved in similar acyl transfer reactions, such as the TGases.

Figure 4: The “ping-pong” mechanism utilized by cysteine proteases is very similar to that of the transglutaminases, and both enzymes initiate the catalytic reaction with an active site thiol.



1.4.3 High Sequence Homology within the Transglutaminase Family

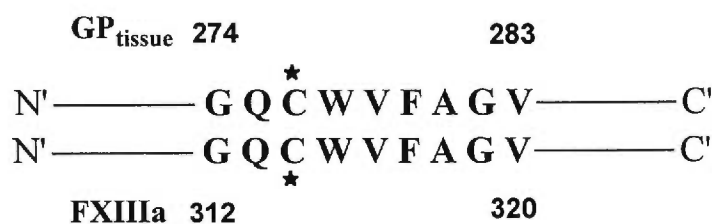
The overall homology between the primary amino acid sequences of 15 different members of the TGase family is only in the 25 – 45 % range (5). However, a highly conserved central core has been identified. The result is a striking 136 of 180 conserved residues in this central core. It is believed that this region contains all of the necessary elements needed to accommodate catalysis. Regions of low homology are attributed to varying substrate requirements for different members of the TGase family.

Within the highly conserved core region is a nine amino acid sequence surrounding the catalytic cysteine residue, which is *identical* for all six members of the TGase family in humans (5). More surprisingly, this homology extends to all animal species from which TGase has been isolated, including human, mouse, rat, rabbit, guinea pig and calf. A comparison of the primary amino acid sequence surrounding the active site thiol of guinea pig liver TGase and FXIIIa is shown in **Figure 5** (page 34). These results extend our notion of a common catalytic mechanism within all members of the TGase family, and validate the designation of guinea pig liver TGase as model enzyme for the broader transglutaminase family.

Some interesting questions emerge from these results. Why is conservation in the core region essential? What insights regarding the catalytic mechanism are discernable? Based on the mechanism of the cysteine proteases, it is logical to verify if there are any *histidines* among the conserved residues of the central core. Indeed, three conserved histidine residues have been identified (5), and it was investigated if one of these histidines was a viable partner to the catalytically essential cysteine. One first approach was the interpretation of the three-dimensional X-ray crystallography structure of FXIIIa, the only member of the transglutaminases to have been crystallized to date. The data regarding the FXIIIa active site reveals that Cys-314 and *His-373* are in close enough proximity ($S^{\gamma}-N^{\delta 1}$ distance is 3.2 Å) to be partnered through a hydrogen bond, thus forming the typical thiolate–imidazolium ion pair observed in the cysteine proteases (see **Figure 6** on page 35 for the PDB structure of FXIIIa) (9). This three dimensional topography of the enzyme's active site confirms

the possibility for thiolate-imidazolium ion pair formation, based strictly on spacial criteria. This is an important piece of information since the minimal requirement for the formation of such a pair is indeed proximity.

Figure 5: A highly conserved active site is present in *all* members of the TGase family, as revealed by primary amino acid sequence analysis. For illustration, below is the sequence alignment surrounding that active site thiol of Factor XIIIa and guinea pig liver tissue TGase (GP_{tissue}).

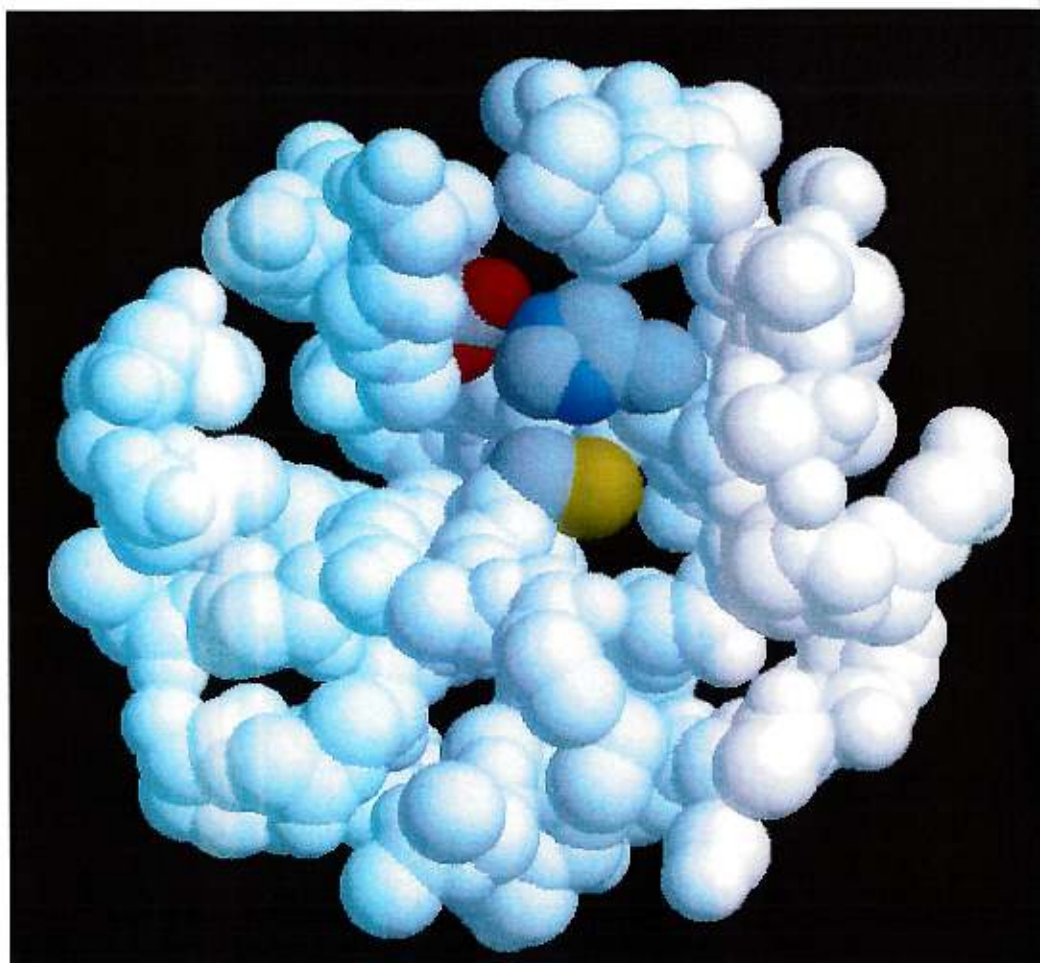


★ = catalytically active cysteine

G = glycine
 Q = glutamine
 A = alanine
 W = tyrosine
 V = valine
 F = phenylalanine

Another means of determining the putative residues in the active site is through site-directed mutagenesis. To test conclusions made from the three-dimensional structure of FXIIIa regarding His-373, all three conserved histidines (His-64, His-342 and His-373) were systematically mutated to Asn in order to determine which was catalytically essential (26). Activity was drastically impaired only upon mutation of the His-373, supporting observations made from the X-ray crystallographic structure of the appropriate orientation of the His-373 for potential catalytic involvement.

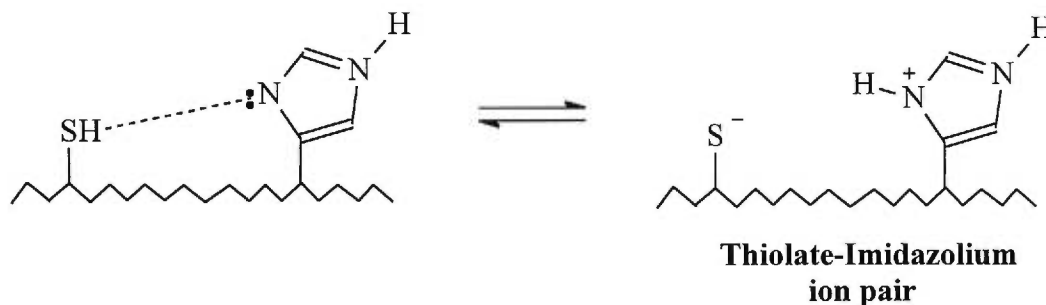
Figure 6: A three-dimensional structure of the active site of Factor XIIIa as determined by X-ray crystallography. The structure was downloaded from the PDB and modified in Rasmol. Represented below is the active site surrounded by a 14 Å shell of residues. In yellow is the catalytic Cys-314 thiol, in blue are the oxygens of Asp-337, and in red are the nitrogens of the imidazole ring of His-373. These are the three residues suspected to be involved in the TGase Cys-His-Asp catalytic triad.



1.4.4 Conclusion

These lines of evidence, taken together, provide strong testimony for a chemical solidarity between cysteine and histidine, which facilitate the acylation and deacylation steps of the TGase-catalyzed reaction (see **Figure 7** below) through formation of a thiolate-imidazolium ion pair, and help support our premise.

Figure 7: The thiolate-imidazolium ion pair. When in close proximity to an imidazole group, the thiol group of cysteine will generally predominate in its deprotonated form, thereby becoming a more efficient nucleophile.



1.5: RESEARCH METHODOLOGY

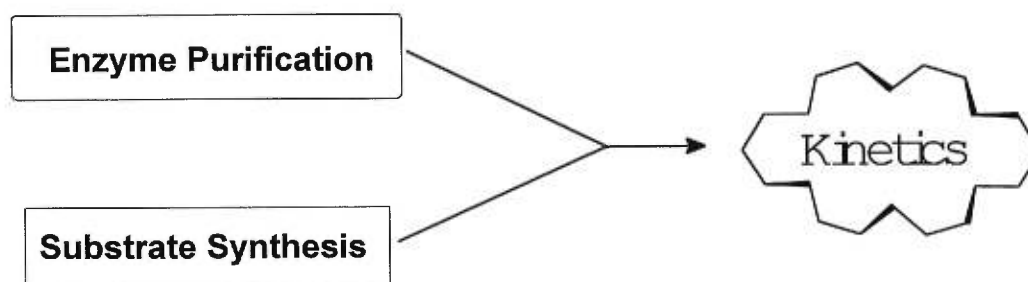
1.5.1 The Study of the Deacylation Step Catalyzed by Tissue Transglutaminase

The objective of this research was to selectively study the TGase-catalyzed deacylation step. More specifically, we were interested in probing the TGase-catalyzed nucleophilic attack of a primary amine (or water) on the thiolester acyl-enzyme intermediate. Our hypothesis was that deacylation must be catalyzed by a general base, and we believed the identity of this base to be a histidine.

Our challenge was three-fold: isolate a highly purified enzyme, synthesize a viable substrate analogue, and investigate the mechanism of deacylation using different kinetic techniques. We therefore took a multidisciplinary approach, as

outlined in **Figure 8** (page 37), by combining three major areas: protein purification, synthesis, and kinetic studies.

Figure 8: Despite our multidisciplinary approach to research, kinetic studies are at the heart of our research interests.



1.5.2 Enzyme Purification

To accurately investigate enzyme mechanisms *via* kinetic studies, a source of highly purified enzyme is required. Since high purity guinea pig liver TGase was not commercially offered, our initial objective was to purify the enzyme to its highest grade (measured as specific activity) and in the greatest yield. Although existing purification protocols were available from the literature (18,19,27), it was necessary to adapt the conditions to our laboratory.

The purification was a multistep process requiring several days of manipulation. In brief, five steps were involved: tissue homogenization/centrifugation, ion exchange chromatography, precipitation/extraction, and size exclusion chromatography. Finally, the enzyme was stored after lyophilization. Details of the purification will be discussed in **Chapter 2**.

1.5.3 Substrate Synthesis

First considerations in the selection of a substrate for kinetic studies on TGase were solubility and stability of the substrate in an aqueous environment. Other important criteria which guided the final decision for appropriate substrate included:

1. the need for the substrate to have a good binding affinity towards the enzyme.
2. it was essential that the substrate accommodate a rapid acylation of the enzyme (*i.e.* deacylation must be rate-limiting).
3. it was preferable that the substrate contain a UV-active group to be liberated during the course of the reaction, to provide a continuous assay for kinetic analysis.

The substrate selected, *N*-Cbz-*L*-glutamyl(γ -*p*-nitrophenyl ester)glycine, met all of the above conditions. The substrate was synthesized by several routes in order to compare overall yield achieved and ease of synthesis. Details of the synthetic component of this project will be addressed in **Chapter 3**.

1.5.4 Kinetic Studies on Deacylation

Several kinetic experiments were conceived to test our hypothesis regarding the involvement of a general-base catalyst in the deacylation step. A versatile tool commonly employed by enzymologists for this task is the Brønsted plot. This type of experiment reveals linear free energy relationships between reaction velocity and, in our case, nucleophilicity of the second substrate. Various primary amines were selected with varying basicities (of their conjugate acids) ranging from pK_a 5.6 - 10.5. The catalytic efficiency of the deacylation reaction was therefore compared with the nucleophilicity of the amine in a buffered solution of pH 7.0, yielding critical information as to the involvement of a putative general base in the mechanism.

Kinetic isotope effect studies (Kie), which are conducted in a stringent D_2O environment, are also very useful in deciphering the intricacies of a catalytic mechanism. These experiments are based on the ability of certain groups to exchange protons for deuterons in solution, such as the primary amines, and the observed isotope effects are a projection of increased N-D bond strength in comparison to an N-H bond. These experiments are useful in determining if a proton is being transferred in the activated complex of the rate-limiting step of a reaction. In our case, a solvent kinetic isotope effect is evidence of a general base involved in the abstraction of a proton from the attacking nucleophilic amine.

Since we were also interested in finding the identity the general-base catalyst involved in deacylation, we constructed a pH-rate profile. This profile is obtained by following the deacylation reaction for a given amine at different pH values. If there is a catalytic residue acting as general base in deacylation, the titration of this residue will be observed (as the pH is varied), since the velocity of the deacylation reaction will be influenced by the extent to which the base is protonated. The curve obtained will yield a pK_a for this residue thereby providing some clues as to its identity. The pK_a of a histidine residue, the suspected general base, is generally in the 7.0 – 8.5 range (10), and therefore an inflection point in the plot would be expected in this pH range. Details of the kinetic studies will be discussed further in **Chapter 4**.

Chapter 2

2. PURIFICATION OF GUINEA PIG LIVER TRANSGLUTAMINASE:

2.1: OVERVIEW

Although guinea pig liver transglutaminase can be purified according to previously reported procedures (18,19,27), the adaptation of those procedures to our laboratory gave rise to certain difficulties. It was upon resolution of these difficulties with each consecutive purification that we were eventually able to arrive upon certain key modifications and adjustments which have provided this laboratory with an extremely efficient method of purifying the enzyme. **Table I** compares the overall yield (measure of the efficiency of the purification) and specific activity (measure of enzyme purity) achieved in our laboratory with that obtained in the literature. We report herein a protocol for isolating enzyme in greater yields and higher specific activity than that reported in the literature.

Table I: Summary of results from the purification (herein) of tissue transglutaminase from guinea pig liver, and comparison with results previously reported by Folk and Chung (18). **Steps: 1** = homogenate, **2** = supernatant, **3** = ion-exchange, **4** = extraction, **5** = size exclusion.

Step	Total protein (mg)		Activity ($\mu\text{mol}/\text{min}$)		Specific activity ($\mu\text{mol}/\text{min}/\text{mg}$)		Yield (%)	
	(*)	Herein ¹	(*)	Herein ¹	(*)	Herein ¹	(*)	Herein ¹
1	25,000	22,500	1250	1440	0.05	0.06	100	100
2	10,000	6,930	1100	1310	0.11	0.19	88	91
3	250	371	625	1110	2.5	3.0	50	76
4	56	65	448	520	8.0	8.0	36	36
5	18	25	252	450	14.0	18.0	20	31

* = Literature ref. (18); ¹experimental error on these values is $\pm 5\%$.

2.2: PROTOCOL MODIFICATIONS

2.2.1 The Time Course

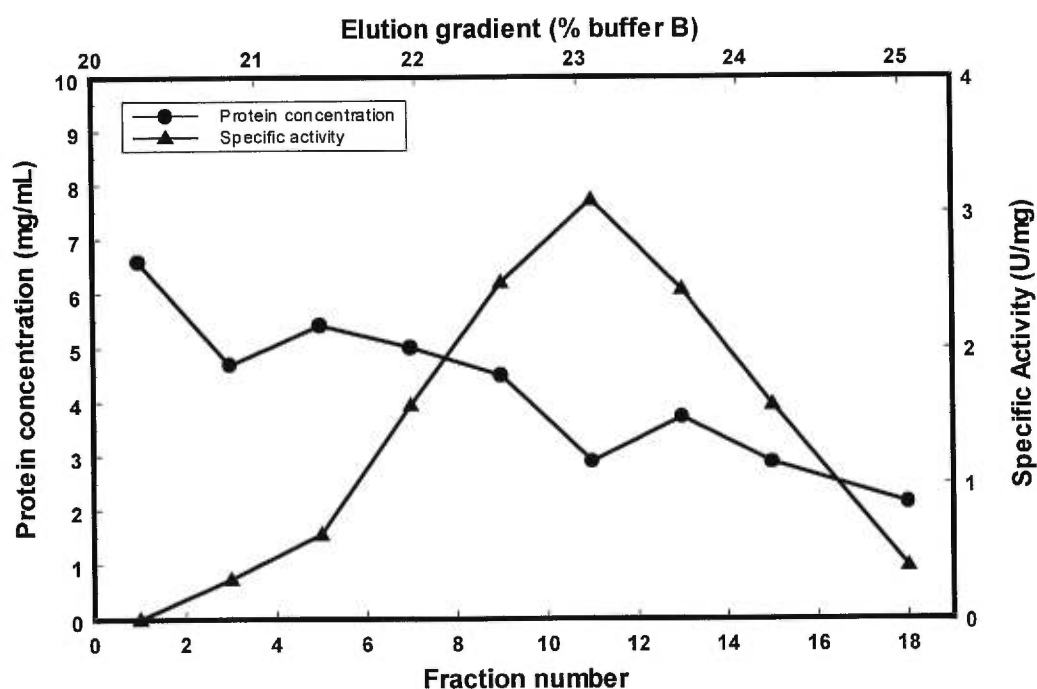
Of first concern was the appropriate time course taken for the purification. It became evident that time between manipulations should be minimized in order to achieve the highest specific activity possible. Fresh guinea pig livers were homogenized and centrifuged (**Appendix A-3; Step 1**, page 98) immediately upon arrival in order to minimize loss of TGase activity due to oxidation of the active site thiol or proteolysis. The supernatant fraction was found to remain stable at -20 °C for several months without apparent loss in activity, and therefore the purification could be interrupted at this point if necessary. We observed that interrupting the purification by storing the protamine sulfate precipitate (**Appendix A-3; Step 3**, page 99) in 0.2 M Tris-acetate (pH 6.0) at 4 °C, even for 24 hrs, led to as much as 50 % losses in activity. These observations are in contradiction to those reported by Folk *et al.*, where the partially purified enzyme was stable for up to three days, as the protamine sulfate precipitate, without appreciable loss in activity (19). It is our experience that an uninterrupted purification is the best measure. The purification was accomplished in a three day time course.

2.2.2 Ion Exchange Resin

To maximize the specific activity of the final purified enzyme solution, we had to optimize the ion-exchange column chromatography procedure (**Appendix A-3; Step 2**, page 98), which proved to be a consistent limiting factor in the protocol. It was only upon changing the ion exchange resin that we were able to ameliorate the results. The ion exchange step in the literature protocol is reported (18) to accommodate an approximate 15-fold increase in specific activity (to 2.5 U/mg), and provide an overall yield of 50 %. The support we were using (DEAE Bio-gel A) based on the Folk protocol (18) was frequently crushed, even at the minimal suggested flow rate of 5 mL/min, causing elevated back pressures and impeding eluant flow. Consequently we were unable to obtain the expected results. By switching to Bio-Rad Macro-Prep DEAE resin (see **Figure 9**, page 42), a much more rigid support, these problems were

resolved. In fact, this modification led to a 76 % yield and a specific activity of 3.0 U/mg (see **Table I**, page 40), representing a significant improvement over reported values of 50 % and 2.5 U/mg (18).

Figure 9: Chromatogram of the ion exchange column showing specific activity and protein concentrations of collected fractions as a function of gradient eluant composition. Fractions 7 – 15 were pooled for subsequent purification.



2.2.3 TGase Precipitation

Through fine tuning we were able to improve upon expected results for the precipitation and extraction step (**Appendix A-3; Step 3**, page 99). This step proved to be a delicate procedure requiring a very gradual, dropwise addition of the 1% protamine sulfate solution, with mild stirring, in order to selectively precipitate the anionic TGase without provoking undue denaturation. It was determined that the optimal volume of protamine sulfate solution used to precipitate the enzyme should be

12 - 15 % (v/v) of the enzyme solution. Secondly, extractions were conducted with decreasing volumes, since the use of equally large volumes of extraction buffer for the second or third extraction typically resulted in an unnecessary decrease in specific activity, without the compensation of a significantly increased yield.

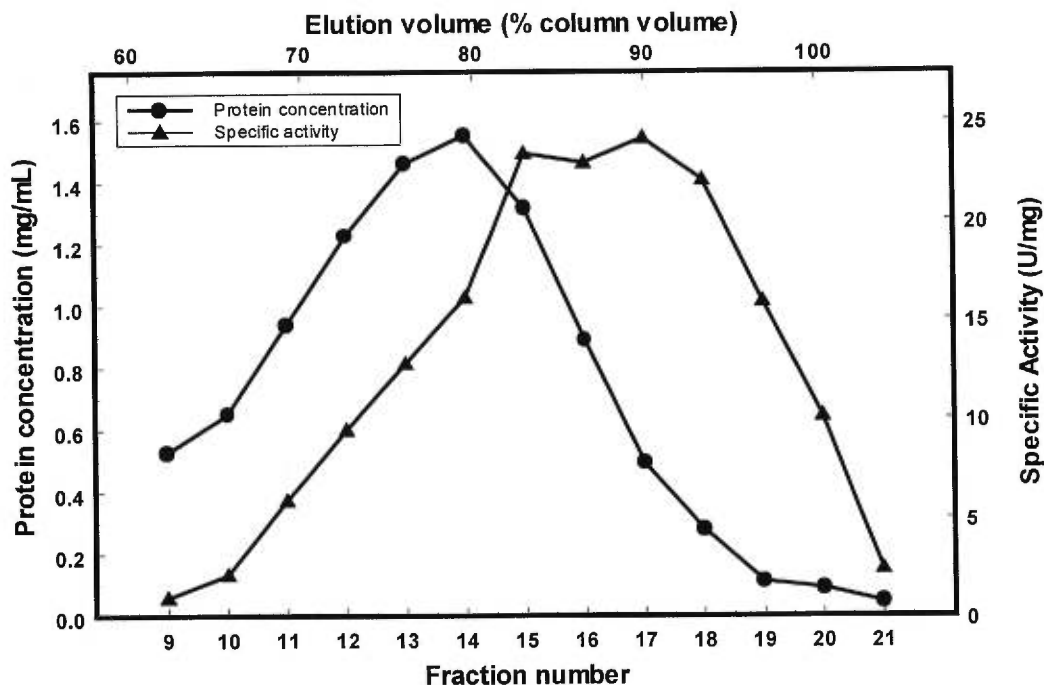
2.2.4 An Alternative Concentration Step

The substantial difference between our modified procedure and the Folk protocols (18,19,27) on which it is based, is the omission of the concentration step through ammonium sulfate precipitation following precipitation/extraction. According to the Folk protocols, a large quantity of ammonium sulfate was added to the extracts, followed by a centrifugation to collect the resulting precipitate, and finally a re-dissolution of the precipitate in an appropriate buffer prior to size exclusion chromatography. In our experience, however, the ammonium sulfate precipitation posed two major obstacles: incomplete precipitation lowered the yield of recovered enzyme, and the high concentration of ammonium in the resulting solutions appeared to interfere with the activity assay, leading to a degree of uncertainty regarding the true activity of the enzyme in the ensuing steps. As an alternative, we have found that concentrating the extracts through centrifugal filtration (Amicon Centri-Prep 30 tubes, 30 000 molecular weight cut-off) over a few hours at 4 °C is suitable for reducing the solution volume (1 to 4 mL) without significant loss in yield or specific activity. This modification offers a more rapid and sensitive alternative.

2.2.5 Size Exclusion Chromatography

Once the volume of the combined extracts has been suitably reduced, the solution is loaded onto a size exclusion chromatography column (**Appendix A; Step 4**, page 100), based on the previously reported procedure (18). Fractions high in TGase activity normally elute after a half-column volume, as shown in **Figure 10** (page 44). The Folk protocol (18) specifies that fractions rich in enzyme activity after size exclusion chromatography were combined, and then concentrated through ultrafiltration to at least 10 mg/mL, and frozen.

Figure 10: Chromatogram of the size exclusion column showing specific activity and protein concentrations of collected fractions as a function of column volume eluted. Fractions 13 – 19 were pooled.



2.2.6 Storage of Lyophilized TGase

The enzyme was reportedly stable at - 20 °C for many months at a high concentration of > 10 mg/mL (18). However, we have experienced ongoing problems with purified TGase stability associated with this method of storage reported by Folk. We have observed losses in activity of more than 50 % after 4 days of storage at - 20 °C, and complete losses of activity after one month of storage. Oxidation of the active site thiol could presumably play some role in the loss of enzyme activity during storage. The tendency of the active thiol group to rapidly oxidize has been illustrated through the addition of thiol reducing agents, such as dithiothreitol (DTT), which was able to partially restore TGase activity lost during long-term storage (18). However, the addition of DTT to our solutions of purified TGase as a preventative measure was undesirable since DTT interfered with our kinetic studies. In addition, storage of

solutions purged with nitrogen at $-20\text{ }^{\circ}\text{C}$ offered no marked improvement in long-term stability, suggesting that the inactivation that takes place during storage is not entirely due to a process related to active site thiol oxidation.

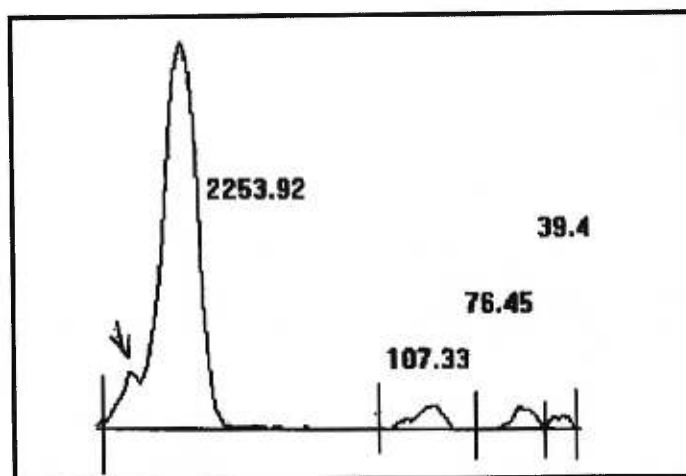
In a review article, Folk *et al.* briefly described “a contaminating impurity” occasionally found in the final solutions of some enzyme preparations (28). The impurity was identified as a liver esterase, since activity was inhibited by treatment with low levels of diisopropyl phosphorofluoridate. This may explain the cause of the rapid and significant loss in activity we have observed. In a separate article, it was claimed that *rat* liver tissue transglutaminase was co-purified by gel filtration and ion exchange chromatography with a widely distributed protease which was capable of inactivating the rat liver TGase (29). It therefore seems evident that there are other proteins routinely co-purified with TGase. We have solved the problem of storage instability by lyophilizing the enzyme directly after size-exclusion chromatography (see **Appendix A-3, Step 4**, page 100). The lyophilized enzyme remains active to within 90 % of its original activity even after several months.

2.2.7 Assessment of TGase Purity

We were interested in quantifying the purity of TGase obtained by our purification protocol. We therefore assessed the purity of the enzyme by performing SDS-PAGE electrophoresis (see **Appendix A-4**, page 100). The gels were analyzed using the Scion Image for Windows program which captures, displays, and analyzes image maps of electrophoretic gels. A linear standard curve was constructed in order to correlate varying optical band intensity with the quantity of protein in that band. To this end, SDS-PAGE gels containing lanes loaded with varying quantities of bovine serum albumine (BSA) (see **Appendix A-5**, page 101) were run in parallel with lanes containing varying quantities of the purified TGase. The gels were then developed by either Coomassie blue or zinc staining techniques, such that a standard curve for each method of development was utilized to analyze the bands in the purified TGase-containing lanes. Note that these lanes had been loaded with 5.0 and 7.5 μg of purified TGase. A peak histogram was generated by Scion Image (see **Figure 11**, page 46) and

the area under each peak was representative of the band intensity. The BSA standard curves served to then convert the area under each peak into a protein quantity.

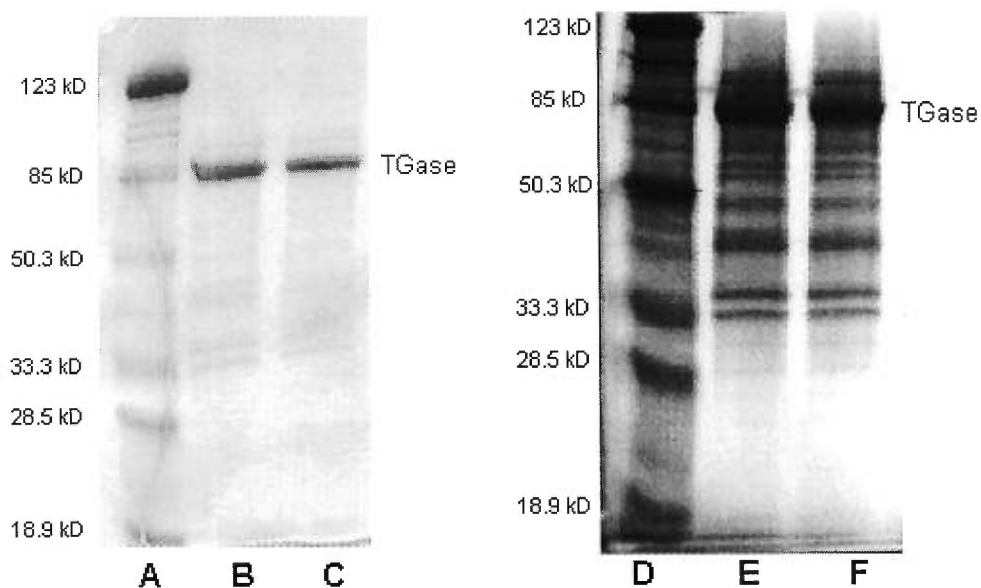
Figure 11: Peak histogram of the purified TGase fraction developed by Coomassie staining (lane B of **Figure 12** on page 47), as generated by Scion Image for Windows. Each peak represents a band and the numeric value represents relative band intensity.



Visual inspection of the gels in **Figure 12** (page 47) reveals that the Coomassie blue staining procedure is much less sensitive than the zinc staining method. The standard Coomassie blue method has a reported lower limit of detection of 0.1 - 1.0 μg , whereas the lower limit of detection for the zinc staining technique is 10 - 100 ng (30). It is possible to detect three faint bands in addition to the band representing TGase (90 kDa) on the gel stained by the Coomassie blue staining technique. These bands migrate with apparent molecular weights between 31, 32, and 40 kDa, and their identity is suspected to be an esterase or protease. Consequently, the Coomassie stained TGase preparation appears satisfyingly pure (four barely visible bands and one highly intense band for TGase). The zinc stained TGase preparation, however, reveals as many as nine bands of varying optical intensity, and the purity appears to be much lower. As confirmed by the Scion Image analysis, the Coomassie blue

stained gel reveals an 85 % TGase purity, whereas the zinc stained gel establishes a TGase purity of 60 %. Previous reports in the literature regarding the purification of TGase to apparent *homogeneity* have been based upon the results of SDS-PAGE experiments using Coomassie blue staining. Our current results suggest that the choice of staining method may significantly affect conclusions regarding the purity of the TGase preparation.

Figure 12: SDS-PAGE gel analysis of the final purified TGase solution. **Lanes A-C** were stained with Coomassie blue; lanes **D - F** were developed using zinc staining (30). **Lanes A** and **D** were loaded with pre-stained molecular weight markers; **lanes B** and **E** were loaded with 7.5 μg TGase; **lanes C** and **F** were loaded with 5.0 μg TGase.



2.3: CONCLUSION

The superior specific activity of the final TGase preparation attests to the high purity of the enzyme and efficiency of the purification protocol, despite apparent impurities by SDS-PAGE electrophoresis. The modifications made in our laboratory to the standard purification protocol (18) have yielded a 28 % increase in specific activity and 55 % increase in overall yield, while reducing the number of steps to the purification. As a result of these modifications we are able to report the highest yields and specific activities for guinea pig liver transglutaminase in the literature.

Chapter 3

3. SYNTHESIS OF SUBSTRATE ANALOGUE:

3.1: OVERVIEW

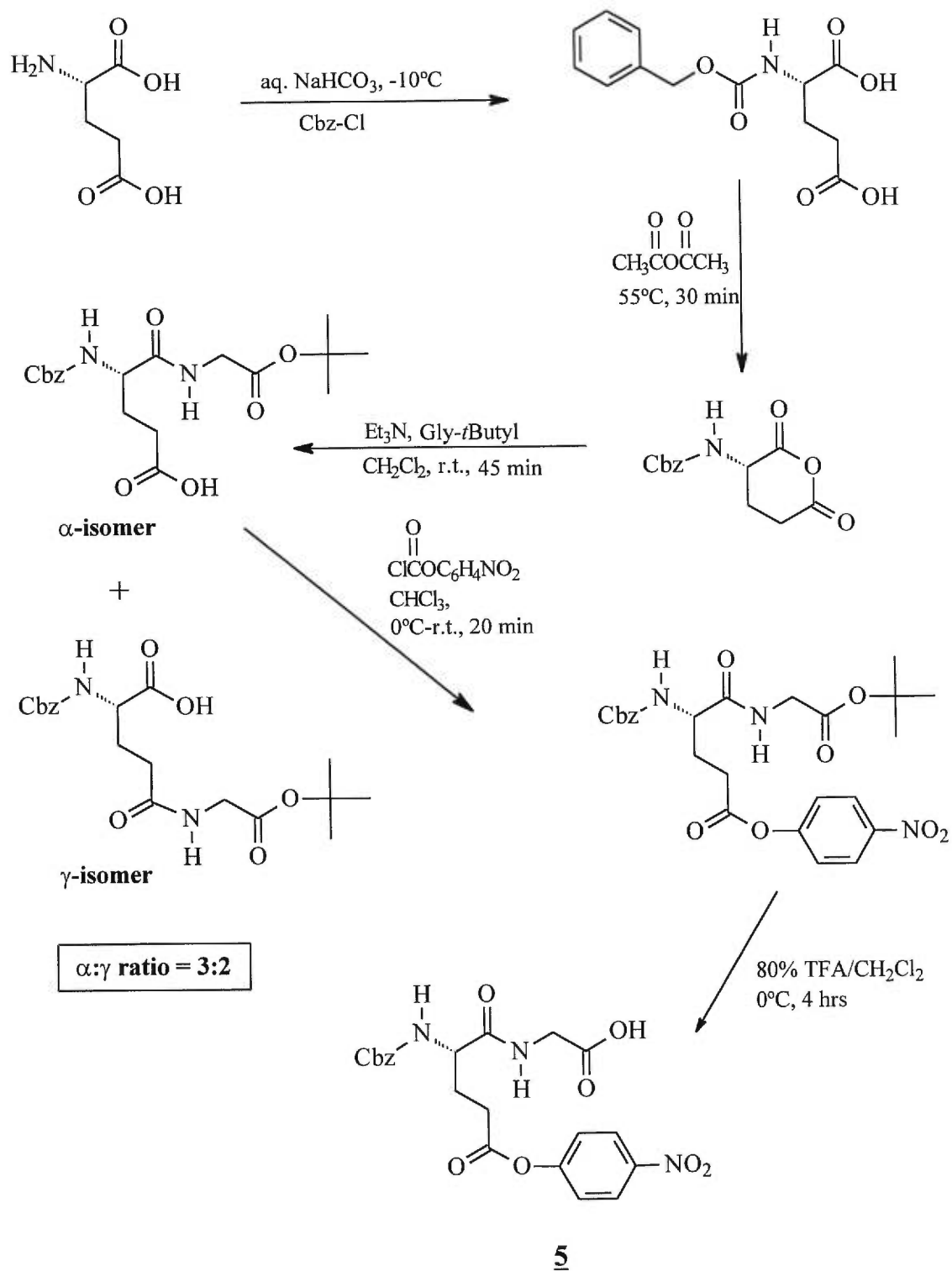
N-Cbz-L-Glutamyl(γ -*p*-nitrophenyl ester)glycine (**5**) was prepared for use as a substrate analogue for kinetic studies on the TGase-catalyzed deacylation step because it satisfied certain essential criteria. Namely, the peptide framework was known to confer good affinity for the TGase binding site (7), the active ester moiety had proven capabilities for rapidly acylating the enzyme making the deacylation step rate-limiting (8), and the reaction product released upon acylation of the enzyme (*p*-nitrophenolate) is an excellent chromophore, permitting progress of the enzymatic reaction to be followed spectrophotometrically. The validation of this substrate for kinetic studies was based largely on the pioneering research of Dr. J.E. Folk on the general TGase mechanism.

Research on the molecular and catalytic properties of TGase conducted by Folk and Chung (28) prompted the discovery that a γ -positioned *p*-nitrophenyl ester of L-glutamic acid was a particularly effective acylating substrate for TGase. An important observation was that TGase activity towards both the active ester substrate (*N*-Cbz-L-Glu(γ -*p*-nitrophenyl ester)Gly) and the glutamine substrate (*N*-Cbz-L-GlnGly) proceeded by *identical* modified “ping-pong” mechanisms (8). Furthermore, it was determined that the D isomer of each compound was far less efficient a substrate towards TGase, and could even act as competitive inhibitor of its correspondant L isomer. For instance, the progression of the transamidation reaction (V_{\max}) was 3800-fold slower with *N*-Cbz-D-GlnGly in the presence of glycine ethyl ester than with the L-isomer (8). For the active ester substrate, effects of stereochemistry were shown to be less pronounced; however, V_{\max}/K_M values remained quite different for the L- and D-isomers at 5800 and 220 min per mg of enzyme, respectively. This variance was judged largely due to the reduced binding affinity of the D-isomer, as made evident by a 30-fold higher K_M value.

An interesting feature of the active ester substrate, however, was a demonstrated 15-fold faster V_{\max} for hydrolysis than that obtained for the hydrolysis of *N*-Cbz-L-GlnGly (8). It was later revealed that the rate-limiting steps were different for each substrate, such that acylation was limiting for *N*-Cbz-L-GlnGly and deacylation was rate-limiting in the case of *N*-Cbz-L-Glu(γ -*p*-nitrophenyl ester)Gly. Kinetic studies mapping the minimal requirements regarding the peptide framework of these substrate analogues revealed that the Cbz-protecting group utilized during dipeptide substrate synthesis was complementary to the binding with TGase. In fact, omission or replacement of this group by formyl, acetyl, benzoyl, or propionyl reduced the maximum velocity for hydroxamate formation (*i.e.* activity assay) by 55 – 99 % (28).

Although a synthetic route to substrate analogue **5** was published in 1970 (18), several different synthetic routes to **5** are proposed herein which apply more recent synthetic methodologies. Based on the integral role of this substrate in our research, it was important to find an efficient synthesis which would optimize yield while minimizing the degree of possible racemization, given that the D-isomer has a demonstrated higher K_M value (8). It must be noted that the Cbz protective group, although beneficial for binding, has a greater propensity than other protective groups to permit racemization during amino acid coupling reactions *via* intermediate 5(4H)-oxazolone formation, a feature common to all *N*-alkoxycarbonyl protective groups (31). Four synthetic routes were proposed: two for the synthesis of the L-isomer, as well as two for the synthesis of the D-isomer. These synthetic routes applied the principles of orthogonal synthesis, such that the protecting groups used, where necessary, were compatible with the reaction conditions and could be positioned and removed selectively. The different approaches taken are illustrated in **Schemes 2 – 5** of this chapter.

Scheme 2: Synthesis of *N*-Cbz-*L*-glutamyl(γ -*p*-nitrophenyl ester)glycine (**5**) via glutamic acid anhydride formation and ring opening with glycine *tert*-butyl ester.

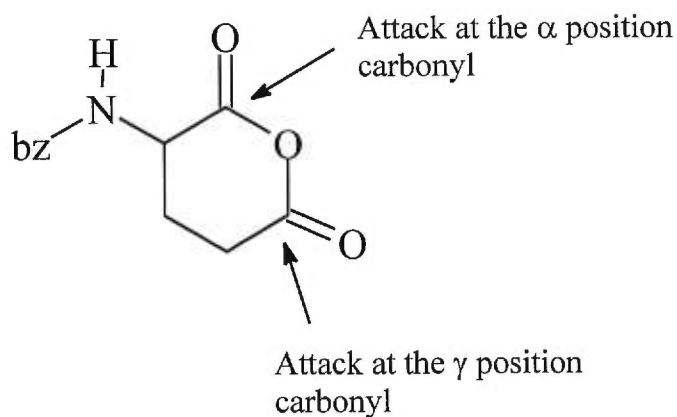


3.2: SYNTHESIS OF *N*-CBZ-L-GLUTAMYL (γ -*p*-NITROPHENYL ESTER)GLY

3.2.1 L-Glutamic Acid Cyclic Anhydride Formation: Use of Glycine *tert*-Butyl Ester and *p*-Nitrophenyl Chloroformate in the Synthetic Route

The synthesis of the dipeptide framework (**Scheme 2**, page 51) was initiated by the straightforward protection of the α -amino group of L-glutamic acid with the benzyloxycarbonyl (Cbz) group, and afforded a white powder in 92 % yield (refer to **Appendix B-2** starting on page 103 for all reactions outlined in **Scheme 2**). The interesting feature of this proposed synthetic scheme is a reduction in the number of steps through activation of the carbonyl function *via* cyclic anhydride formation. Subsequent coupling with glycine *tert*-butyl ester was achieved by direct nucleophilic attack on the activated carbonyl(s). The anhydride intermediate contains two viable electrophilic centers, and therefore two isomers can be generated from nucleophilic attack, as depicted below in **Figure 13**. It was our objective to obtain, in a regiospecific manner, the α -isomer of the coupling reaction.

Figure 13: Two electrophilic centers are available for nucleophilic ring opening of *N*-Cbz-L-glutamic acid cyclic anhydride.



Previous work in this laboratory has demonstrated that the regioselective ring opening of *N*-Cbz-*L*-glutamic acid cyclic anhydride with anilines can be strongly influenced by the careful choice of solvent (32). Complete regioselectivity for the α -isomer was possible in the presence of an apolar solvent, such as benzene or dichloromethane. Unfortunately, the selectivity observed with the anilines appears to be a feature specific to these aromatic primary amines and not as broadly applicable to aliphatic primary amines, such as glycine *tert*-butyl ester and glycine allyl ester. Our attempts in optimizing the regioselective formation of the desired α -isomer upon reaction with glycine esters, either by varying the polarity of the solvent or by using different ester groups, were only modestly successful as revealed in **Table II** (page 54).

The greatest regioselectivity for the α -isomer, using glycine *tert*-butyl ester, was observed in the presence of chloroform (60 % α -isomer). With the more hydrophobic solvents, regioselectivity for the γ -isomer was largely favored. For instance, the reaction in toluene yielded 87 % γ -isomer and benzene yielded 81 % γ -isomer. The regioselectivity is apparently not influenced by the structure of the ester protective group on glycine. Comparison of reactions in dichloromethane reveal that regioselectivity for the α -isomer is 50 % with glycine allyl ester as well as with glycine *tert*-butyl ester. Although the regioselectivity for the α -isomer was much lower than anticipated, the overall efficiency of the reaction was excellent, with yields in the 88 – 96 % range (see **Table II**). Fortunately, the isomers were easily separable by flash column chromatography.

Formation of the *p*-nitrophenyl ester at the γ -carboxyl position was accomplished using *p*-nitrophenyl chloroformate, according to a procedure (33) developed in our laboratory, resulting from a slight modification of a published protocol (34). This coupling method is surprisingly effective, providing good yields of highly pure *p*-nitrophenyl ester product in relatively short reaction times (20 minutes). Yields were in the 80 % range and losses were due mostly to hydrolysis of the *p*-nitrophenol group during rigorous aqueous work-up. Deprotection of the *tert*-butyl

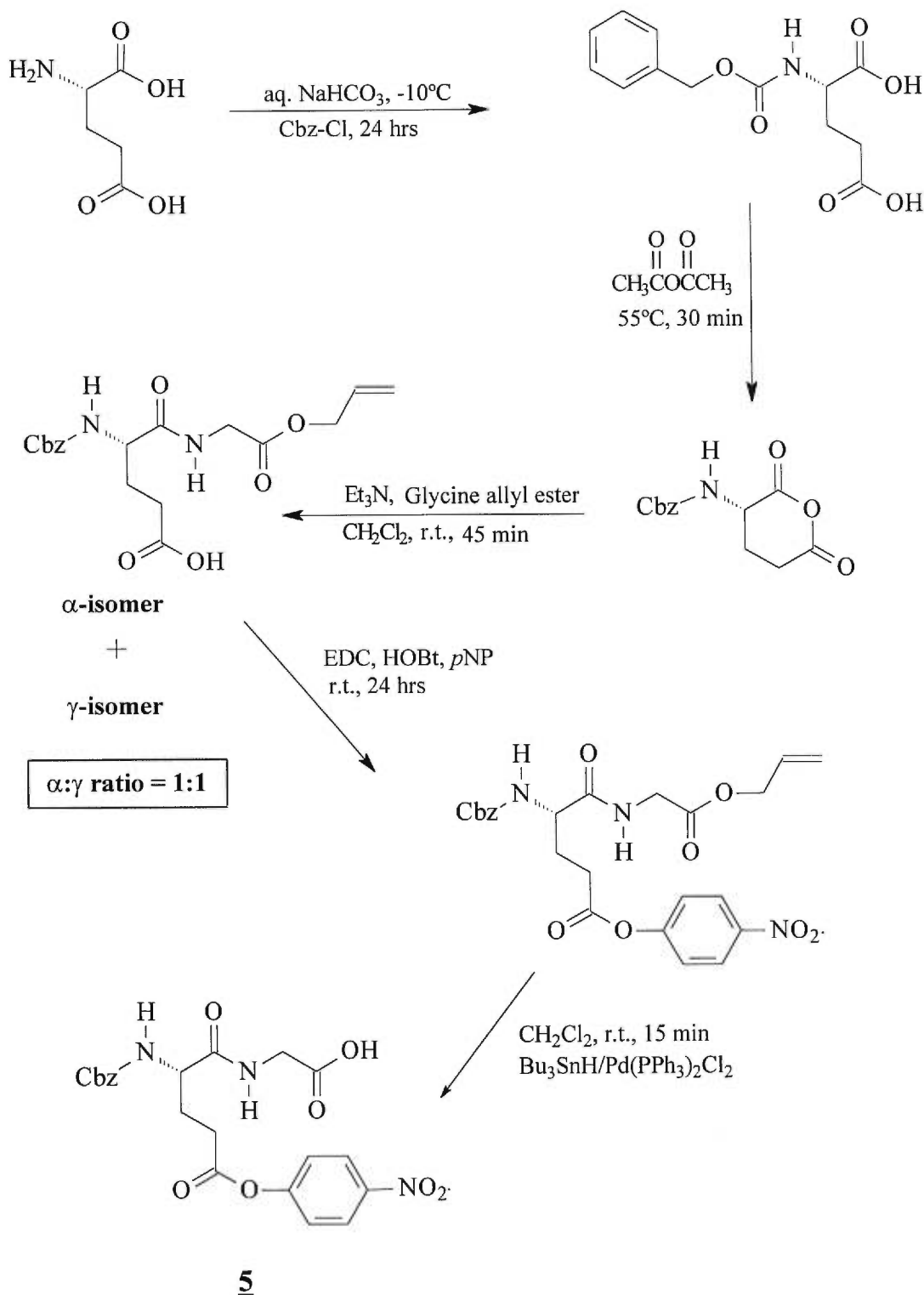
group was achieved in 80 % TFA, requiring 4 hours at 0 °C. The *tert*-butyl ester protective group proved compatible in this synthetic scheme, since its deprotection conditions did not affect the labile *p*-nitrophenyl ester bond. The overall yield for this five step synthesis was 30 %, compared to 9 % for the previously reported synthesis of substrate analogue **5** (8).

Table II: Regioselectivities observed upon varying the polarity of the solvent, or by using different ester protective groups of glycine (nucleophile), on the *N*-Cbz-L-glutamic acid cyclic anhydride ring opening reaction.

Solvent ^a	Amine	Major product	Yield ^b (%)	Regioselect. (α:γ)
DCM	Gly <i>t</i> -butyl ester	α = γ	96	1:1
CHCl ₃	Gly <i>t</i> -butyl ester	α	96	3:2
Toluene	Gly <i>t</i> -butyl ester	γ	95	1:6.5
Benzene:DCM (8:1)	Gly <i>t</i> -butyl ester	γ	88	1:4.3
DCM	Gly allyl ester	α = γ	88	1:1
THF:DCM (8:1)	Gly allyl ester	γ	96	2:3

^a DCM was used as co-solvent in situations of poor solubility; ^b Overall yield of the reaction (α-isomers + γ-isomers) obtained after purification by flash column chromatography.

Scheme 3: Synthesis of *N*-Cbz-L-glutamyl(γ -*p*-nitrophenyl ester)glycine (**5**) via L-glutamic acid cyclic anhydride formation and ring opening with glycine allyl ester, and EDC/HOBt coupling of *p*-nitrophenol.

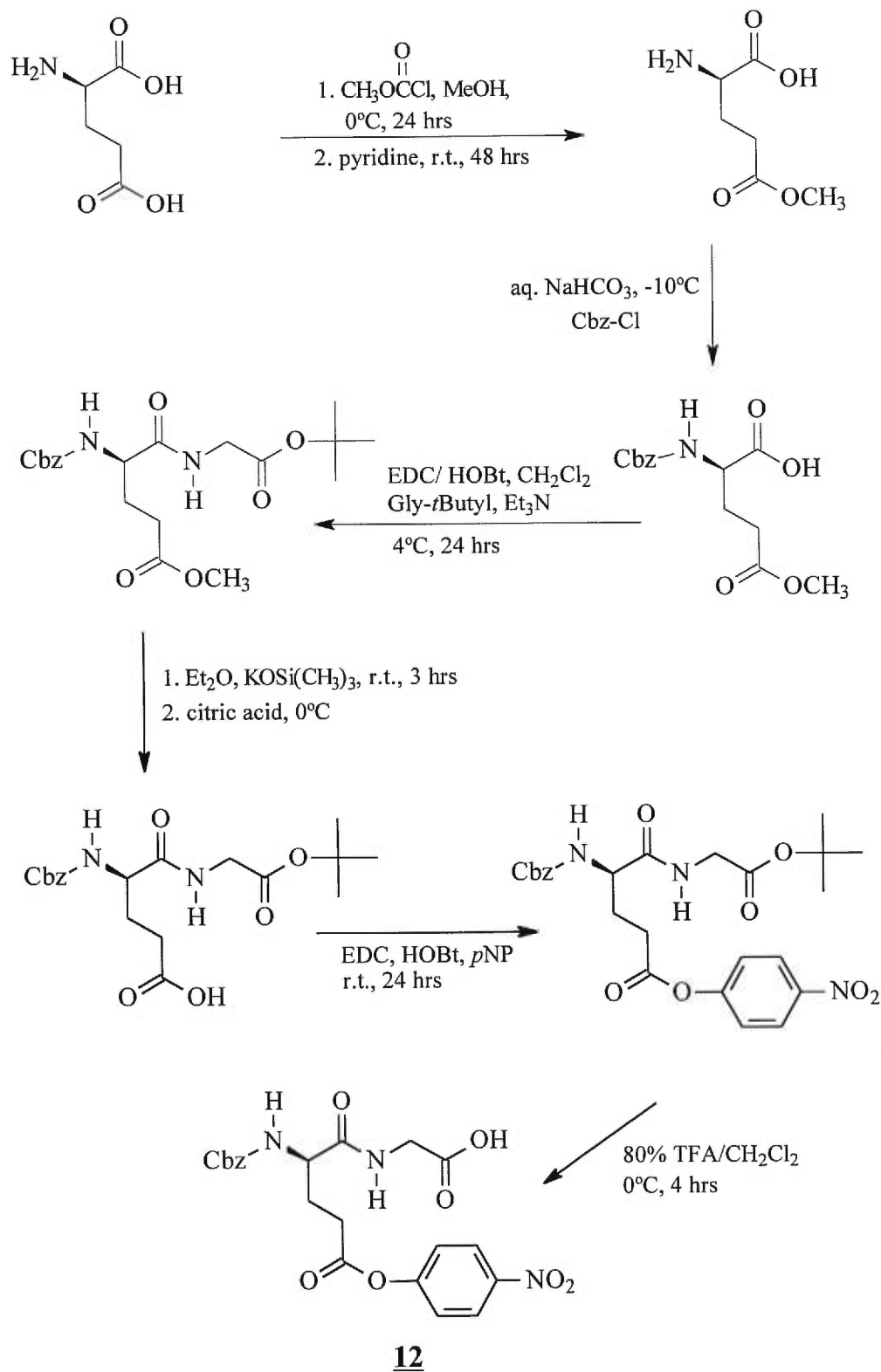


3.2.2 L-Glutamic Acid Cyclic Anhydride Formation: Use of Glycine Allyl Ester and EDC/HOBt Coupling of *p*-Nitrophenol in the Synthetic Route

As mentioned above, the versatility of the cyclic anhydride ring opening reaction was tested by using glycine with different ester protective groups, with no apparent improvement on regioselectivity. The allyl protective group, however, was an interesting option since it was not as labile as the *tert*-butyl group, which can be cleaved even under mild acidic conditions (35). Thus amidation of L-glutamic acid anhydride with glycine allyl ester and coupling of *p*-nitrophenol with the traditional EDC/HOBt method represents the variations introduced to synthetic **Scheme 3** on page 55 (refer to **Appendix B-3** starting on page 109 for all reactions outlined in **Scheme 3**). The coupling of *p*-nitrophenol at the γ -carboxyl position with the carbodiimide, EDC, was less impressive than the *p*-nitrophenyl chloroformate coupling method. The EDC coupling reaction required 24 hrs for completion and repeated washing with water did not entirely eliminate the water soluble urea by-product of the reaction, thereby necessitating flash column chromatography for final product purification. Although no stereocentres are involved in this coupling reaction, HOBt was introduced as an additive to drive the equilibrium towards product formation (36).

The allyl ester deprotection proved successful in the presence of the labile *p*-nitrophenyl ester, under the mild deprotection conditions afforded by using tributyl tin hydride and a dichlorotriphenylphosphene palladium catalyst. This reaction was very efficient, requiring only 10 min for completion. The only drawback of this synthesis involving the allyl protecting group is that the palladium catalyst employed in deprotection is not easily purified even after column chromatography from the product. The overall number of steps in this synthetic scheme remained at five, but two additional flash chromatography columns were required, thereby reducing the overall yield to 25 %.

Scheme 4: Synthesis of *N*-Cbz-*D*-glutamyl(γ -*p*-nitrophenyl ester)glycine (**12**) via a complete and sequential protection/deprotection synthetic route.



3.3: SYNTHESIS OF N-CBZ-D-GLUTAMYL (γ -p-NITROPHENYL ESTER)GLY

3.3.1 A Sequential Protection/Deprotection Synthetic Approach

A third synthetic approach was the conventional protection/deprotection strategy requiring six steps (**Scheme 4**, page 57). Initial selective γ -methyl protection of L-glutamic acid was effected, requiring three days and providing a very low yield (46 %) (refer to **Appendix B-4** starting on page 112 for all reactions outlined in **Scheme 4**). Unfortunately, there are no alternative reactions for the selective methyl protection of a γ -positioned acid, and the compound was commercially unavailable. Protection at the *N*-terminus with benzyloxycarbonyl provided excellent yields. Amino acid coupling was achieved by the EDC/HOBt strategy. Glycine *tert*-butyl ester was selected as the second amino acid, based on orthogonal principles of synthesis. It had been reported that the *tert*-butyl group is stable under specific γ -methyl deprotective conditions involving potassium trimethylsilanoate as a mild base (37). For the peptide coupling methodology, EDC was chosen over DCC since the latter generates a urea by-product which is theoretically not soluble in most organic solvents (and thus removable by filtration), but in practice is known to remain as a contaminant in the presence of other dissolved material (36). Since racemization is known to occur at the carboxyl amino acid coupling partner during the peptide coupling reaction, and more pronouncedly so when the amino acid is Cbz-protected (31), the additive, 1-hydroxybenzotriazole (HOBt), was introduced to the coupling reaction. This compound minimizes racemization by reducing the lifetime of the reactive O-acylisourea intermediate, and diminishes side reactions conducive to racemization (38). It has also been demonstrated that reducing the temperature of the reaction mixture minimizes the chance of racemization, so the reaction was effected at $-4\text{ }^{\circ}\text{C}$ (31). An overall yield of 80 % after flash column chromatography was achieved for the coupling reaction. The deprotection of the γ -methyl group, based on a previous protocol (37), afforded yields as high as 85 %, but proved difficult to reproduce. The possibility of hydrolysing the *tert*-butyl despite the mild conditions was anticipated, and attempts to improve the yield by adding solid citric acid (a very mild acidifying

agent) at - 4°C, adding smaller quantities, and acidifying to a limit of pH 5, supplied no improvement in yield.

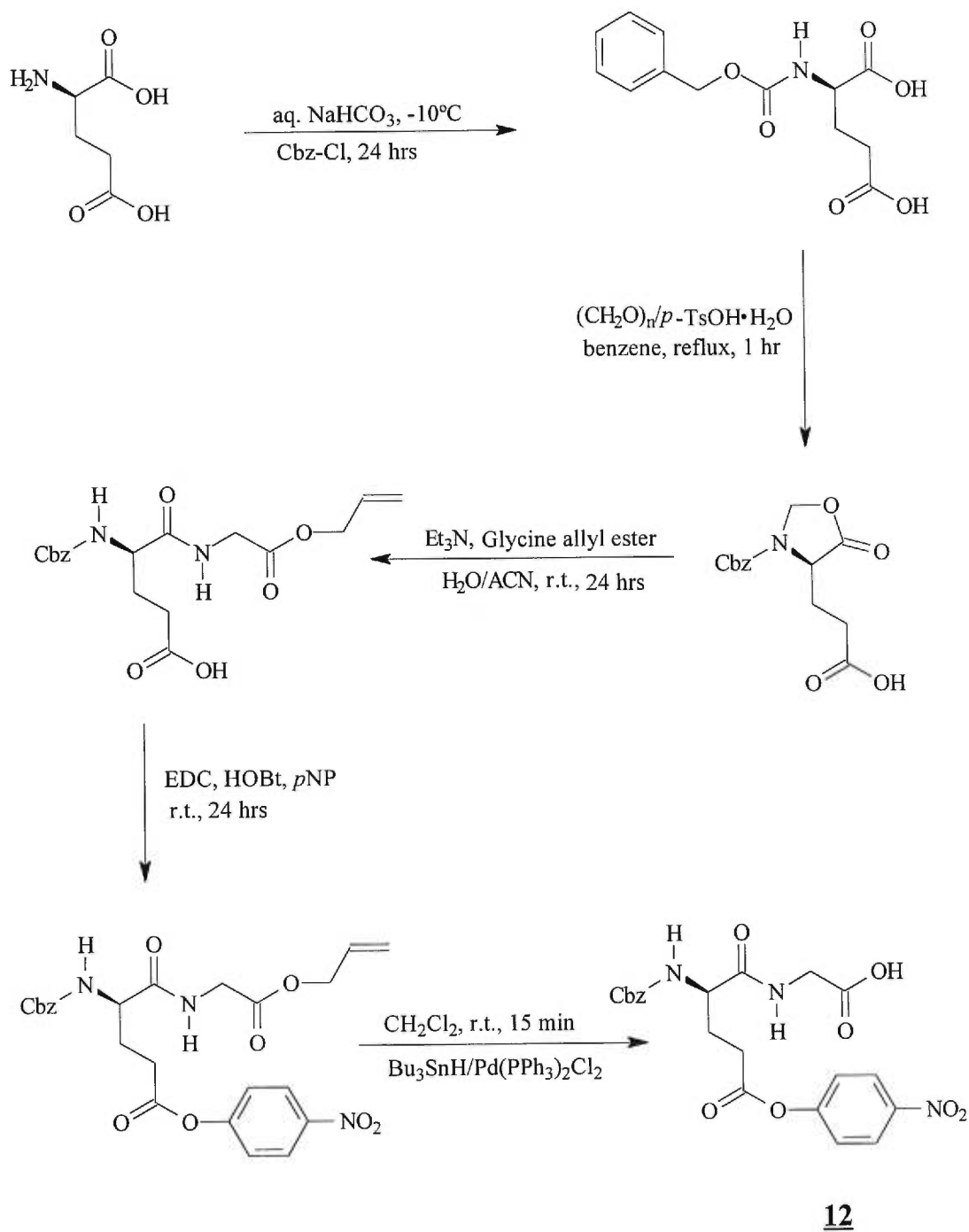
The subsequent coupling of *p*-nitrophenol was achieved again with EDC/HOBt, at room temperature. The overall yield for this reaction was 80% after purification. The *tert*-butyl group was removed by bubbling HCl at - 4 °C (HCl gas has a higher solubility at low temperature). The HCl gas was generated by the reaction between ammonium chloride and sulfuric acid and delivered to the reaction vessel *via* a Nalgene tube fitted with a glass pipette. A drawback to *tert*-butyl deprotection with HCl *vs* TFA is a longer reaction time and subsequent product degradation as evidenced by TLC analysis. The final product was purified by flash column chromatography and the yield for *tert*-butyl deprotection was 85 %.

This six step synthesis imparts a significant reduction in overall yield (20 %), mostly as a consequence of the very low yields of the γ -methyl protection step. Finally, the increase in number of steps as well as longer reaction times for several of these steps signifies larger time constraints using this synthetic approach.

3.3.2 Formation of the 5-Oxazolidinone Derivative of *N*-Cbz-*D*-Glutamic Acid

An alternative approach to the synthesis of *N*-Cbz-*D*-glutamyl-(γ -*p*-nitrophenyl ester)glycine was to eliminate the need for protection of the γ -carboxylate functionality deemed disadvantageous in the previous synthetic methodology. The intermediate chosen was the oxazolidinone derivative of *N*-Cbz-*D*-glutamic acid (see **Scheme 5**, page 60). The 5-oxazolidinones are generally prepared from the α -amino acids and serve as interesting intermediates in peptide synthesis because they generate activated esters (39). Furthermore, the resultant peptides obtained *via* coupling show virtually no racemization. Thus the oxazolidinone approach seemed a viable alternative (refer to **Appendix B-5** starting on page 118 for all reactions outlined in **Scheme 5**).

Scheme 5: Synthesis of *N*-Cbz-D-glutamyl(γ -*p*-nitrophenyl ester)glycine (**12**) via formation of 5-oxazolidinone derivative of *N*-Cbz-D-glutamic acid and nucleophilic ring opening with glycine *tert*-butyl ester.



The oxazolidinone derivative was synthesized, based on a previous protocol (40), by reaction with paraformaldehyde and *N*-Cbz-*D*-glutamic acid under reflux with a Dean-Stark condenser in the presence of a catalytic amount of *p*-toluenesulfonic acid. The reaction was stopped after one hour since progression beyond this reaction time proved to generate significant degradation products. The reaction was very efficient with 94 % yield.

In a previous article, it was demonstrated that the reaction between the 5-oxazolidinone derivative of *N*-Cbz-*L*-glutamic acid and various primary amines (methylamine, ethylamine, 2,2-dimethylethylamine) resulted in complete regioselectivity for the α -isomer with yields of 75 – 90 % (41). The reaction was conducted in water in the presence of 6 eq of primary amine at room temperature (5 hrs) or under reflux (2 hrs). The ability to regioselectively attack the α -carboxylate of the oxazolidinone derivative with an amino group in a coupling step was an exciting prospect. First, we encountered low solubility of the oxazolidinone derivative in water, so the compound was dissolved in a minimum of DCM before diluting with water. Both of our reported amidation approaches were attempted using glycine allyl ester. Heating to reflux generated mainly degradation products. The reaction at room temperature required 24 hrs before completion was observed by TLC analysis, and the product was purified by flash column chromatography. The overall yield was 65 %, somewhat lower than the yields observed with the aliphatic primary amines. However, regioselectivity appeared to completely favour the α -isomer which was very pleasing.

Coupling with *p*-nitrophenol was achieved with the EDC/HOBt yielding, after flash column chromatography, 82 % product. Allyl deprotection was achieved in 85 % yield. The overall yield for this 5 step reaction scheme was therefore 38 %, the highest reported among those synthetic routes described herein.

3.4: CONCLUSION

These different approaches have mapped out some synthetic possibilities using modern organic chemistry techniques for achieving the synthesis of substrate analogue **5**, as summarized in **Table III** (page 63). The results, based on overall yield, indicate that synthetic **Scheme 5** affords the best methodology. However, based on our experience, synthetic **Scheme 2**, involving the glutamic acid cyclic anhydride formation, ring opening with glycine *tert*-butyl ester, and esterification with *p*-nitrophenyl chloroformate proved the easiest route with respect to practicality and rapidity.

Finally, it is unfortunate that time constraints impeded the scheduled chiral HPLC analysis of the four products. The intention was to determine the percentage of racemization incurred by each method and comment as to which synthetic route resulted in minimal racemization. Also, it would have been of interest to quantitate the percentage of the D-isomer present in the substrate analogue **5** sample, based on the proven inhibitory behaviour of the D-isomer. Nevertheless, we accomplished the primary objective of comparing several synthetic routes in search of new and expedient approaches to the synthesis of substrate **5**, with yields on the order of 25 - 38 % in comparison with the 9 % yield previously reported (8).

Table III: Summary of results for the proposed synthetic schemes in the synthesis of *N*-Cbz- (L or D)-glutamyl(γ -*p*-nitrophenyl ester)glycine.

Synthetic Scheme	Number of Steps	Isomer Synthesized	Overall Yield (%)
2	5	L	30
3	5	L	20
4	6	D	25
5	5	D	38

Chapter 4

4. KINETIC STUDIES ON THE DEACYLATION STEP:

4.1: OVERVIEW

An enzymologist is generally interested in reaching three levels of understanding of an enzymatic mechanism: the reaction pathway as far as order of substrate addition and product release; relative rates of the various steps in the mechanism, with the identification of the rate-limiting step; and finally to discover through kinetic experimentation the way in which the enzyme catalyzes each discrete chemical reaction. This section focuses on the final and most complex level of understanding, namely the elucidation of the precise enzymatic events leading to the deacylation reaction of TGase.

Kinetic studies are essential to enzymology. They will serve as a tool in expanding our knowledge of the TGase catalyzed reaction, by allowing us to probe each step leading to formation and subsequent breakdown of the transient tetrahedral intermediate. Conclusions drawn in this chapter will be based on a Brønsted correlation, kinetic isotope effect studies and pH-rate profile studies. The results of these studies will contribute to our understanding of the deacylation mechanism by allowing us to determine if general-base catalysis is involved.

4.2: GENERAL CONSIDERATIONS FOR KINETIC STUDIES ON ENZYMES

At their most fundamental level, kinetic studies involve determining the effects of varying substrate concentration variable on the reaction rate. Results are expressed in terms of a rate law, and the challenge is to interpret this rate law in terms of a mechanism. The Michaelis-Menton equilibrium equation, or that of Briggs-Haldane for steady-state reactions, are among the first models devised to provide guidelines for the study of enzyme mechanisms (see **Figure 32**, page 141, for schematic representation of the Briggs-Haldane rate equation) (42). These models describe a simple enzymatic reaction involving one substrate and one product, and also define

certain elementary terms and kinetic parameters, such as steady state, ES complex, K_M , V_{max} and k_{cat} , which today are central to enzymology (see **Appendix D-2**, page 142 for definitions of these terms). The rate equations resulting from these models are identical except in their definition of the K_M constant. An important condition for application of these models, however, is that substrate concentration far exceed enzyme concentration at all times.

The mechanism of Briggs-Haldane introduces the concept of a “steady-state” level of the enzyme-substrate complex (ES) during the reaction. Under this definition, the enzyme experiences different “states” (42). One such state is attained immediately after mixing enzyme and substrate, and involves a rapid disappearance of substrate and free enzyme, as their chemical union results in the formation of the ES complex (transient phase). A steady-state is attained after this initial transient phase, where the formation of the ES complex is balanced by its rate of decomposition, $d(ES)/dt = 0$, and thus the rate of product formation is constant. This forms the basis for steady-state kinetics, and describes the principles we have applied for our own kinetic data acquisition. The rate equation for the TGase modified “Ping Pong Bi Bi” mechanism is shown in **Figure 33** (page 143)

4.3: SPECIFIC CONSIDERATIONS FOR KINETIC STUDIES ON TGASE

Judicious implementation of control experiments is necessary for the justified interpretation of kinetic results. The following section will identify issues of concern encountered as our kinetic methodology was being established, and emphasize the conditions we believe should provide justification for the interpretation of our kinetic data.

4.3.1 Calcium Requirements

The catalytic proficiency of TGase is dependent on the concentration of calcium (Ca^{2+}). This Ca^{2+} binding step, which is necessary to activate TGase, is considered a means for the metabolic regulation of TGase activity *in vivo* (43). Through calcium-binding studies it was revealed that TGase has different activation mechanisms for its hydrolysis and transfer reactions, as revealed by large differences

in their calcium dependence (44). The transfer reaction exhibits a much larger Ca^{2+} requirement than hydrolysis, and this was explained by the presence of two binding sites on the enzyme, which were coined the ‘catalytic’ and ‘binding’ sites, respectively. It was rationalized that both sites must be occupied to accommodate the transfer reaction; however, the hydrolysis reaction can occur if one (catalytic site) or both sites are occupied, thereby increasing the number of viable intermediates leading to product.

A fixed concentration of 50 mM Ca^{2+} was used in all kinetic experiments in order to guarantee that the Ca^{2+} ion requirement for the transfer reaction was respected. The Ca^{2+} ion dissociation constant (K_D) for the transfer reaction was found to be 8×10^{-3} M, and so a 4-fold K_D was used to ensure saturation of the enzyme (43).

4.3.2 Microscopic Reversibility

Due to microscopic reversibility principles, all enzyme catalyzed steps are theoretically reversible. The reversibility of the TGase-catalyzed transfer reaction has been demonstrated by the reaction between *N*-Cbz-L-GlnGly and glycine ethyl ester. The product of the forward reaction, *N*-Cbz-L-Gln(γ -Gly ethyl ester)Gly, was synthesized, and in the presence of TGase, slow formation of *N*-Cbz-L-GlnGly was observed chromatographically (21). The reversibility of the deacylation reaction does not pose a problem for our kinetic studies because initial velocities are measured at less than 10 % disappearance of substrate. In so doing, the concentration of product never reaches significant proportions which could have an impact on the observed kinetic rates. This limitation was applied to all kinetic experiments. The maximal absorbance representing complete saponification of 0.1 mM *N*-Cbz-L-glutamyl(γ -*p*-nitrophenyl ester)glycine (this represents the concentration of substrate analogue **5** used in all *transamidation* reactions) was determined at all pH values studied (results not shown). Maximal absorbance at pH 7.0, for example, was determined to be 0.6 absorbance units, and the reaction was therefore followed over a maximal change of 0.06 absorbance units. This scale was well within the detection capabilities of the Cary 100 Varian Spectrophotometer used since it registers

sensitivity to four decimal places during absorbance measurements. By implementing this limitation, initial rate conditions were ensured for all kinetic experiments.

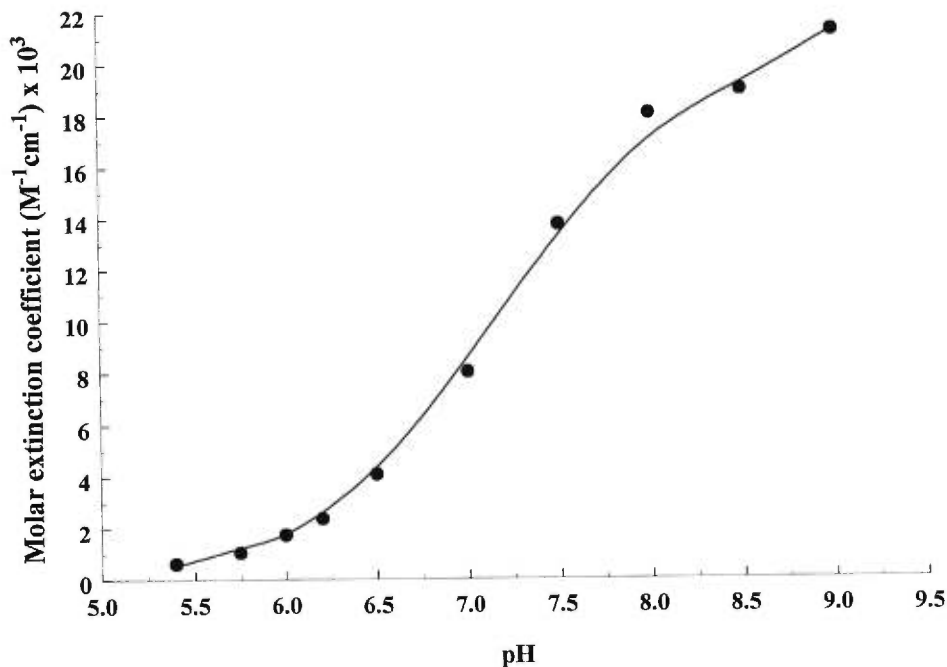
4.3.3 Extinction Coefficient

The primary kinetic data were initially obtained as slopes of absorbance *vs* time, since the TGase-catalyzed reaction was being followed spectrophotometrically by detection of *p*-nitrophenol liberated during acylation of substrate analogue **5**. In order to obtain the appropriate kinetic parameters, units of absorbance were converted into units of concentration by use of the molar extinction coefficient for *p*-nitrophenol. More precisely, the dissociated species (*p*-nitrophenolate) was being followed since it is strongly UV-active at 400 nm. The *p*-nitrophenolate has a pK_a of 7.16 (45), and therefore the extinction coefficient (ϵ) for this species will be pH-dependent over the range of pH values (6.0-8.5) studied. Standard curves were thus constructed at each of the pH values studied (see **Appendix C-2.1**, page 125 for the experimental section), by measuring the absorbance of different concentrations of *p*-nitrophenol at 400 nm. The slopes of absorbance *vs* concentration were then used to obtain the respective extinction coefficients. Finally, the Beer-Lambert equation, which incorporates the extinction coefficient, was used to convert absorbance values obtained from kinetic runs into concentration values (Equation 1). The representative sigmoidal plot of pH *vs* ϵ for *p*-nitrophenolate can be seen in **Figure 14** (page 68).

$$A = \epsilon [J] l \tag{1}$$

where, J = molar concentration of absorbing species J (mol/L)
 ϵ = molar absorption coefficient (L/mol/cm)
 l = path length (cm)

Figure 14: A graphical representation of the sigmoidal pH-dependence of the molar extinction coefficient of *p*-nitrophenolate.



4.3.4 Background Hydrolysis and Enzyme Stability

An important consideration for our enzyme kinetic studies is the pseudo-first order background hydrolysis reaction involving active ester substrate analogue **5** and hydroxide (OH^-) ions in solution. The rate of background hydrolysis will be influenced by the concentration of substrate analogue **5** and by the pH of the reaction medium. Surprisingly, the primary amine concentration for all primary amines studied did not influence this rate, so that intermolecular transamidation was not competing with the enzymatic reaction (results not shown). Background hydrolysis was accounted for by subtracting the velocity of the background reaction from the velocity of the TGase-catalyzed reaction (see **Appendix C-4.1.1**, page 132 for the method). Blanks for all kinetic studies contained all the components of the kinetic run *except* enzyme.

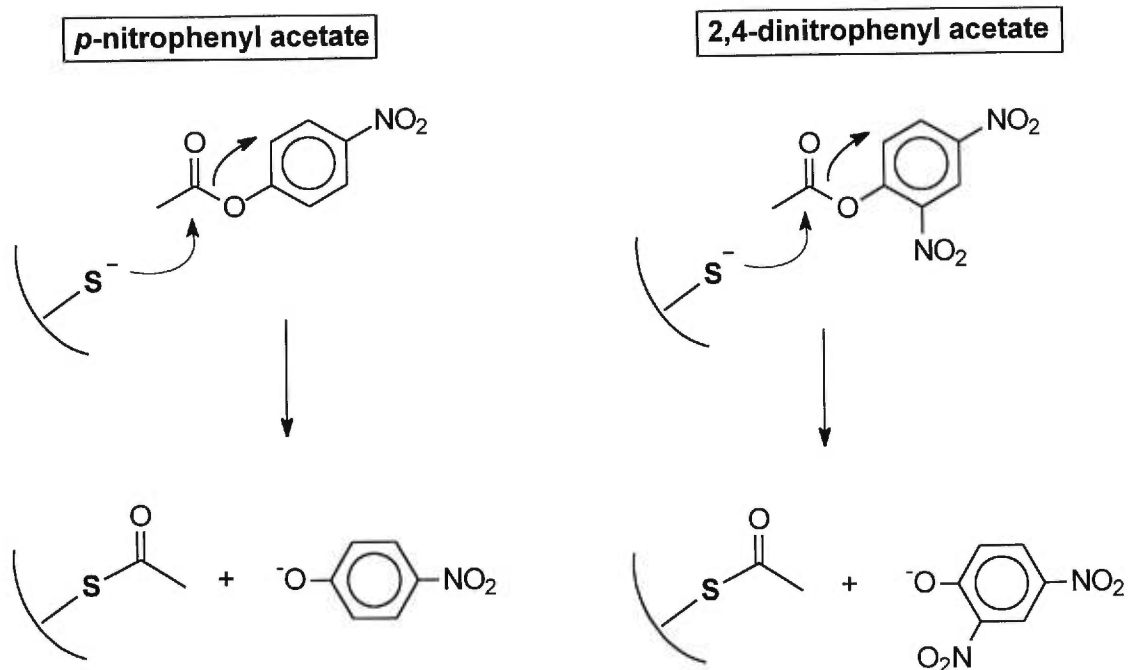
There was also an element of concern for the stability of the enzyme under various pH conditions, as well as over time. The enzyme stability varied between 83 –

95 % within the pH range studied (see **Table XI**, page 136). The largest losses in activity were observed in the more basic kinetic conditions employed (pH 8 - 8.5), where enzyme denaturation was anticipated to occur. Also, the stability of the enzyme over time was verified at pH 7.0, revealing that one hour of incubation at 37 °C did not contribute appreciable losses in enzyme activity. Since kinetic runs took place over a *maximum* of 10 minutes, time related loss in activity was not an issue during all kinetic studies.

4.3.5 Corroboration that Deacylation is Truly Rate-Limiting

It was important to test whether deacylation was truly rate-limiting in the presence of substrate analogue **5** as first substrate. Two active esters resembling our substrate in their leaving group (LG) moiety, *p*-nitrophenyl acetate (*p*NPA) and 2,4-dinitrophenyl acetate (2,4-DNPA), were used as substrates in the TGase-catalyzed hydrolysis reaction (see **Appendix C-4.1** on page 129 for the experimental section). In theory, there should be no LG effect on the reaction rate if acylation is functioning at its optimal velocity. The 2,4-dinitrophenol ($pK_a = 4.02$) (46) is a better LG than *p*-nitrophenol ($pK_a = 7.16$) (45); however, it was anticipated that the catalyzed hydrolysis of their respective acetates would occur at similar rates. As depicted in **Figure 15** (page 70), these substrates generate the same acetyl-acyl enzyme intermediate, and therefore vary only in their LG portion. Results presented in **Table IX** (page 130) reveal their V_{max}/K_M values are nearly identical at **0.79** for *p*NPA (see **Figure 28**, page 131) and **0.78** for 2,4-DNPA (see **Figure 29**, page 131). This would indicate that once binding constants are brought into consideration, the maximum velocities are identical, confirming a rate-limiting acylation. The reduction in K_M for 2,4-DNPA could be a consequence of improved binding affinity due to the presence of a second nitro substituent.

Figure 15: Rate of TGase-catalyzed hydrolysis as a function of leaving group capabilities. Effect of leaving group on the rate of acylation.



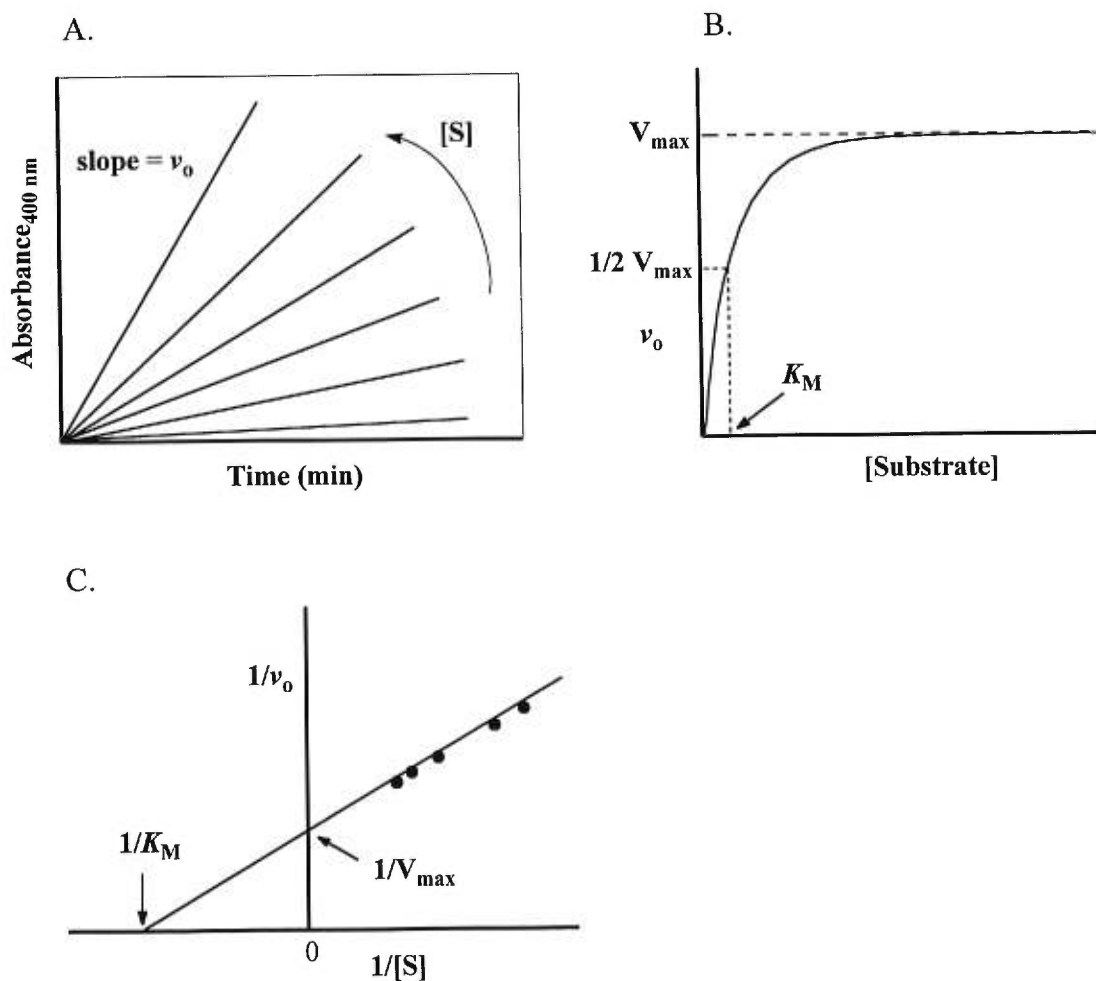
- Acyl-enzyme intermediate generated is identical
- Only the leaving group capabilities are different

4.3.6 Data Acquisition for TGase-Catalyzed Hydrolysis and Aminolysis

Primary data obtained from the TGase-catalyzed hydrolysis reaction are subjected to a series of graphical manipulations in order to arrive at the desired kinetic parameters, K_M and V_{max} . As described above, the reaction was followed spectrophotometrically with the release of *p*-nitrophenolate. The concentration of substrate analogue **5** was varied and slopes of absorbance vs time are obtained as shown in **Figure 16(a)** (page 71). These slopes were then converted into concentration vs time yielding v_o ("observed rate") values for each substrate concentration. These were plotted to give the "Michaelis-Menton saturation curve" as exemplified in **Figure 16(b)** or the "Lineweaver-Burke plot" in **Figure 16(c)**. The kinetic parameters for

hydrolysis of substrate analogue **5** ($V_{\max} = 0.2$ mM/min/mg and $K_M = 0.02$ mM; see **Figure 30**, page 132) for example were obtained by constructing the Michaelis-Menton graph.

Figure 16: (a) Plot of absorbance vs time as a consequence of varying substrate concentration. (b) Michaelis-Menton saturation curve generating kinetic parameters V_{\max} and K_M . Note that **[Substrate]** = *N*-Cbz-*L*-glutamyl(γ -*p*-nitrophenyl ester)glycine, or, primary amine at fixed concentration of *N*-Cbz-*L*-glutamyl(γ -*p*-nitrophenyl ester)glycine. (c) Lineweaver-Burke plots are useful for obtaining V_{\max} and K_M in circumstances when saturation cannot be reached.



For all kinetic studies performed in the presence of varying primary amine acceptor substrates (transamidation), it was important to choose reaction conditions that would ensure rapid acylation. The appropriate saturating concentration of substrate analogue **5** was determined to be **0.1 mM** or a concentration 5-fold its K_M . Under these conditions, the acyl-donor binding site will be saturated at all times and a rapid acylation is assured, such that ensuing kinetic results can be interpreted strictly in terms of deacylation phenomenon.

It is interesting to note that substrate analogue **5** and *p*NPA have identical LG's, but yield two very different acyl enzymes. The marked difference between values of V_{max}/K_M obtained for *p*NPA (**0.79**) and substrate **5** (**10.0**), suggest that under these conditions, the steady-state turnover rate is dependent on the acyl portion of the substrate, consistent with rate-limiting deacylation. With the framework for meaningful kinetic experimentation in place, the deacylation step of the TGase-catalyzed reaction was investigated.

4.4: STRUCTURE-ACTIVITY RELATIONSHIP (BRØNSTED PLOT)

To test our hypothesis on the involvement of a general-base catalyst during deacylation, we embarked upon a structure-activity study. This section will deal with physical organic chemistry concepts including the Brønsted theory, nucleophilicity and basicity, as well as discuss key mechanistic findings such as the structure of the transition state of the rate-limiting step in the TGase-catalyzed deacylation reaction.

Linear free-energy relationships (LFER), as revealed by Brønsted plot analysis, assist in delineating transition state structures for enzyme-catalyzed reactions (46b). The Brønsted plot is generated as a consequence of charge or dipole separation in the transition state compared to the ground state. For the TGase catalyzed deacylation reaction the ground state is the thiolester acyl-enzyme intermediate (47). The polar substituent effect, β , which is obtained from the slope of the Brønsted plot, is used to interpret these charge differences (47b). Using the Brønsted theory, primary amine acceptor substrates were varied in order to correlate nucleophilicity with the efficiency of deacylation step.

The rate-determining step during the nucleophilic attack of an amine on a carbonyl involves either formation or subsequent breakdown of the transient tetrahedral intermediate. The actual nucleophilic attack is said to proceed through five stages (48):

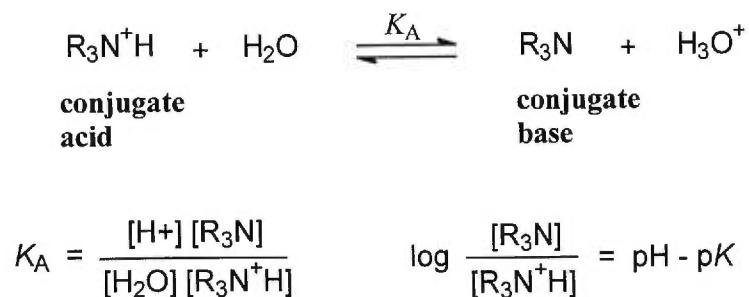
1. approach of nucleophile
2. passage through the first transition state (attack)
3. formation of a tetrahedral intermediate
4. passage through a second transition state (decomposition)
5. the formation of new amidic bond

We can visualize this reactional pathway from the perspective of the thioester acyl-enzyme intermediate, as the reaction progresses from the nucleophilic attack on the acyl-enzyme to the regeneration of free enzyme. The emerging question then is whether this reactional pathway is assisted by a general-base catalyst, acting as a proton ‘trap’ for the attacking nucleophile during deacylation. The term ‘general-base catalysis’ refers to proton abstraction at the same time as heavy bond rearrangement, as opposed to ‘specific-base catalysis’, which describes a rapid pre-equilibrium proton removal (42). The amine is therefore participant to two collective events if general–base catalysis is involved: nucleophilic attack on the carbonyl *and* the relinquishment of a proton to the general base. By using a series of primary amines of varying pK_a for their conjugate acids (pK_{NH^+}), we can integrate effects of acidity and nucleophilicity on the observed rates of deacylation. It is the slope of the Brønsted plot, therefore, which will provide information as to the degree of importance of each event on the rate–limiting step.

The concepts of nucleophilicity and pK_{NH^+} have a fine line of distinction. In aqueous solution, a primary amine can be present either as a base (RNH_2) or as its conjugate acid (RNH_3^+). The equation used in determining the pK_{NH^+} for a primary amine is given in **Figure 17** (page 74)(49). The pK_{NH^+} of an amine represents the pH at which equal proportions of protonated and neutral forms are present in solution. It has been suggested that only the neutral form of the amine can be bound by TGase (50). Given that the native substrate for TGase is a peptide-bound lysine, it is apparent that at physiological pH, about 99.9 % of the ϵ -amino group will be present in the

protonated state. Therefore, it seems reasonable to assume that TGases are capable of recognizing and binding primary amine substrates in both protonation states. However, the enzyme catalyzed deacylation reaction could be influenced by the availability of the neutral form of the amine. If this were true, the fact that the Brønsted study was conducted at pH 7.0 would affect the proportion of the reactive form for each amine (*i.e.* neutral form) as a function of their pK_{NH^+} . Correction for the effective neutral amine concentration, however, was deemed unnecessary for the interpretation of the Brønsted plot. When in fact a correction for effective neutral amine concentration was applied, a sharp break in the slope of the Brønsted plot was generated (from $\beta_{\text{nuc}} = -0.37$ below $pK_{\text{NH}^+} 7$ to $\beta_{\text{nuc}} = 0.59$ above $pK_{\text{NH}^+} 7$) from the previous *linear* correlation observed between amine pK_{NH^+} and $\log(\text{deacylation rates})$. The deviation from linearity introduced by this treatment of the data argues against its validity. The linearity, in fact, tells us that we are observing a 'true' relationship.

Figure 17: Acid-base equilibrium for a primary amine in aqueous solution. Determination of the pK_{NH^+} for an amine.



Also pivotal in the interpretation of the Brønsted plot is the concept of amine nucleophilicity. Generally, the higher the pK_{NH^+} , the more nucleophilic the amine. Attempts to correlate kinetic (*i.e.* $\log V_{\text{max}}/K_M$) and equilibrium phenomena (pK_a) are not always successful because some nucleophiles, while being strong conjugate acids (towards H^+), can still be powerful nucleophiles (towards electrophilic centres such as carbonyls) (51). All the nucleophiles in this study, however, belong to the same class

of ‘hard’ nucleophiles and possess key structural similarities which ensure good correlation between basicity (measures the ‘hard’ nucleophilic character) and nucleophilicity (total capacity for electron pair donation) (see **Table IV**, page 76 for the listing of primary amines utilized in this study)(51).

To summarize on issues related to interpretation of the Brønsted data, concern has been raised for the possible need to correct for effective concentration of free amine in deacylation kinetics involving amines of varying basicity. Also the validity in correlating pK_{NH^+} and nucleophilicity for the purpose of Brønsted plot analysis has been questioned. In addressing these questions, we are now confident that the experimental methodology applied herein is sound.

Because the impetus is on generating a meaningful Brønsted plot, the pK_{NH^+} of each amine was determined under our experimental conditions (see **Appendix C-3** on page 129 for the experimental section). This was deemed necessary because the pK_a can be influenced by conditions of ionic strength and solvent composition (see **Table V** on page 77 for the kinetic results of the transamidation reaction at pH 7.0) (51). The Brønsted plot for the transamidation reaction involving a series of primary amine acceptor substrates and donor substrate analogue **5**, is represented in **Figure 18** (page 78).

Several mechanistic deductions can be made from the Brønsted plot based on the following considerations: (1) there is a *linear* correlation between pK_{NH^+} and $\log(V_{\text{max}}/K_M)$; (2) a *negative* slope is obtained; (3) a relatively *small* β_{nuc} value of 0.37 (shallow slope) is observed. The significance of each of these will be discussed below.

Table IV: Summary of the primary amines chosen for construction of the Brønsted plot, their $pK_{\text{NH}_3^+}$ values determined herein, and an illustration of their comparative structures.

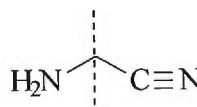
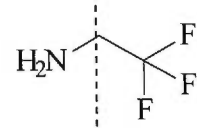
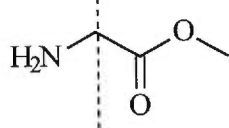
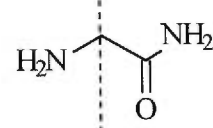
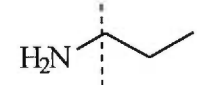
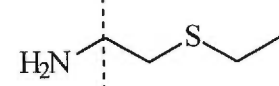
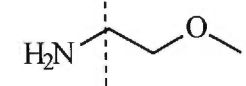
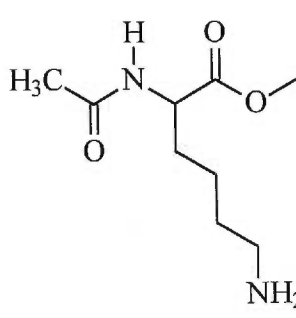
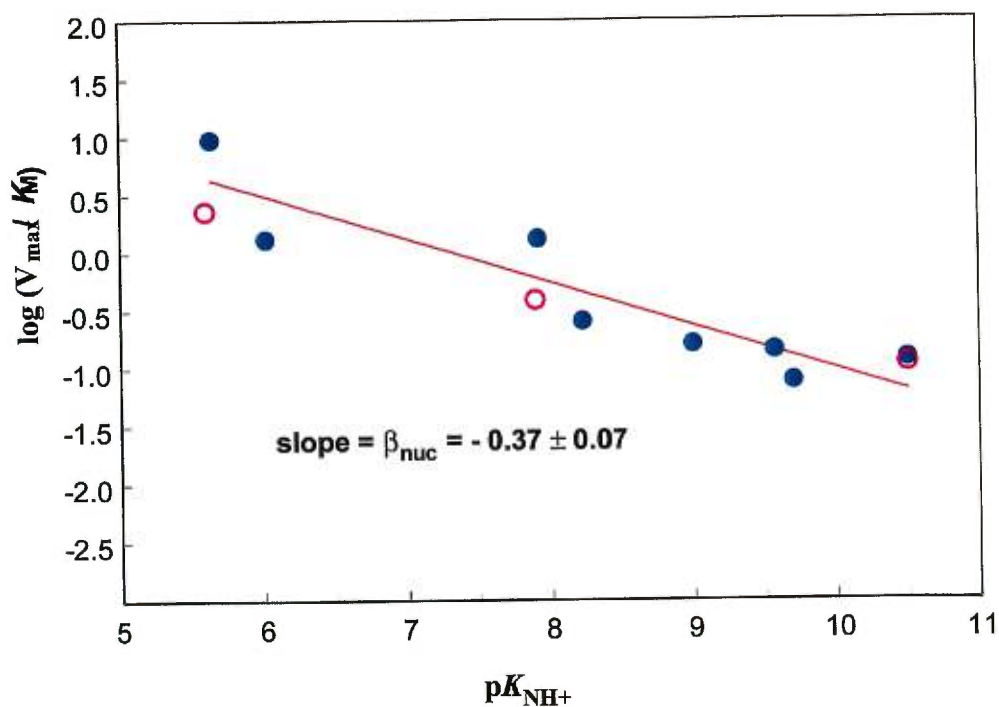
Primary Amine	$pK_{\text{NH}_3^+}$	Structure
Aminoacetonitrile	5.64	
2,2,2-Trifluoroethylamine	6.02	
Glycine methyl ester	7.92	
Glycinamide	8.23	
Propylamine	9.00	
2-Ethylthioethylamine	9.70	
2-Methoxyethylamine	9.57	
<i>N</i> -Acetyl-L-lysine methyl ester	10.50	

Table V: Kinetic parameters (V_{\max} , K_M and $\log(V_{\max}/K_M)$) obtained according to Equation 4 for the TGase catalyzed transamidation reaction in the presence of 0.1 mM substrate **5** and a series of primary amine acceptor substrates at 25 °C and pH 7.0 (0.1 M MOPS), and the respective $pK_{\text{NH}_4^+}$ values determined under kinetic experimental conditions.

	Ammonium pK_a	V_{\max}^b (mM/min/U)	K_M^c (mM)	V_{\max}/K_M^d (min/mg)	\log^e (V_{\max}/K_M)
Aminoacetonitrile	5.64	1.38	0.14	7.50	0.98
2,2,2-Trifluoroethylamine	6.02	0.69	0.52	1.33	0.12
Glycine methyl ester	7.92	0.82	0.62	1.32	0.12
Glycinamide	8.23	1.24	4.68	0.255	-0.59
Propylamine	9.00	0.71	4.35	0.163	-0.79
2-ethylthioethylamine	9.57	2.76	19.2	0.143	-0.84
2-Methoxyethylamine	9.70	3.13	40.0	0.078	-1.11
N-Acetyl-L-lysine methyl ester	10.50	0.33	2.80	0.118	-0.93

^a Measured herein (see Appendix C-3, page 128); ^{b, c, d} reported values have 10 % error; ^d reported values have 20 % error.

Figure 18: The Brønsted slope β was obtained according to Equation 5 for the aminolysis reaction involving the thiolester acyl-enzyme intermediate of TGase and various primary amines ranging in basicity (closed circles). The same reaction in D_2O for several of the amines is shown as open circles. There is a 20 % experimental error associated with each value.



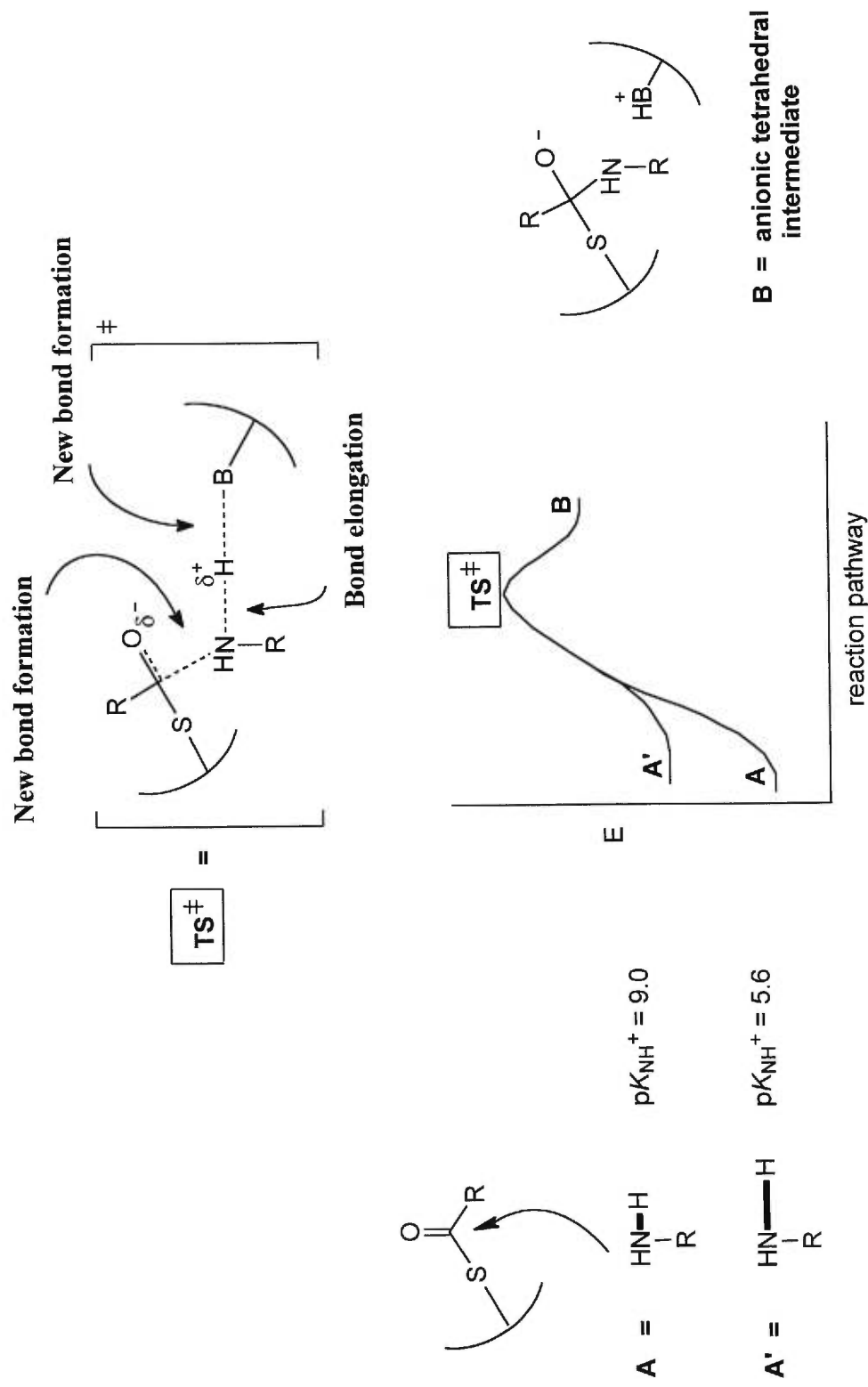
First, the Brønsted-type plot features good linearity over the broad range of amine basicities studied ($r = 0.840$), confirming in all cases, that a *linear* relationship exists between the pK_{NH^+} and $\log(V_{max}/K_M)$ for the TGase-catalyzed deacylation reaction. In contrast, the plot of $\log(V_{max})$ vs pK_{NH^+} was extremely scattered (results not shown). The fact that it is necessary to implicate the K_M values of the amines studied in order to observe a linear free-energy relationship signifies that rate constants for equilibrium substrate binding are incorporated into the rate law for the enzymatic

deacylation process. This suggests that the rate-limiting step is a function of the events leading up to the formation of the tetrahedral intermediate, and not the decomposition. Therefore the rate-limiting step most likely involves the formation of a covalent bond between the substrate and the enzyme.

Secondly, the negative β_{nuc} slope reveals that amine *acidity*, and not nucleophilicity, has the most significant impact on the deacylation kinetics. The rationale is that amines of greater acidity are characterized by elongated N–H bonds, and therefore facilitate the formation of the transient tetrahedral intermediate. The Hammond postulate explains that “if a TS^\ddagger and an unstable intermediate (*i.e.* tetrahedral intermediate) occur consecutively during a reaction process and have nearly the same energy content, their interconversion will involve only a small reorganization of structure” (52). By supplying a more acidic amine we are effectively decreasing the activation energy for tetrahedral intermediate formation by reducing the investment of energy needed to effect N–H bond elongation, as illustrated in **Figure 19** (page 80). The influence of amine acidity on the reaction rate is also strong evidence for general-base catalysis. The β_{nuc} parameter may be viewed as an empirical index of the fraction of charge transferred to the nucleophile, and reflects the degree of bond formation/cleavage in the transition state (51,53). The value of 0.37 ± 0.07 can be interpreted in terms of little charge separation between the ground and transition states at the rate-limiting step of deacylation. The important conclusion from the Brønsted data is that the reactivity of amines toward the ES complex is not significantly influenced by the basicity of these nucleophiles, since bond formation between the amine and the carbon of the carbonyl is not extensive in the transition state.

Thirdly, the shallowness of the slope of the Brønsted plot provides a measure of the efficiency of the deacylation reaction. The shallowness presumably reflects the summation of two competing factors, namely, increased amine nucleophilicity with increasing basicity and increased ease of proton abstraction with decreasing basicity.

Figure 19: A general trend revealed by the Brønsted plot is the increased reaction velocity with increasing primary amine acidity, which is explained schematically by application of the Hammond postulate.

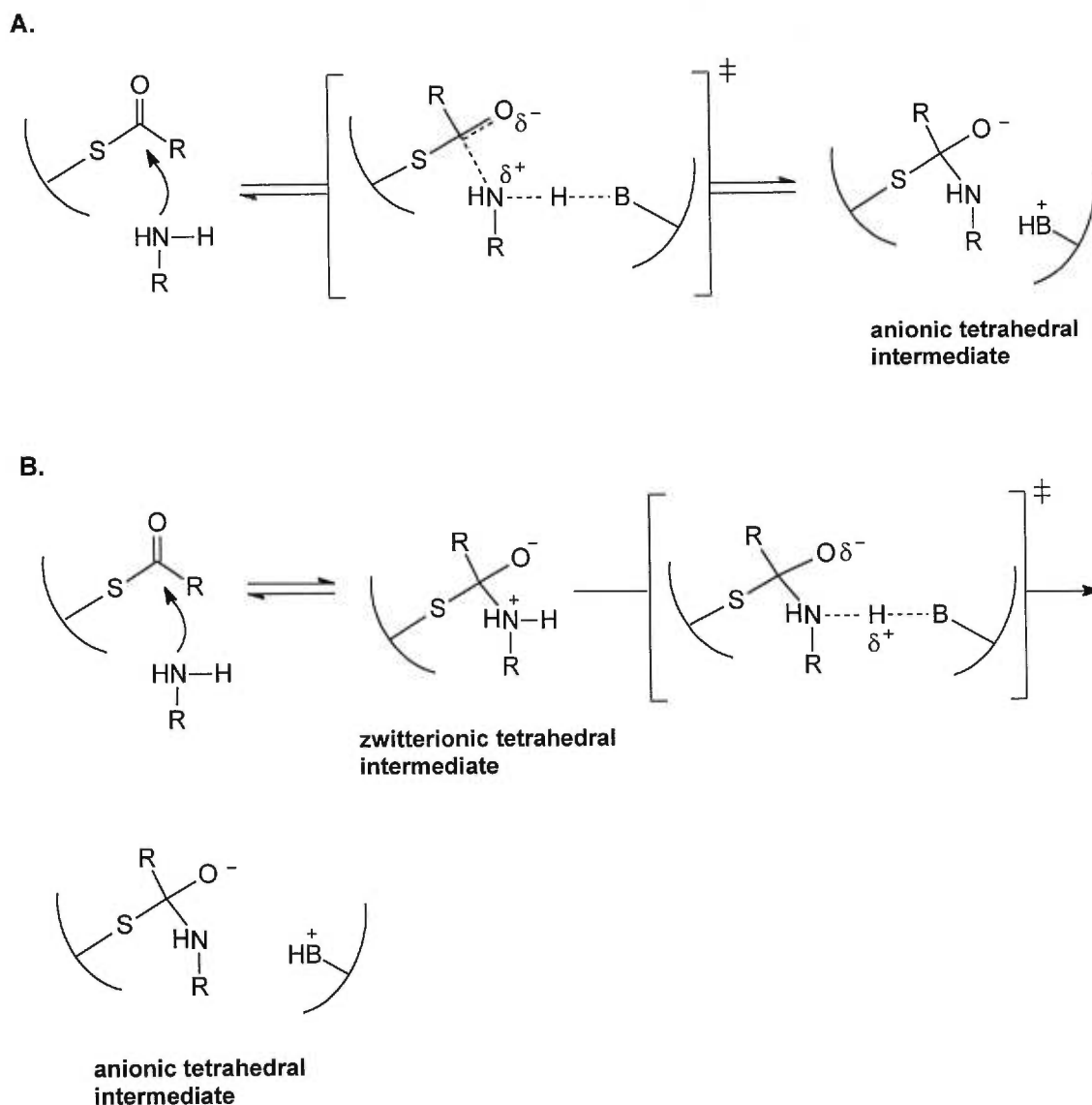


Given that the Brønsted theory supports our premise for general-base catalysis, attention can be drawn to the preferred mechanistic pathway for deacylation by guinea pig TGase. **Figure 20** (page 82) illustrates the two possible reactional pathways involving proton transfer during amine nucleophilic attack on thioesters. Nucleophilic attack of the amine can occur concomitantly with removal of one of its protons by a general base to generate an anionic tetrahedral intermediate, which then decomposes into products. This is known as a *concerted* mechanism and is a feature of general-base catalyzed reactions. Also, addition of the amine to the carbonyl can provide a zwitterionic tetrahedral intermediate, with the subsequent removal of a proton by a base in a *stepwise* process (54). Differentiation between these two pathways is satisfied by the negative slope of the Brønsted plot, which implies that amine acidity affects the rate of deacylation and signals a general-base catalyzed process. Interestingly, studies on an analogous non-enzymatic reaction involving nucleophilic attack on thioesters, such as *p*-nitrophenyl thiolacetate, displayed a large positive slope ($\beta_{\text{nuc}} = +0.83$), which was attributed to a stepwise mechanism involving a rate-limiting decomposition of the tetrahedral intermediate (55). The preferred mechanistic route for the enzyme-catalyzed reaction appears different than for the non-enzymatic, and the fundamental difference is probably that the catalyst (enzyme) has all of the machinery in place for each requirement of a concerted reaction.

We have specified that the negative Brønsted slope is reflective of general-base catalysis, but another possibility for this result is a rate-limiting *proton removal* rather than a proton abstraction accompanying the rate-limiting tetrahedral intermediate formation. The former pathway would consist of a rapid nucleophilic attack prior to or after proton abstraction, and would yield a steep negative slope, due to a strong correlation between $\text{p}K_{\text{NH}^+}$ and reaction rate. The shallowness of the slope in **Figure 18** (page 78) contradicts this possibility. Finally, we could also be observing a phenomenon where a basic group such as the amine itself, or an amino acid residue, is acting as a nucleophilic catalyst during deacylation, and not as a general base. Results obtained from our isotope effect studies, which will be discussed in the following section, allow us to eliminate these possibilities. Large

isotope effects were observed, which imply a proton transfer by a general-base catalyst in the transition state of the rate-limiting step.

Figure 20: There are two plausible mechanisms involving nucleophilic attack during the TGase-catalyzed deacylation step: **A.** the *concerted* and **B.** *stepwise* mechanisms.



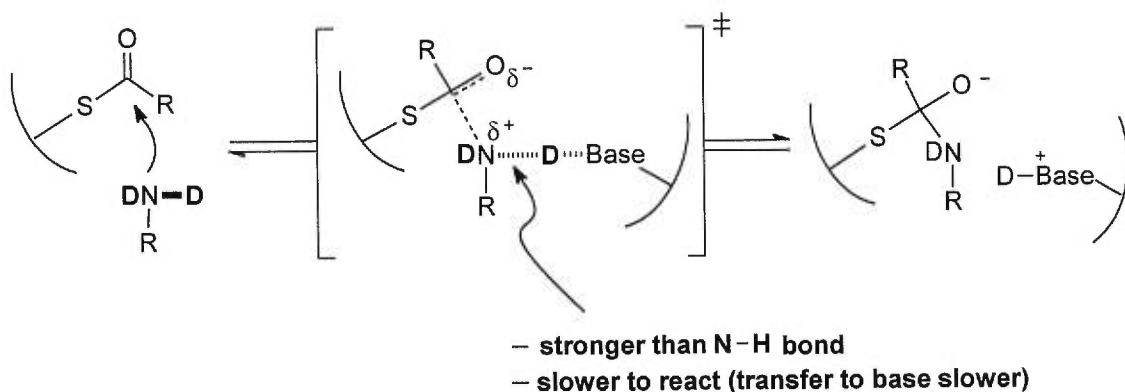
Notice that the Brønsted plot conveys information regarding the enzymatic reaction in connection with amine nucleophilicity, as it occurs at the *specific* pH of 7.0. Therefore it must be stressed that all mechanistic interpretations made to this point regarding the deacylation step of guinea pig liver TGase are for events occurring at neutrality. An interesting future experiment would be to construct a Brønsted plot at various pH values and investigate if a change in the mechanism occurs in response to pH.

In conclusion, these results add to the longstanding belief that enzyme-mediated catalysis *via* proton transfer between electronegative atoms provides an important contribution to observed rate accelerations (56). More specifically, in the isolated case of the TGase-catalyzed reaction we have confirmation that general-base catalysis provides the driving force for the deacylation reaction.

4.5: ISOTOPE EFFECT STUDIES (Kie)

Solvent kinetic isotope effects (Kie) measure changes in reaction rates that result upon replacement of exchangeable protons with deuterons. While isotopic substitution has no effect on the qualitative chemical reactivity of the substrate, it often has an easily measured effect on the rate at which the reaction occurs (56). The magnitude of a primary kinetic isotope effect is generally in the order of 1.0 to 7.0, where a value of 1.0 reflects no effect and a value of 7.0 represents a very large isotope effect. We will be focusing our discussion on *primary* kinetic isotope effects which involve bond breaking at the isotopically-substituted atom (N–D). In this case, the principles behind observed isotope effects stem from the differing zero-point energies of a protium- and a deuterium-substituted nitrogen. Any N–H bond has characteristic vibrations which impart some energy to the molecule in its ground state, called its zero-point energy (52). The energy associated with these vibrations is directly proportional to the mass of the vibrating atoms. Due to the greater mass of deuterium, naturally the N–H bond is weaker than the N–D bond by a significant amount resulting from the two-fold difference in mass between hydrogen and deuterium. Thus substitution with deuterium lowers the zero-point energy of the molecule and consequently N–D bond cleavage is more difficult requiring a larger activation energy (see **Figure 21**, below).

Figure 21: Solvent kinetic isotope effects result from the greater strength of the nitrogen-deuteron bond in comparison to the nitrogen-hydrogen bond.



If the negative slope of **Figure 18** (page 78) derives from general-base catalysis during deacylation, as we propose, then the putative proton ‘in flight’ at the rate-limiting transition state will expectedly give rise to a kinetic isotope effect. In order to assess this possibility, kinetic parameters were obtained in D₂O for three acceptor substrates: aminoacetonitrile, glycine methyl ester and *N*-acetyl-L-lysine methyl ester. The results of these experiments are summarized in **Table VI** below and shown in **Figure 18** as *open circles*.

Table VI: Kinetic parameters (V_{\max} and K_M) obtained according to Equation 4 and kinetic isotope effects ($(V_{\max}/K_M)^{H_2O} / ((V_{\max}/K_M)^{D_2O})$) for the reaction of TGase in D₂O, at 25 °C at pD 7.0 (0.1 M MOPS), with 0.1 mM of substrate analogue **5** in the presence of three different primary amine acceptor substrates.

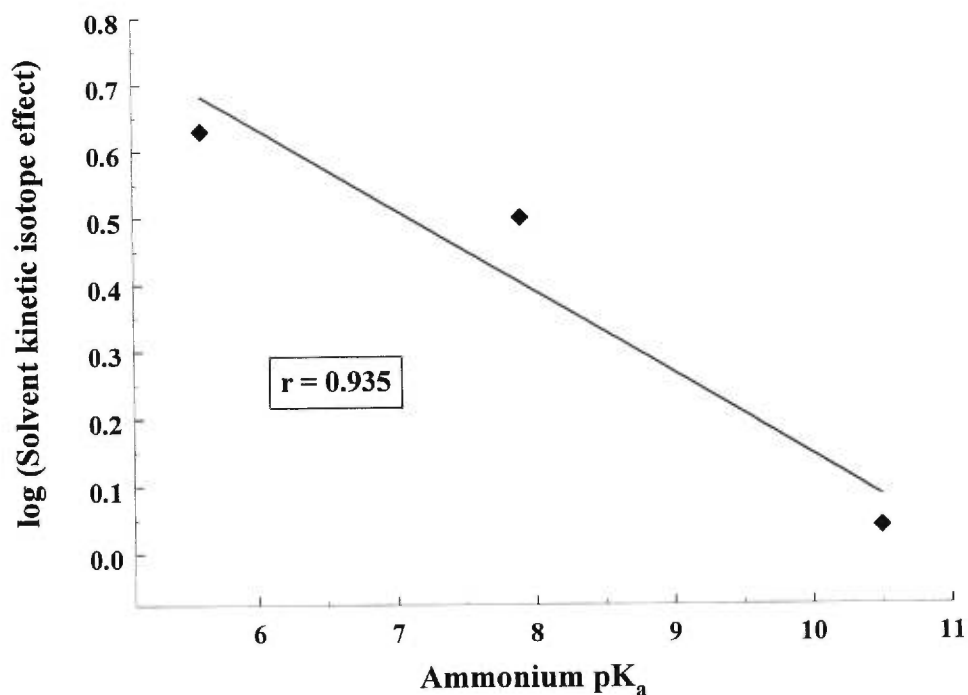
Amine: H ₂ NCH ₂ - <i>R</i>	<i>H</i> ₂ O			<i>D</i> ₂ O			Kie ^d	p <i>K</i> _{NH} ⁺
	V_{\max} ^a	K_M ^b	$\frac{V_{\max}}{K_M}$ ^c	V_{\max}	K_M	$\frac{V_{\max}}{K_M}$		
-CN	1.38	0.14	9.85	0.46	0.20	2.3	4.3	5.6
-CO ₂ CH ₃	0.82	0.62	1.32	0.29	0.74	0.39	3.4	7.9
Ac-L-Lys-O-Me	0.33	2.80	0.12	0.35	3.10	0.11	1.1	10.5

^a (mM/min/mg); ^b (mM); ^c (min/mg); ^d error associated with Kie is 20 % of the values.

In each case, a Kie was observed for V_{\max}/K_M , in the range of **4.3** for aminoacetonitrile, **3.4** for glycine methyl ester and **1.1** for *N*-acetyl-L-lysine methyl ester, suggestive of general-base catalysis. The magnitude of the observed Kie, which appears to be proportional to amine acidity, reflects the structure of the transition state (TS[‡]), or more precisely, the degree of proton transfer at the TS[‡]. A maximum effect is expected for a transition state which reflects 50 % proton transfer. Also, when bond

breaking is more or less than 50 % at the transition state, the Kie value will be < 7 , representing a TS^\ddagger which is more reactant *or* product-like, respectively (52). It is important to note that a significant kinetic isotope effect implies that proton restructuring is occurring during the reaction, but does not provide information regarding either the number of protons involved or their surrounding environment (56). A similar study looking at Kie on k_{cat} for the papain-catalyzed hydrolysis of active ester substrates reported an effect in the order of 2.2 - 3.3 (57), which was interpreted as evidence for general-base catalysis. The correlation between the magnitude of the Kie and the $\text{p}K_{\text{NH}^+}$ of the primary amine is a rather interesting feature of our results. The Kie values are apparently inversely proportional to $\text{p}K_{\text{NH}^+}$, and the plot of $\log(\text{Kie})$ vs $\text{p}K_{\text{NH}^+}$ reveals a significantly linear ($r = 0.935$) relationship as illustrated in **Figure 22** below.

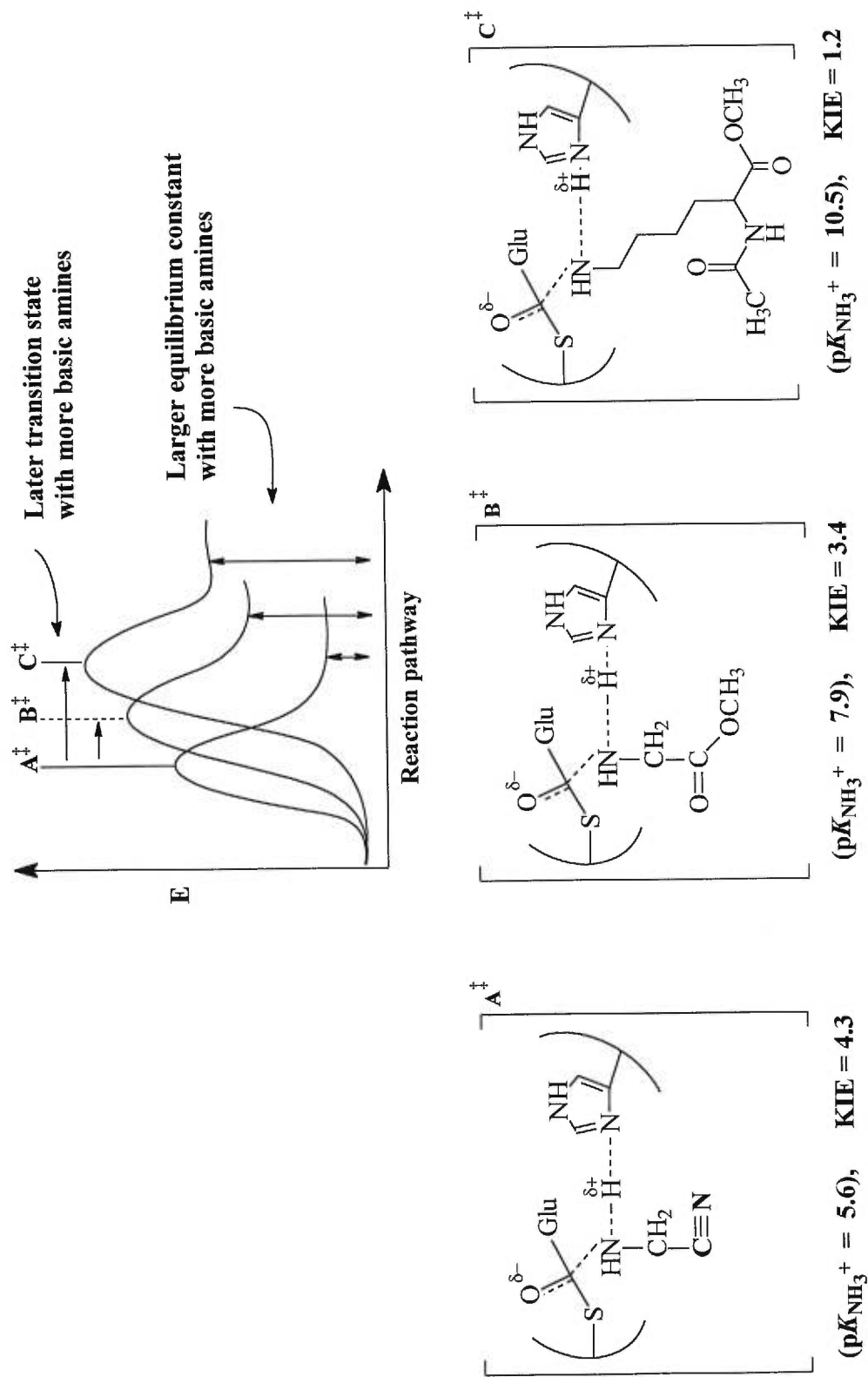
Figure 22: Linear correlation observed between the solvent kinetic isotope effect on the $\text{p}K_{\text{NH}^+}$ of the primary amine.



With the most acidic amine (aminoacetonitrile, $pK_{\text{NH}^+} = 5.6$), the N–H bond is already considerably elongated in its ground state. The transition state, with respect to proton transfer, is expected to be the *earliest*. This simply means that the proton is nearly 50 % transferred to the base in the TS^\ddagger . As illustrated in **Figure 23** (page 88), proton transfer for an acidic amine should be characterized by a small equilibrium constant reflecting the similar energies of reactant and product. Increasingly less pronounced Kie are observed with the decreasingly acidic amines, whose *later* TS^\ddagger feature higher degrees of proton transfer. For a basic amine, such as glycine methyl ester ($pK_{\text{NH}^+} = 7.9$), proton transfer is thermodynamically more uphill, since the proton is shielded by strong amine basicity. A larger structural rearrangement must occur prior to proton transfer, and therefore a *later* transition state is observed. Under these circumstances, the TS^\ddagger resembles more the product (*i.e.* the proton transfer > 50 %). With *N*-acetyl-L-lysine methyl ester ($pK_{\text{NH}^+} = 10.5$), the impact of the proton transfer on Kie is very small due to significant bond elongation occurring before the TS^\ddagger is reached (again because the TS^\ddagger is much later).

Kie have allowed us to confirm suppositions regarding general-base catalysis during the deacylation step of TGase brought on by the Brønsted results. These studies, however, do not provide any information regarding the identity of the general base. In order to unveil the number of residues involved in the enzymatic reaction as well as shed some light as to their identity, construction of a pH-rate profile of the TGase-catalyzed reaction was undertaken. The ensuing section discusses results of the pH-rate profile of the deacylation step.

Figure 23: Diagrammatic representation of the speculative degree of proton transfer realized at the transition state of the general-base catalyzed deacylation reaction in D₂O according to the relative acidity of the primary amine.



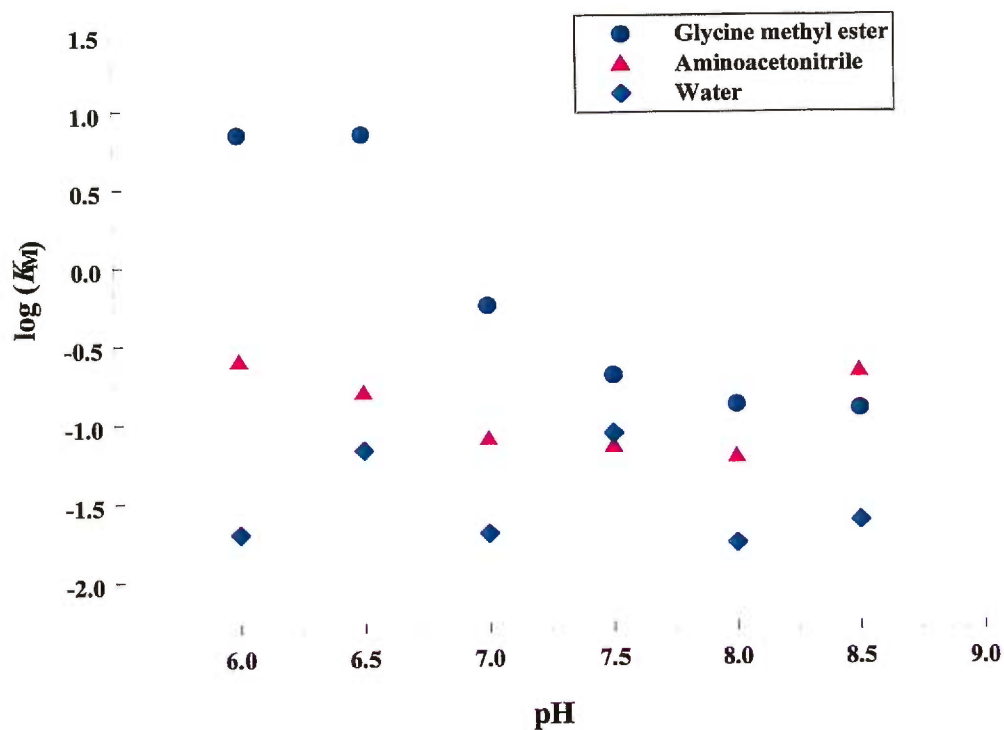
4.6: pH-RATE STUDIES

There are several reasons why rates may vary with pH. The two main competing reasons are that either the substrate must undergo an ionization in order to be an effective substrate, or that some catalytic group on the enzyme must exist in a given state of protonation for reaction to occur effectively (58). We are interested in the second case and careful examination of any pH-rate profile is necessary in order to ensure that the first case is not at the source of the observed pH-rate profile. Residues necessary for substrate binding may also show up if their state of protonation is critical for subsequent catalysis. Another cause of rate changes associated with pH may be an enzyme conformational change. These effects are usually only partial at best, and are generally ignored. Finally, the pK_a value of a given residue in the active site can vary tremendously according to its surrounding environment. Thus it is often a cumbersome task identifying specific residues based on the determination of the pK_a value from the pH-rate profile (59). Nonetheless, pH-rate studies can reveal information regarding the preferred ionization states of the enzyme's catalytic residues.

The pH-rate profiles for the TGase-catalyzed reaction with water, glycine methyl ester and aminoacetonitrile were obtained. The pH vs K_M plot for all three substrates is illustrated in **Figure 24** (page 90). There appears to be no pH effect on the availability of water in the active site as revealed by a fairly constant flux in K_M in the hydrolysis reaction. This would signify that little conformational change is occurring at the active site over the broad range in pH as to exclude water. A more interesting profile is observed in the case of the amines, where the ionization of a residue with an apparent pK_a of **6.5** influences the binding of the amine. More specifically, the deprotonation of this residue is associated with increased binding affinity of the amine. The effect is most pronounced for glycine methyl ester, with a 100-fold improvement in binding at pH's greater than 7.5. The logical explanation is that different binding affinities exist for the protonated and neutral forms of this amine. At low pH mainly the protonated amine species is present with a low binding affinity. At pH 7.0, a residue in the enzyme active site exists in its unprotonated form to assist in proton abstraction from the entering protonated amine. This generates the neutral amine which is better bound and consequently primed for nucleophilic attack. Thus there

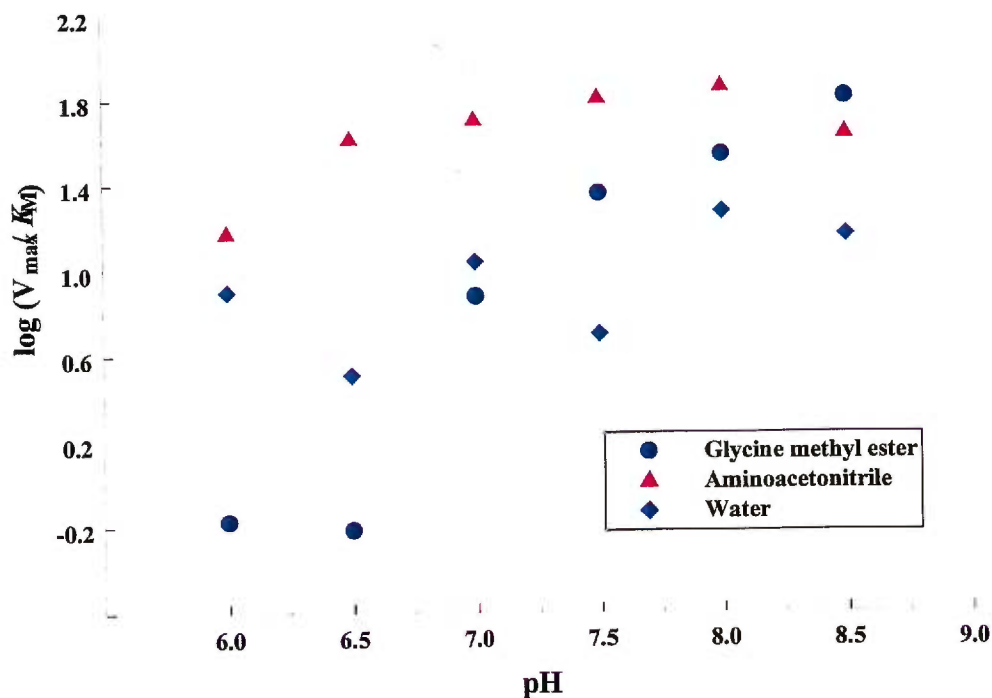
appears to be a binding-associated deprotonation event involving a residue in the active site. An explanation for the more pronounced effect with glycine methyl ester than with aminoacetonitrile is that the $pK_{\text{NH}_4^+}$ is 7.9 for the former compared to 5.6 for the latter, such that a significant amount of the protonated glycine methyl ester species exists at pH 6.5. Aminoacetonitrile, on the other hand, exists in its deprotonated state over the entire pH range studied. The possibility that the observed ionization is due to titration of the amine and not an active site residue seems fallible based on the fact that similar pH- K_M profiles are obtained for aminoacetonitrile and glycine methyl ester despite their different $pK_{\text{NH}_4^+}$ values.

Figure 24: The effect of pH on $\log(K_M)$, obtained according to Equations 3 and 4, for the TGase-catalyzed hydrolysis reaction, and the aminolysis reactions involving aminoacetonitrile and glycine methyl ester as primary amine nucleophiles.



The $\log(V_{\max}/K_M)$ vs pH profile for each substrate is depicted in **Figure 26** below. Again, the hydrolysis reaction is generally unaffected by variances in pH. The transamidation reaction, especially for glycine methyl ester, appears to increase dramatically over the pH range; however, it must be noted that this trend is mainly a consequence of increased binding affinity at high pH (as revealed by **Figure 24** on page 90) and not an increased efficiency in deacylation at higher pH (as revealed by **Figure 25** on page 91).

Figure 26: The effect of pH on $\log(V_{\max}/K_M)$, obtained according to Equations 3 and 4, for the TGase-catalyzed hydrolysis reaction and the aminolysis reactions involving aminoacetonitrile and glycine methyl ester as primary amine nucleophiles



In theory, the presence of a general base should be visualized in the form of an inflection point in the curve of pH vs $\log(V_{\max})$, as the ability of the base to abstract a proton (independent of any binding events) will be gravely impaired upon its protonation at lower pH. Several possibilities could serve to explain the relatively flat

slopes in **Figure 25**. Perhaps the inflection point exists at pH values either below pH 6.0 or above pH 8.5, such that we are observing a plateau. There appears to be a slight increase in velocity at the higher pH values, however a large degree of uncertainty results from high experimental error at this high a pH.

In general, these pH-rate studies have pointed out that substrate analogue **5**, while being excellent for studies at neutrality, is less practical at low and high pH values. At low pH levels there is a large decrease in sensitivity due to a very low concentration of the UV-active species *p*-nitrophenolate. At high pH there is excessive background hydrolysis (as high as 68 %, see **Table X** on page 132) of the observed enzymatic reaction rate. The high experimental error associated with kinetics conducted at these extremes in pH imposes certain limitations to the methodology developed herein for the study of the TGase catalyzed deacylation reaction. For these reasons, the application of this methodology should be limited to the pH range of 6.5 – 7.5 where all the factors involved in following the deacylation reaction are working optimally.

4.7: CONCLUSION

The methodology developed herein has made feasible the kinetic study of a specific step, the deacylation step, of the TGase-catalyzed reaction. We report the first *kinetic* evidence for the involvement of a general base as confirmed by the Brønsted and kinetic isotope effect studies. The identity of the general base, however, remains to be proven, as the pH-rate profile studies conducted incorporate a significant amount of experimental error and therefore must be classified as inconclusive in this regard. Site-directed mutagenesis experiments could prove useful in confirming the identity of the general base as His-334 in future experiments.

Conclusion

The results reported herein have advanced our understanding of the TGase-catalyzed deacylation reaction. The Brønsted experiment confirmed that nucleophilic attack by a primary amine on the thiolester acyl-enzyme intermediate occurs *via* a concerted mechanism in which a general base is positioned for prompt proton abstraction from the amine. These events ensure that the tetrahedral intermediate decomposes to yield free enzyme and the isopeptide reaction product. We are pleased to have successfully conducted this type of experiment, a first for the transglutaminases. Furthermore, this approach to a Brønsted analysis, involving a series of nucleophilic primary amines, is quite uncommon in the literature and thus far seen only for non-enzymatic studies. It is therefore exciting to be able to compare experimental results obtained from enzymatic and non-enzymatic models with regards to nucleophilic attack on a thiolester intermediate. The kinetic isotope effect studies, which we felt would provide solidarity between our hypothesis and results obtained from the Brønsted plot analysis, did indeed corroborate a general-base catalyzed deacylation step. In fact, this experiment developed into an engaging exercise in mechanistic interpretation, revealing that the transition state structure is dependent on the identity of the primary amine involved. The kinetic isotope effect results could certainly be refined in future research by conducting proton inventory experiments to elucidate the exact number of protons in flight during the rate-limiting step of deacylation, and strengthen the proposed Asp-His-Cys catalytic triad theory regarding the TGase mechanism (which would require at least two protons in flight). The kinetic methodology was tested over a broad range in pH values by conducting pH-rate profile studies, and it was discovered that the methodology was limited at the extremities in pH values studied due to excessive background hydrolysis and loss in sensitivity of detection. The methodology, however, remains rapid, sensitive and accurate at and around neutrality.

Finally, none of these results would have been possible were it not for a successful enzyme purification and substrate synthesis. An amelioration of 55 % in the yield and 28 % in specific activity are recorded as a result of our modifications to

previously published protocols for the purification of guinea pig liver TGase. The consequence of these results is improved enzyme purity which renders kinetic data more sensitive to the mechanistic events unique to the TGase. The lower the purity of the enzyme the more likely that other contaminating enzymes could interfere with kinetics through competitive substrate binding or even consumption of the substrate. The overall yield of substrate analogue **5** (*N*-Cbz-*L*-glutamyl(γ -*p*-nitrophenyl ester)glycine) was achieved with 25 – 38 % yield in comparison with the 9 % reported in literature. This was made possible through experimentation with new and different synthetic approaches to the substrate, initiated by a genuine interest in synthetic organic chemistry.

Appendices

Appendix A: Purification **Materials and Methods**

Materials:

Guinea pig livers were obtained fresh either from Rockland, Inc. (Gilbertsville, PA) or as a generous gift from Dr. S. Rowland of Merck Frosst (Pointe-Claire/Dorval, PQ). Ethylenediaminetetraacetic acid (EDTA), imidazole, sucrose and zinc sulfate were purchased from Aldrich. Hydroxylamine hydrochloride, trichloroacetic acid, and potassium chloride were obtained from Anachemia. Ferric chloride and acetic acid were obtained from BDH. Tris buffer, 250R Coomassie blue, Macro-Prep DEAE Support and Bio-Gel A-0.5m Gel were obtained from Bio-Rad. Salmine protamine sulfate (Grade X), ammonium sulfate (SigmaUltra grade), bovine serum albumin (BSA, Fraction V) and calcium chloride were purchased from Sigma. *N*-Cbz-L-GlnGly was synthesized in our laboratory according to pre-established procedures (18). All aqueous solutions were prepared using water purified with the Millipore BioCell system.

Methods:

A-1: PROTEIN CONCENTRATION

Concentrations of total protein were determined using the Bio-Rad D_C Protein Assay, a method based on the Lowry assay (60) (using BSA as a standard) at all stages of the purification, except for fractions obtained after size exclusion chromatography. For these fractions, TGase was considered to be of high purity, so that protein concentrations were determined using the extinction coefficient for TGase ($A_{280\text{ nm}}^{1\%} = 15.8$) (18). Color development for Lowry assays took place over 15 minutes, and absorbance values were measured using a Milton-Roy Spectronic 1201 spectrophotometer at $\lambda=740\text{ nm}$. Standard curves were performed daily.

A-2: TRANSGLUTAMINASE ACTIVITY

TGase activity was measured by the colorimetric hydroxamate assay procedure using 30 mM *N*-Cbz-L-GlnGly, 1 mM EDTA, 5 mM CaCl₂, and 0.1 M hydroxylamine in 0.2 M Tris-acetate at pH 6.0 and 37 °C (19). The activity assay solution was prepared fresh daily. One unit of enzyme activity (U) is defined as the amount of TGase required to catalyze the formation of 1 μmol of γ-glutamylhydroxamic acid per minute. Specific activity is given as units per mg of protein.

A-3: ENZYME PURIFICATION PROTOCOL

All purification steps were conducted at 4 °C or on ice, all solutions and buffers were prepared fresh daily, and all column chromatography was conducted using the Bio-Rad Econo Chromatography System.

STEP 1 - Preparation of liver supernatant solution: Guinea pig livers were obtained fresh (packed on ice) and immediately homogenized with a 0.25 M sucrose solution (2.2 mL/g liver) at 15 000 rpm for 1.5 min using a Polytron PT 3000 Homogenizer (Brinkmann Instruments). Portions of 50 g of liver were homogenized in a 5 × 15 cm glass cylinder. Homogenization must occur within 3 days of the animal sacrifice in order to obtain the highest activity. The homogenate was centrifuged at 105,000 × g for 1 hr (Beckman L-70; 45 Ti rotor), and the supernatant fraction was then filtered through eight layers of cheesecloth (Veratec). The filtered supernatant solution can be frozen and stored at -20 °C for many months without apparent loss in activity. The present purification was conducted on 140 g of liver, yielding 300 mL of homogenate and finally 190 mL of supernatant solution.

STEP 2 - Ion-exchange chromatography: Two fractions each of 95 mL of supernatant solution, corresponding to an equivalent of 70 g of liver, were pumped onto a 2.5 × 5 cm column of Macro-prep DEAE, in consecutive runs. The equilibrating buffer was 5 mM Tris-Cl, pH 7.5 containing 2 mM EDTA (buffer A). The gradient buffer was 5 mM Tris-Cl, pH 7.5 containing 2 mM EDTA and 1 M NaCl (buffer B).

At a flow rate of 5 mL/min the following elution program was initiated: a 75 mL wash of equilibrating buffer (buffer A) was passed through the column, 95 mL of supernatant solution was loaded, and a 550 mL gradient was applied. The gradient consisted of 100 mL equilibration with buffer A, 375 mL linear gradient from 0 to 100 % buffer B, and a 75 mL wash with 100 % B. The final stage of the chromatography elution profile was a 100 mL regeneration with buffer A. Fractions of 5 mL were collected over the 20 to 60 % buffer B gradient range. The enzyme rich fractions emerge from the column between 25 % and 45 % buffer B (see **Figure 9**, page 42).

STEP 3 - Protamine sulfate precipitation and extraction: Fractions with specific activities of over 2.0 U/mg from the two Macro-prep DEAE chromatography runs performed overnight were pooled. A 1 % protamine sulfate (w/v) solution was prepared fresh, allowed to completely dissolve, and 12 mL was added dropwise with gentle stirring over a 20 min period to the 90 mL pool. The precipitated enzyme was collected by centrifugation (Beckman L-70; 45 Ti rotor) at $14,600 \times g$ for 15 min. The resultant pellets were combined and washed with 10 mL of 0.2 M Tris-acetate buffer (pH 6.0), by homogenizing with the Polytron PT 3000 for 1 min at 3000 rpm. The suspensions were then centrifuged (Beckman GS-6R, GH-3.8 rotor) at $2500 \times g$ for 2 min, and the pellet was then transferred to a 2.2×8 cm glass cylinder to undergo extraction. Each extraction consisted of homogenization (with the Polytron at 4000 rpm) three times at 30 sec intervals with 1 min intermittent breaks for cooling on ice. An initial extraction with 10 mL of a fresh solution of 0.05 M ammonium sulfate in 5 mM Tris-Cl, pH 7.5, 2 mM EDTA (buffer A) was conducted. The homogenate was centrifuged (Beckman GS-6R) at $2500 \times g$ for 2 min to recover the precipitate. The TGase rich supernatant was stored at 4°C. The pellet was then extracted a second time in a similar fashion with 7 mL of the ammonium sulfate solution. A third extraction revealed that the enzyme was already completely recovered. The first two extracts, having specific activities greater than 8.0 U/mg, were pooled to give a final volume of 17 mL. The volume was reduced by centrifugation over a 30,000-molecular weight cutoff membrane (Amicon Centri-Prep 30 concentrators) at a maximum speed of 1500

× g, to a final volume corresponding to 1-5 % of the following size exclusion column volume. Several hours were required to reduce the volume to 3.3 mL.

STEP 4 - Size exclusion chromatography: The extract was loaded onto a 2.5 × 23 cm column (Bio-Gel A-0.5m, fine mesh) at a flow rate of 0.5 mL/min. The elution was conducted overnight using 10 mM Tris-acetate buffer, pH 6.0 containing 1 mM EDTA and 0.16 M KCl for 336 min. Fractions of 4 mL were collected between 67 and 246 min. The TGase emerges from the column after a half-column volume has eluted. All fractions relating to high protein concentrations on the chromatogram, judging by their absorbance at 280 nm, were tested for specific activity (see **Figure 10**, page 44). Fractions with high specific activities were pooled to give a final volume of 21 mL and a combined specific activity of 18.0 U/mg. The solution was then divided equally (1.05 mL aliquots) into 20 Eppendorf micro-centrifuge tubes and placed on dry ice/acetone for 5 min. These frozen solutions were then lyophilized for 6 hrs using a speed vac (Savant SC110) under vacuum at 4 °C (0.25 Torr), and stored at -20 °C.

A-4: ELECTROPHORESIS

Separation of proteins by sodium dodecylsulfate polyacrylamide gel electrophoresis (SDS-PAGE) was conducted using the Bio-Rad Mini-Protean II electrophoresis cell according to procedures of Laemmli (61) using pre-cast minigels (8 × 10 cm, Bio-Rad) prepared with 12 % Tris-HCl resolving gel, 4 % stacking gel, and 2.6% crosslinker concentrations. Protein bands were revealed using both 250R Coomassie blue and zinc (30) staining techniques. The pre-stained SDS-PAGE broad range molecular weight markers (Bio-Rad) used as standards included aprotinin ($M_r = 7,800$), lysozyme ($M_r = 18,900$), soybean trypsin inhibitor ($M_r = 28,500$), carbonic anhydrase ($M_r = 33,300$), ovalbumin ($M_r = 50,300$), bovine serum albumin ($M_r = 85,000$), β -galactosidase ($M_r = 123,000$) and myosin ($M_r = 213,000$).

A-5: ENZYME PURITY ANALYSIS

In order to determine the purity of TGase in the purified preparation, an electrophoresis gel imaging technique called Scion Image for Windows was employed (see Figure 12, page 47). A standard curve of varying quantities of BSA was established by loading 0.5, 1, 2.5, 5.0 and 7.5 μg of BSA onto five lanes of an SDS-PAGE gel. Two lanes were reserved for the final purified TGase solution which was loaded in both 5.0 and 7.5 μg quantities (see **Figure 12**, page 47). After electrophoresis, gels were developed using both standard Coomassie blue and zinc (30) staining techniques. Photographs were taken of the zinc stained gels, while the Coomassie blue stained gels were dried. The photographs and dried gels were scanned using a flatbed document scanner at 400 dpi resolution. The scanned images were then analyzed using the program Scion Image for Windows (distributed freely on the internet at http://www.scioncorp.com/pages/scion_image_windows.htm), which has extensive image analysis capabilities for one-dimensional electrophoretic gels (see **Figure 11**, page 46).

Appendix B: Synthesis Materials and Methods

Materials:

1-Hydroxybenzotriazole hydrate (HOBt), benzyl chloroformate, triethylamine, acetic anhydride, *p*-nitrophenyl chloroformate, trifluoroacetic acid, 1{3-(dimethylamino)-propyl}-3-ethylcarbodiimide (EDC), *p*-nitrophenol, tributyl tin hydride, acetyl chloride, potassium trimethylsilylate, formaldehyde, 4-dimethylaminopyridine and *p*-toluenesulfonic acid monohydrate were purchased from Aldrich. Glycine *tert*-butyl ester, L-glutamic acid hydrochloride and D-glutamic acid hydrochloride were obtained from Sigma. Sodium bicarbonate (NaHCO₃), sodium carbonate (Na₂CO₃), magnesium sulfate (MgSO₄) and sodium sulfate (NaSO₄) were purchased from Omega. Glycine allyl ester hydrochloride (**18**) was synthesized in this laboratory according to the procedure given on page 122.

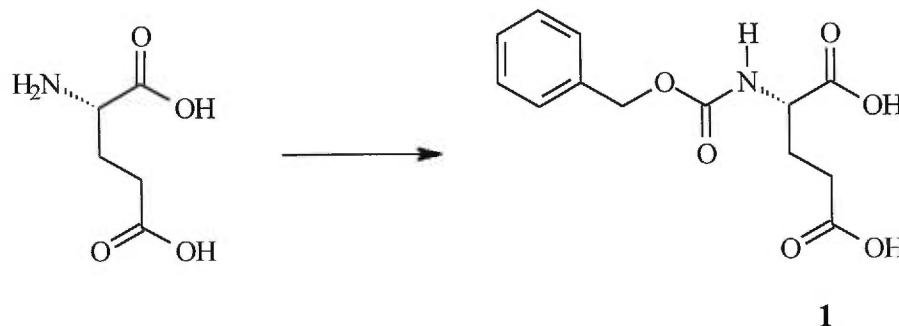
Methods:

B-1: General Aspects of Synthesis

Acetonitrile and dichloromethane were distilled from CaH₂; triethylamine was first distilled from ninhydrin and then from CaH₂; acetic anhydride was fractionally distilled over P₂O₅; HOBt was dried at 110 °C over toluene in a drying piston; *p*-nitrophenyl chloroformate was purchased from Aldrich and recrystallized from petroleum ether and hexanes prior to use. Flash column chromatography was performed on 230-400 mesh silica gel; TLC's were performed on aluminum-backed silica plates. Reported melting points are uncorrected. ¹H and ¹³C NMR experiments were recorded on a Bruker AMX300 (300 MHz) and a Bruker AMX400 (400 MHz) NMR spectrometer. The chemical shifts are reported in ppm (δ units) downfield of the internal tetramethylsilane ((CH₃)₄Si). Coupling constants are in Hz. The spectra were analyzed using WinNMR when necessary.

B-2: Synthesis of N-Cbz-L-Glutamyl(γ -p-Nitrophenyl Ester)Glycine Via L-Glutamic Acid Cyclic Anhydride Formation and Ring Opening with Glycine tert-Butyl Ester

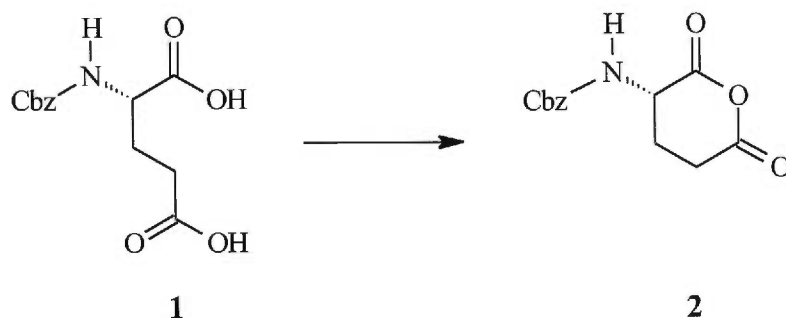
N-carbobenzyloxy-L-glutamic acid (**1**)



Sodium bicarbonate (57.8 g, 0.680 mol, 10 eq) was dissolved in 600 mL of water. L-Glutamic acid (15.0 g, 0.100 mol, 1.50 eq) was added, and the reaction mixture was stirred at -10 °C until completely dissolved. Benzyl chloroformate (9.63 mL, 0.068 mol, 1.00 eq) was added dropwise (0.5 mL/min), and the reaction was left stirring for 2 hrs at -10 °C followed by warming to ambient temperature. The reaction was complete after 24 hrs, at which point the aqueous phase was washed three times with ether (3 × 100 mL) and acidified to pH 1.0 with concentrated HCl. The precipitated product was extracted three times with 100 mL EtOAc. The extracts were pooled and washed once with water. The organic phase was dried over NaSO₄ and evaporated to give 17.8 g (93%) of *N*-Cbz-L-glutamic acid (**1**) as a white granular dense solid.

mp 119-120 °C (lit 120-121 °C) (*61b*).

¹H NMR (CD₃OD): δ = 1.89-1.98 (m, 1H); 2.15-2.24 (m, 1H); 2.42 (t, J = 7.72, H); 4.24 (q, J = 4.8, 1 H); 5.10 (s, 2H); 7.27-7.38 (m, 5H).

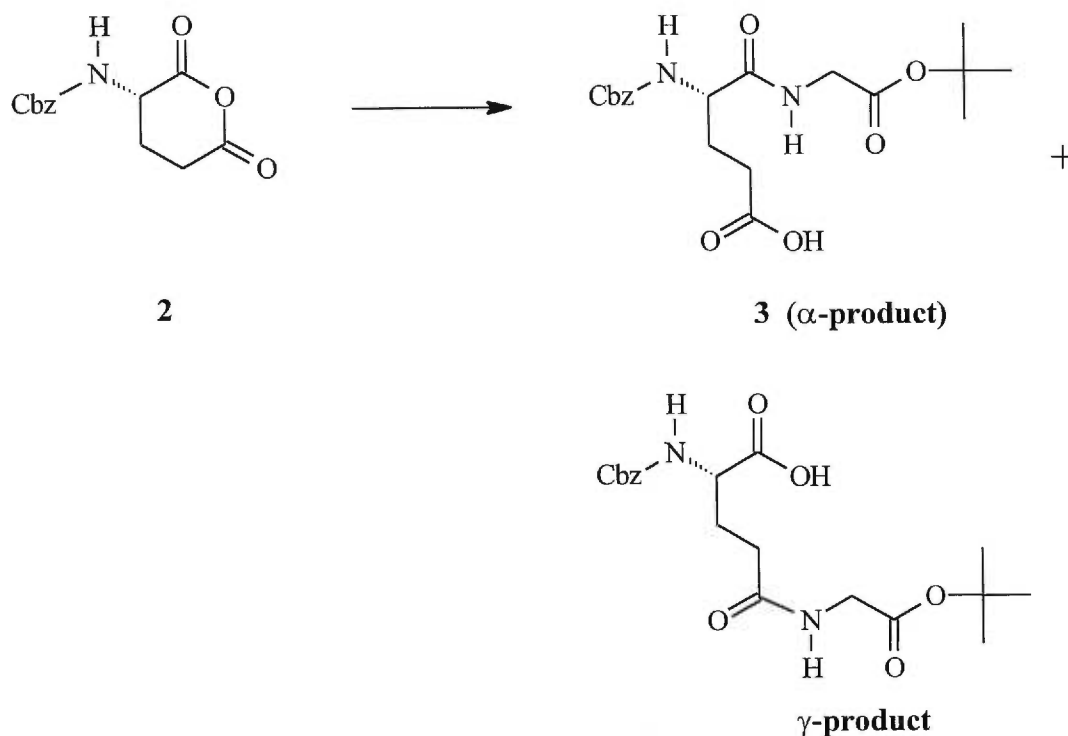
N-Cbz-*L*-glutamic acid cyclic anhydride (**2**)

N-Cbz-*L*-glutamic acid (**1**) (7.80 g, 28.0 mmol, 1 eq) was added to 60 mL of distilled acetic anhydride. The flask was fitted with a reflux condenser and the reaction mixture was warmed very slowly to 55 °C. After 10 min at 55 °C (complete dissolution of *N*-Cbz-*L*-glutamic acid), the reaction was complete. The byproducts, acetic acid and unreacted acetic anhydride, were removed by evaporation with a rotovap fitted to a vacuum pump, with heating at a temperature below 55 °C. Excessive heating during evaporation is undesirable due to degradation of **2**. Evaporation gave **2** as an oily residue. The product was recrystallized in 150 mL ether with a small quantity of EtOAc to help dissolve the product, and then left at – 20 °C overnight. The product was collected by filtration and dried *in vacuo* for several hours, to afford 5.63 g (76 %) of small shiny white needles.

mp 91 °C (lit 93 – 94 °C)(62)

¹H NMR (CDCl₃): δ = 1.91 (dd, *J* = 13.2, 5.7, 1H); 1.97 (dd, *J* = 18.3, 10.7, 1H); 2.47 (t, *J* = 6.8, 1H); 2.84-3.08 (m, 2H); 4.47 (t, *J* = 6.5, 1H); 5.14 (s, 2H); 5.62 (br s, 1H); 7.37 (s, 5H).

¹³C NMR (CDCl₃): δ = 23.3, 29.5, 51.0, 67.4, 128.1, 128.3, 128.5, 135.6, 155.7, 164.7, 166.6.

N-Cbz-*L*-glutamylglycine *tert*-butyl ester (**3**)

N-Cbz-*L*-glutamic acid cyclic anhydride (**2**) (1.00 g, 3.80 mmol, 1 eq) was dissolved in 40 mL of distilled DCM along with triethylamine (53.0 μ L, 3.80 mmol, 1 eq) and glycine *tert*-butyl ester hydrochloride (0.637 g, 3.80 mmol, 1 eq). The reaction mixture was stirred at room temperature for 30 min under nitrogen. Flash column chromatography with a gradient of 40 % - 60 % ethyl acetate/1 % AcOH/ hexanes yielded the α -isomer, which is known to have a higher R_f than the γ -isomer (1:1 EtOAc/DCM) (44). Elution of γ -isomer required 95 % EtOAc/4.0 % MeOH/1 % AcOH. The isomers were recrystallized from CHCl_3 and Et_2O , to provide white powders consisting of 0.66 g of the α -isomer and 0.72 g of the γ -isomer. The overall yield for the reaction was 92 % at a mixture ratio of 1.1:1 (α : γ).

α -isomer

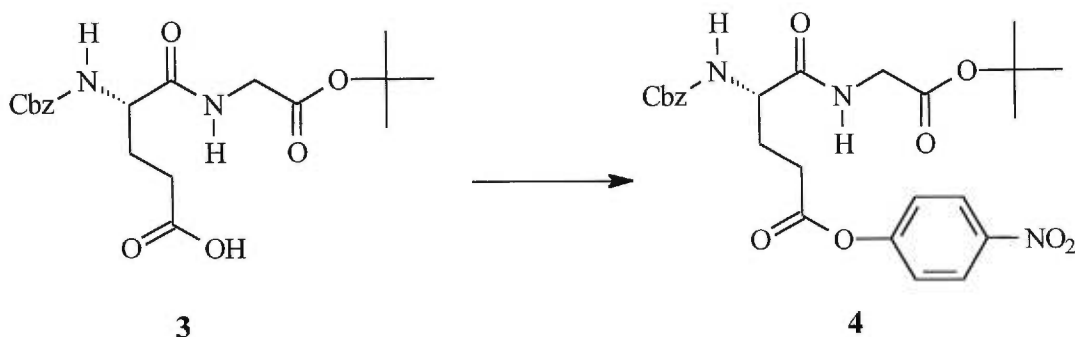
^1H NMR (CDCl_3): $\delta = 1.45$ (s, 9H); 1.92-2.08 (m, 1H); 2.12-2.17 (m, 1H); 2.42-2.58 (m, 2H); 3.88 (dd, $J = 5.1, 17.7$, 1H); 3.96 (dd, $J = 5.2, 18.4$, 1H); 4.46 (d, $J = 5.9$, 1H); 5.10 (s, 2H); **5.91** (d, $J = 8.5$, 1H, NH_{Glu}); 7.33 (s, 5H).

^{13}C NMR (CDCl_3): $\delta = 27.9, 28.0, 42.0, 45.7, 53.6, 67.1, 82.4, 127.9, 128.1, 128.4, 135.9, 156.4, 168.7, 171.7, 176.3$.

 γ -isomer

^1H NMR (CDCl_3): $\delta = \delta = 1.44$ (s, 9H); 1.89-2.06 (m, 1H); 2.12-2.17 (m, 1H); 2.40-2.51 (m, 2H); 3.84 (dd, $J = 5.1, 17.7$, 1H); 3.91 (dd, $J = 5.2, 18.4$, 1H); 4.36 (d, $J = 5.9$, 1H); 5.12 (s, 2H); **6.92** (d, $J = 8.2$, 1H, NH_{Glu}); 7.30 (s, 5H).

N-Cbz-*L*-glutamyl(γ -*p*-nitrophenyl ester)glycine tert-butyl ester (**4**)

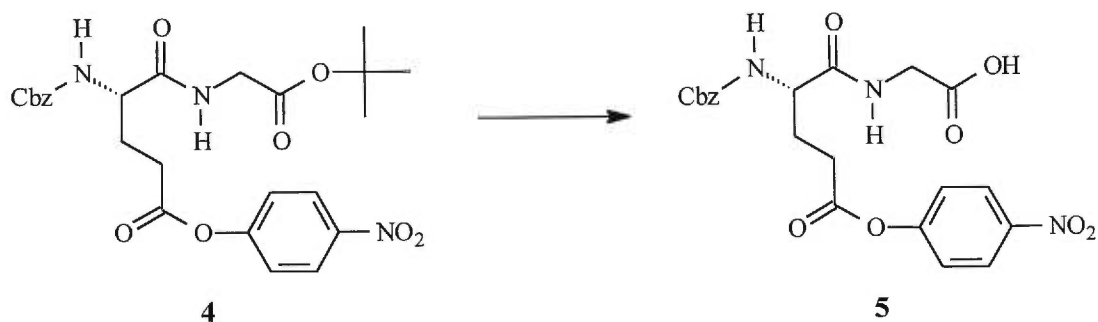


The α -isomer **3** (1.00 g, 2.53 mmol, 1 eq) was dissolved in DCM, and triethylamine (390 μ l, 2.78 mmol, 1.1 eq) was added. The solution was then cooled to 0 °C. DMAP (31 mg, 10 mol %) was added to the solution and the reactive intermediate was allowed to form over a 20 minute period, at which point *p*-nitrophenyl chloroformate (562 mg, 2.78 mmol, 1.1 eq) was added. The reaction, kept under nitrogen, was complete after 20 min by TLC analysis. The solvent was evaporated and the product redissolved in CHCl_3 . A solution of 25 % saturated NaHCO_3 was used to successively wash the organic phase (approximately 10 washes) until the aqueous phase did not acquire a yellow colour after washing of the organic phase. The organic phase was dried over MgSO_4 and evaporated to yield an oily residue. The product was recrystallized by dissolving in a minimum of Et_2O (with mild heating) followed by addition of hexanes. It is necessary to scratch the flask with a glass rod to initiate crystallization. The flask was left at -20 °C overnight. The product (**4**) was collected by successive filtration in a yielded 1.0 g (77 %); mp = 55 – 57 °C.

^1H NMR (CDCl_3): δ = 1.47 (s, 9H); 2.03-2.12 (m, 1H); 2.28-2.36 (m, 1H); 2.70-2.87 (m, 2H); 3.91 (dd, J = 5.1, 18.2, 1H); 3.99 (dd, J = 5.5, 18.3, 1H); 4.43 (d, J = 4.8, 1H); 5.12 (td, J = 12.2, 7.8, 2H); 5.62 (d, J = 7.8, 1H); 6.55 (br s, 1H); 7.26-7.34 (m, 2H), 7.36 (s, 5H); 8.22-8.26 (m, 2H).

^{13}C NMR (CDCl_3): δ = 27.9, 28.0, 30.2, 41.9, 53.5, 67.2, 82.5, 122.4, 125.1, 128.0, 128.2, 128.5, 135.8, 145.3, 155.1, 156.1, 168.4, 170.7, 170.9.

N-Cbz-*L*-glutamyl(γ -*p*-nitrophenyl ester)glycine (**5**)



To *N*-Cbz-*L*-glu(γ -*p*-nitrophenyl ester)gly *tert*-butyl ester (**4**) (0.810 g, 1.57 mmol, 1 eq) was added 8 mL of 99 % TFA and 1 mL of DCM. The reaction mixture was stirred at 0 °C for 4 hrs. The solvents were evaporated, and the oily residue was redissolved several times in CHCl₃ to remove all traces of TFA. *N*-Cbz-*L*-glu(γ -*p*-nitrophenyl ester)gly (**5**) was obtained as a flaky light beige solid (0.78 g, 95 % yield).

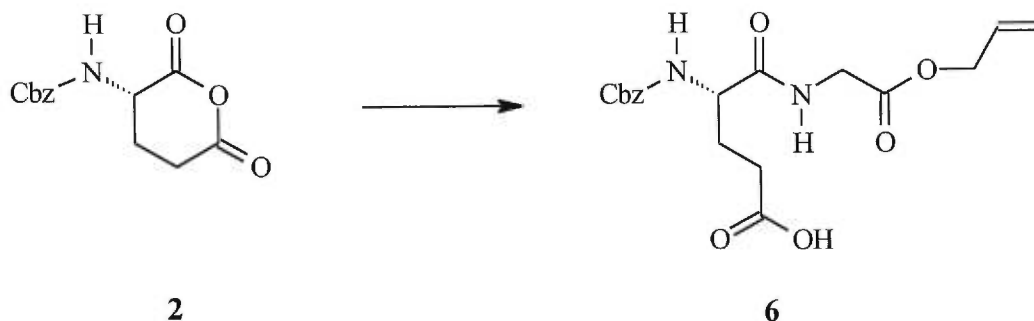
mp: 137°C (lit. 139°C) (18)

¹H NMR (CD₃OD): δ = 2.01-2.11 (m, 1H); 2.25-2.33 (m, 1H); 2.77-2.81 (m, 2H); 3.85-4.03 (m, 2H); 4.32-4.38 (m, 1H); 5.06-5.18 (m, 2H); 6.55 (s, 1H); 7.27-7.37 (m, 6H), 8.26 (d, J = 9.0, 2H); 8.37-8.40 (m, 1H).

¹³C NMR (CD₃OD): δ = 27.9, 28.2, 53.5, 67.8, 82.5, 123.9, 126.0, 128.9, 129.0, 129.4, 135.8, 145.3, 155.1, 156.1, 168.4, 170.7, 170.9.

B-3: Synthesis of *N*-Cbz-*L*-Glutamyl(γ -*p*-Nitrophenyl Ester)Glycine Via the *N*-Cbz-*L*-Glutamic Acid Cyclic Anhydride Formation and Ring Opening with Glycine Allyl Ester

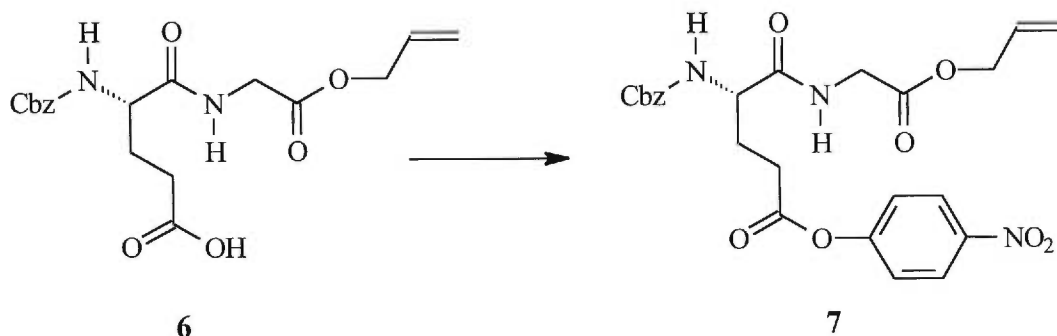
N-Cbz-*L*-glutamylglycine allyl ester (**6**)



The starting material (*N*-Cbz-*L*-glutamic acid anhydride) was obtained from procedures described in **Appendix B-2** (page 103). *N*-Cbz-*L*-glutamic acid anhydride (**2**) (2.63 g, 10.0 mmol, 1.05 eq), glycine allyl ester hydrochloride (1.44 g, 9.50 mmol, 1 eq) and triethylamine (1.32 mL, 9.50 mmol, 1 eq) were dissolved in 60 mL of distilled DCM, and reaction mixture was stirred at ambient temperature for 45 minutes under nitrogen. The two isomers, generated due to competing nucleophilic attack on the α and γ -carbonyl of the cyclic anhydride, were separated by flash column chromatography (18 \times 5 cm, elution with 0 % - 15 % ethyl acetate in DCM and 0.2 % acetic acid). The α -isomer (**6**) was recovered as a white powder (1.45 g, 40 %) by recrystallizing from CHCl_3 and hexanes. The ratio of α : γ was 1.1:1, and the overall yield of the reaction was 96 %. mp = 97 – 98 $^\circ\text{C}$

$^1\text{H NMR}$ (CD_3OD): δ = 1.93-1.97 (m, 1H); 2.04-2.15 (m, 1H); 2.40-2.55 (m, 2H); 3.98 (dd, J = 5.0, 18.1, 1H); 4.11 (dd, J = 5.3, 17.3, 1H); 4.42 (d, J = 5.7, 1H); 4.61 (d, 2 H, J = 5.8); 5.12 (td, J = 5.0, 18.1, 2H); 5.62 (d, J = 5.0, 18.1, 1H); 6.55 (s, 1H); 7.35 (s, 5H).

N-Cbz-*L*-glutamyl(γ -*p*-nitrophenyl ester)glycine allyl ester (**7**)

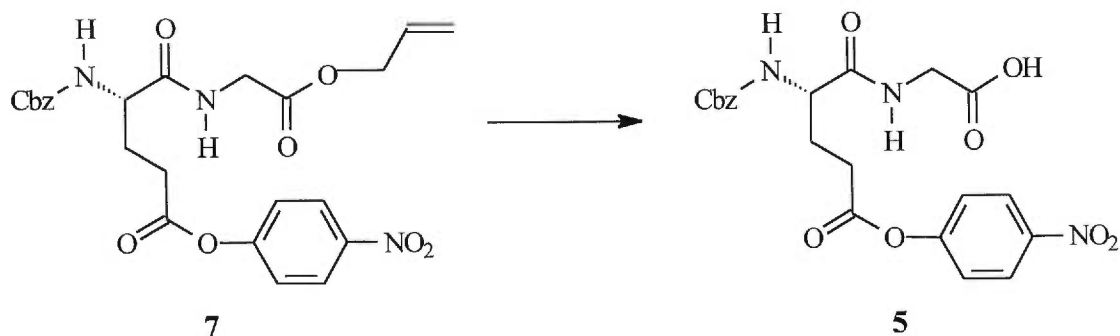


The *N*-Cbz-*L*-glutamylglycine allyl ester (**6**) (0.500 g, 1.32 mmol, 1 eq) was dissolved in 30 mL of distilled DCM. Then EDC-methiodide (0.470 g, 1.58 mmol, 1.2 eq), HOBT (0.180 g, 1.32 mmol, 1 eq) and *p*-nitrophenol (0.220 g, 1.58 mmol, 1.2 eq) were all added and the reaction mixture was stirred at r.t. overnight under nitrogen. After 24 hrs, the reaction was washed with water (5 × 10 mL), until the organic phase was clear and yellow. During each wash, small volumes of saturated NaCl solution were added to aid in phase separation. The product (**7**) was purified by flash column chromatography (2 × 15 cm, 20 – 50 % EtOAc/Hexanes) to remove contaminating *p*-nitrophenol. Evaporation and drying *in vacuo* yielded 550 mg (83 %) of a pure white powder.

mp = 116 – 117 °C

¹H NMR (CDCl₃): δ = 1.92-1.99 (m, 1H); 2.09-2.17 (m, 1H); 2.42-2.58 (m, 2H); 3.98 (dd, *J* = 5.0, 18.1, 1H); 4.11 (dd, *J* = 5.3, 17.3, 1H); 4.42 (d, *J* = 5.7, 1H); 4.61 (d, 2 H, *J* = 5.8); 5.12 (td, 2H, *J* = 5.0, 18.1,); 5.25 (dd, 1 H, *J* = 10.4, 1.1); 5.32 (dd, 1 H, *J* = 17.1, 1.4); 5.88 (ddt, 1 H, *J* = 17.1, 5.6, 5.9); 6.55 (d, 1H, *J* = 8.1); 7.28 (m, 2H), 7.35 (s, 5H); 8.24 (m, 2H).

N-Cbz-*L*-glutamyl(γ -*p*-nitrophenyl ester)glycine (**5**)



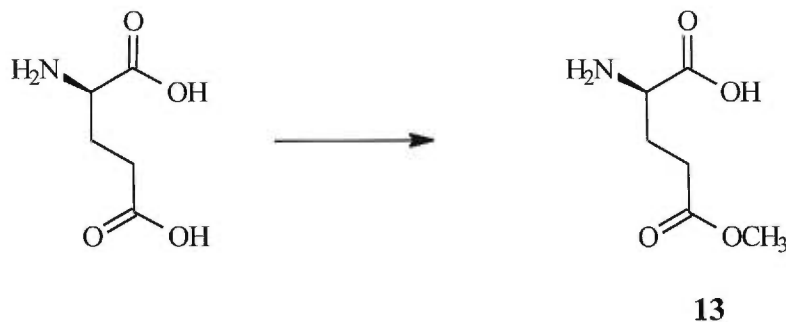
The *N*-Cbz-*L*-Glu(γ -*p*-nitrophenyl ester)Gly (**7**) (0.660 g, 1.32 mmol, 1 eq) was dissolved in 10 mL of DCM (solution A). In a separate flask, 2 mL of distilled and degassed DCM was used to dissolve the tributyltin hydride (2.13 mL, 7.92 mmol, 6 eq) and 1 mol % of palladium catalyst (Pd(PPh₃)₂Cl₂, 10.0 mg) (solution B). All manipulations were conducted under nitrogen. The catalyst (solution B) was added dropwise to solution A. After 15 min the reaction was over by TLC analysis and the solvent was evaporated. The residue was redissolved in ACN and 5 eq (0.400 mL) of acetic acid were added to hydrolyse the resultant tributyltin ester. Several extractions with hexanes were needed to remove palladium and tin byproducts. The pooled hexane fractions were extracted once with ACN to recover any product. The organic phase was pooled and evaporated. Flash column chromatography (15 × 2 cm, a gradient of 30 - 50 % EtOAc/5 % MeOH/Hexanes was used for elution) was conducted to obtain purified **5**. The oily residue was crystallized using EtOH:Et₂O to yield a light beige solid (0.500 g, 83 %). mp = 137 °C (lit. 140 °C) (**8**)

¹H NMR: δ = 1.92-1.99 (m, 1H); 2.09-2.17 (m, 1H); 2.42-2.58 (m, 2H); 3.98 (dd, J = 5.0, 18.1, 1H); 4.11 (dd, J = 5.3, 17.3, 1H); 4.42 (d, J = 5.7, 1H); 5.12 (td, J = 5.0, 18.1, 2H); 6.55 (s, 1H); 7.28 (m, 2H), 7.35 (s, 5H); 8.24 (m, 2H).

¹³C NMR (CD₃OD): δ = 27.9, 28.2, 53.5, 67.8, 82.5, 123.9, 126.0, 128.9, 129.0, 129.4, 135.8, 145.3, 155.1, 156.1, 168.4, 170.7, 170.9.

B-4: Synthesis of N-Cbz-D-Glutamyl(γ -p-Nitrophenyl Ester)Glycine Via a Complete and Sequential Protection/Deprotection Synthesis

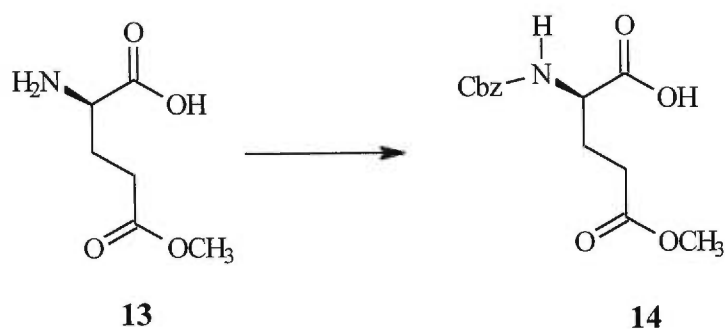
D-glutamic acid γ -methyl ester (**13**)



Acetyl chloride (2.00 mL, 28.0 mmol, 1.08 eq) was added slowly to 25 mL of methanol under agitation, and the solution was cooled in an ice bath. *D*-glutamic acid (3.68 g, 26.0 mmol, 1 eq) was added in small portions. The reaction mixture was stirred for 24 hrs, and then a 2.5 mL portion of pyridine (10 % volume of methanol) was added to the reaction mixture and the reaction mixture was stirred for an additional 48 hrs. The product was recovered by filtration and washed with EtOAc (1 \times 10 mL), Et₂O (1 \times 10 mL) and dried over P₂O₅ at 50 °C. A total of 2.2 g of *D*-glutamic acid γ -methyl ester (**13**), a white powder, was recovered providing an overall yield of 48%.

mp = 170 – 172 °C

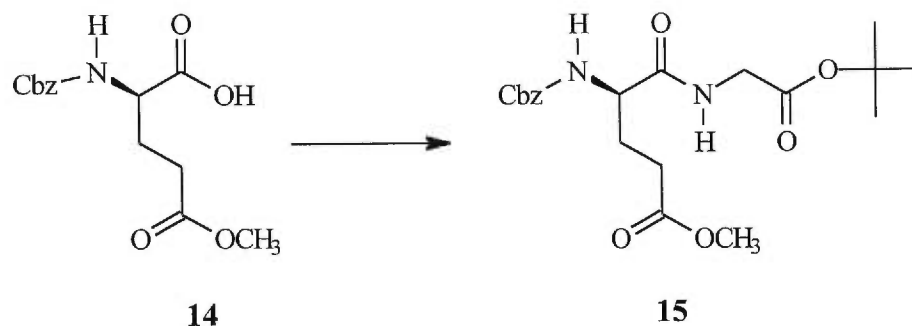
¹H NMR (D₂O): δ = 2.13-2.17 (m, 2 H); 2.53- 2.58 (m, 2 H); 3.69 (s, 3 H); 3.76 (dd, 1 H, J = 6.4,).

N-benzyloxycarbonyl-*D*-glutamic acid γ -methyl ester (**14**)

Cbz protection of the amino group was effected as previously described in **Appendix B-2** (page 103); *D*-glutamic acid γ -methyl ester (**13**) (3.00 g, 18.6 mmol, 1 eq), NaHCO₃ (18.8 g, 0.223 mol, 12 eq), benzyl chloroformate (2.65 mL, 18.6 mmol, 1 eq). Evaporation and drying *in vacuo* overnight gave 5.04 g (92 %) of *N*-Cbz-*D*-glutamic acid γ -methyl ester (**14**) as a white granular solid.

mp: 65 °C

¹H NMR (CD₃OD): δ = 1.89-1.98 (m, 1H); 2.15-2.24 (m, 1H); 2.44 (t, J = 7.7, 2H); 3.65 (s, 3H); 4.24 (q, J = 5.0, 1H); 5.10 (s, 2H); 7.27-7.38 (m, 5H).

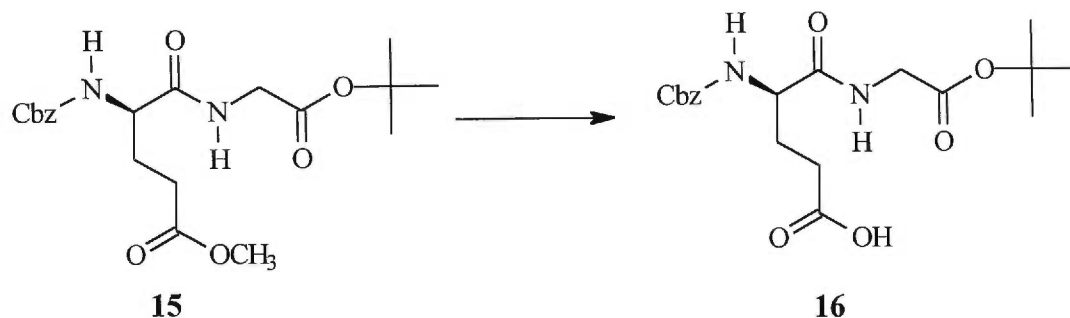
N-Cbz-*D*-glutamyl(γ -methyl ester)glycine *tert*-butyl ester (**15**)

To 40 mL of distilled DCM was added *N*-Cbz-*D*-glutamic acid γ -methyl ester (**14**) (1.27 g, 4.30 mmol, 1.2 eq), dry HOBt (0.58 g, 4.30 mmol, 1.2 eq), and EDC-methiodide (1.28 g, 4.30 mmol, 1.2 eq). The reaction mixture was cooled to 0 °C, and the coupling reaction was initiated by the addition of glycine *tert*-butyl ester hydrochloride (0.600 g, 3.60 mmol, 1 eq) and triethylamine (0.500 mL, 3.60 mmol, 1 eq). The reaction mixture was stirred for 20 hrs at 4 °C under nitrogen. The reaction mixture was washed several times with water, dried over NaSO₄, and evaporated to give **15** as an oily residue. The product was purified by flash column chromatography (15 × 3 cm, gradient of 5 %- 60 % EtOAc in hexanes) to yield 1.2 g (80 %) of *N*-Cbz-*D*-Glu(γ -methyl ester)Gly *tert*-butyl ester (**15**) as a whitish powder.

mp: 66 – 67 °C

¹H NMR (CDCl₃): δ = 1.93-2.20 (m, 2H); 2.38-2.51 (m, 1H); 2.44 (t, J = 7, 2H.); 3.64 (s, 3H); 4.23 (q, J = 5.0, 1H); 5.10 (s, 2H); 5.85 (d, J = 7.64, 1H); 7.22-7.37 (m, 5H).

¹³C NMR (CDCl₃): δ = 27.8, 30.0, 41.8, 51.6, 53.9, 66.8, 82.0, 127.8, 127.9, 128.3, 136.1, 156.1, 168.5, 171.4, 173.5.

N-Cbz-*D*-glutamylglycine *tert*-butyl ester (**16**)

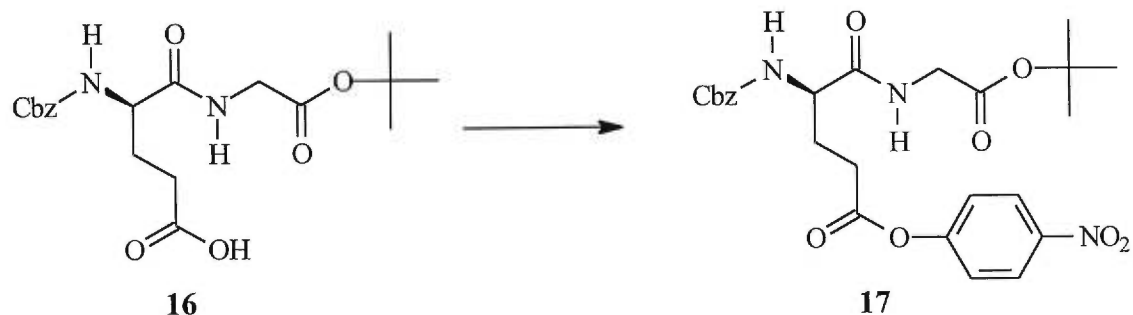
In 50 mL of dry EtO₂ was added *N*-Cbz-*D*-Glu(γ -methyl ester)Gly *tert*-butyl ester (**15**) (1.80 g, 4.34 mmol, 1 eq) and potassium trimethyl silanolate (KOSi(CH₃)₃) (0.28 g, 8.70 mmol, 1.5 eq). The solution turned yellow during the first minutes of the reaction, and an insoluble material (K⁺OMe⁻) soon formed. After 2 hrs another 1 eq of KOSi(CH₃)₃ was added to drive the reaction to completion, which took an additional 2 hrs. To the reaction mixture was added 20 mL of H₂O (in order to dissolve the precipitate). The solution was cooled to 0 °C and solid citric acid (2.25 g, 2.5 eq) was added slowly. The aqueous phase was then extracted with Et₂O (8 × 10 mL), until no more product was visible by TLC in the aqueous phase. The pooled Et₂O fractions were dried over NaSO₄ and evaporation yielded 1.46 g of **16** (85 % yield) as a white powder.

mp = 101 – 103 °C

¹H NMR (CDCl₃): δ = 1.42 (s, 9H); 1.90-2.01 (m, 1H); 2.10-2.12 (m, 1H); 2.41-2.55 (m, 2H); 3.87 (dd, J = 5.1, 17.7, 1H); 3.91 (dd, J = 5.2, 18.4, 1H); 4.40 (d, J = 5.9, 1H); 5.10 (s, 2H); 5.91 (d, J = 8.5, 1H); 7.22-7.39 (m, 5H).

¹³C NMR (CDCl₃): δ = 27.9, 28.0, 42.0, 45.7, 53.6, 67.1, 82.4, 127.9, 128.1, 128.4, 135.9, 156.4, 168.7, 171.7, 176.3.

N-Cbz-*D*-glutamyl(γ -*p*-nitrophenyl ester)glycine *tert*-butyl ester (**17**)



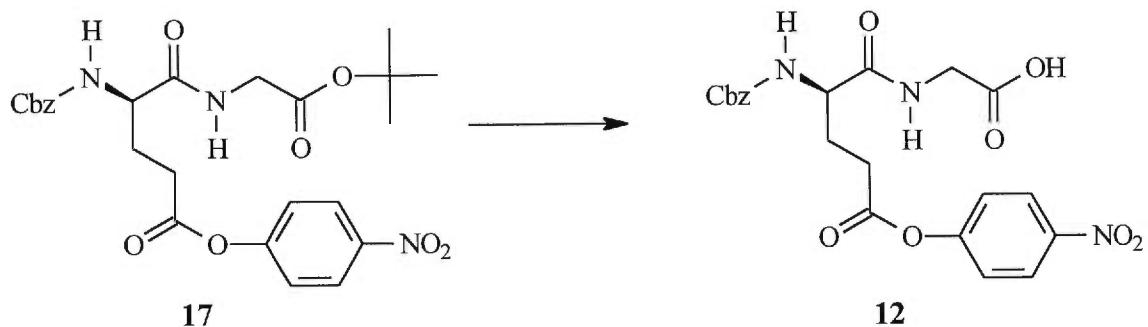
The *p*-nitrophenol coupling was afforded by the procedure described in **Appendix B-3** (page 110). *N*-Cbz-*D*-GluGly *tert*-butyl ester (0.635 g, 1.61 mmol, 1 eq), EDC-methiodide (0.574 g, 1.93 mmol, 1.2 eq), HOBT (0.22 g, 1.61 mmol, 1 eq) and *p*-nitrophenol (0.235 g, 1.69 mmol, 1.05 eq) were reacted to yield a 0.7 g of a white powder (**17**) after recrystallization with Et₂O/hexanes, to give an overall yield of 85 %.

mp = 55 – 57 °C

¹H NMR (CDCl₃): δ = 1.44 (s, 9H); 2.00-2.10 (m, 1H); 2.31-2.39 (m, 1H); 2.69-2.83 (m, 2H); 3.90 (dd, *J* = 5.2, 18.2, 1H); 3.97 (dd, *J* = 5.5, 18.4, 1H); 4.40 (d, *J* = 4.8, 1H); 5.12 (td, *J* = 12.2, 7.8, 2H); 5.66 (d, *J* = 7.8, 1H); 6.51 (br s, 1H); 7.22-7.32 (m, 2H), 7.38 (s, 5H); 8.21-8.25 (m, 2H).

¹³C NMR (CDCl₃): δ = 27.9, 28.0, 30.2, 42.1, 53.5, 67.2, 82.5, 122.2, 125.1, 128.0, 128.2, 128.4, 135.8, 144.9, 155.1, 156.2, 168.2, 170.5, 170.7.

N-Cbz-*D*-glutamyl(γ -*p*-nitrophenyl ester)glycine (**12**)



The *t*-butyl deprotection was afforded by the procedure described in **Appendix B-2** (page 108). *N*-Cbz-*D*-Glu(γ -*p*-nitrophenyl ester)Gly *tert*-butyl ester (**17**) (0.300 g, 0.580 mmol, 1 eq) was added 4 mL of 99 % trifluoroacetic acid (TFA) and 0.5 mL of DCM, to yield a white flaky solid (0.253 g) in 95 % yield.

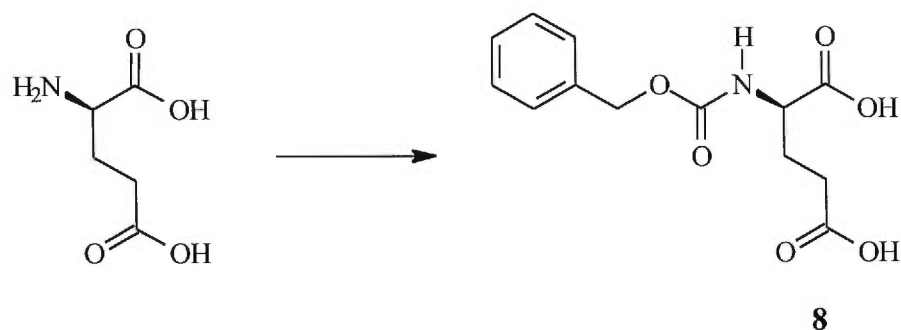
mp = 139 – 142 °C (lit. = 140 °C)(8)

¹H NMR (CD₃OD): δ = 2.01-2.11 (m, 1H); 2.25-2.33 (m, 1H); 2.77-2.81 (m, 2H); 3.85-4.03 (m, 2H); 4.32-4.38 (m, 1H); 5.06-5.18 (m, 2H); 7.27-7.37 (m, 6H), 8.26 (d, *J* = 9.0, 2H); 8.37-8.40 (m, 1H).

¹³C NMR (CD₃OD): δ = 27.9, 28.2, 53.5, 67.8, 82.5, 123.9, 126.0, 128.9, 129.0, 129.4, 135.8, 145.3, 155.1, 156.1, 168.4, 170.7, 170.9.

B-5: Synthesis of N-Cbz-D-Glutamyl(γ -p-Nitrophenyl Ester)Glycine Via Formation of the 5-Oxazolidinone Derivative

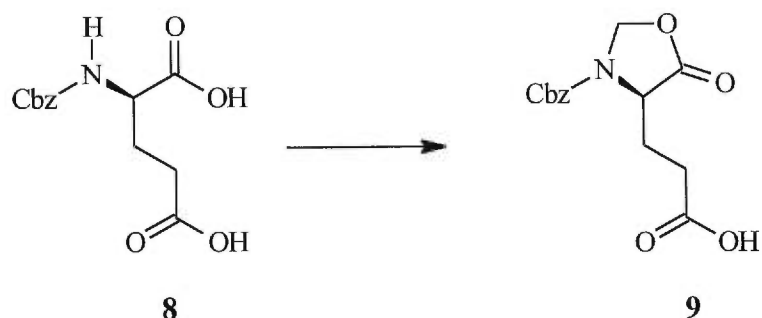
N-Cbz-*D*-glutamic acid (**8**)



Cbz protection of the amino group was effected as previously described in **Appendix B-2** (page 103) . *D*-glutamic acid (1.41 g, 9.58 mmol, 1 eq), NaHCO₃ (9.7 g, 0.115 mol, 12 eq), benzyl chloroformate (2.04 mL, 14.4 mmol, 1.5 eq). Evaporation yielded **8** as a white flaky solid (2.43 g, 90 %).

mp = 119 – 120 °C

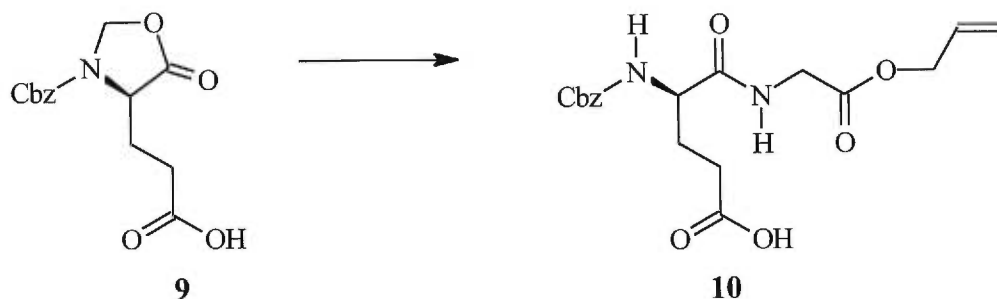
¹H NMR (CD₃OD): δ = 1.89-1.98 (m, 1H); 2.15-2.24 (m, 1H); 2.44 (t, J = 7.7, 2H); 4.24 (q, J = 5.0, 1H); 5.10 (s, 2H); 6.50 (d, J = 8.1, 1H); 7.27-7.38 (m, 5H).

N-Cbz-5-oxo-4-oxazolidinepropanoic acid (**9**)

To 60 mL of toluene was added **8** (2.0 g, 7.1 mmol, 1 eq), formaldehyde (10.5 mL, 0.142 mol, 20 eq) and *p*-toluenesulfonic acid hydrate (0.35 g, 1.8 mmol, 0.25 eq). A reflux apparatus fitted with a Dean-Stark condenser was used to bring the solution to reflux and remove water. After 1 hr the reaction was stopped, and it must be noted that longer reaction times than 1 hr result in product degradation. The toluene was then extracted with 5 % NaHCO₃ solution (4 × 20 mL). The aqueous phase (the pooled NaHCO₃ extracts) was acidified to pH 1.0 with 0.1 N HCl, and extracted with EtOAc (4 × 15 mL). The organic phase was then dried over NaSO₄ yielding **9** (1.93 g, 94 %) as an oily residue. A solid was never obtained even after storage in a minimum amount of EtOAc at – 20 °C overnight, as directed in the literature procedure (40). Other solvent systems also proved unsuccessful for precipitating or crystallizing the product.

¹H NMR (CDCl₃): δ = 2.13-2.30 (m, 2H); 2.46 (s, 2H); 4.37 (dd, *J* = 5.86, 5.80, 1H); 5.15 (s, 2H); 5.22 (d, *J* = 4.30, 1H); 5.47 (br s, 1H); 7.32 (s, 5H).

¹³C NMR (CDCl₃): δ = 25.6, 29.0, 53.8, 60.4, 68.0, 77.8, 128.2, 128.5, 135.2, 153.1, 171.7, 172.5.

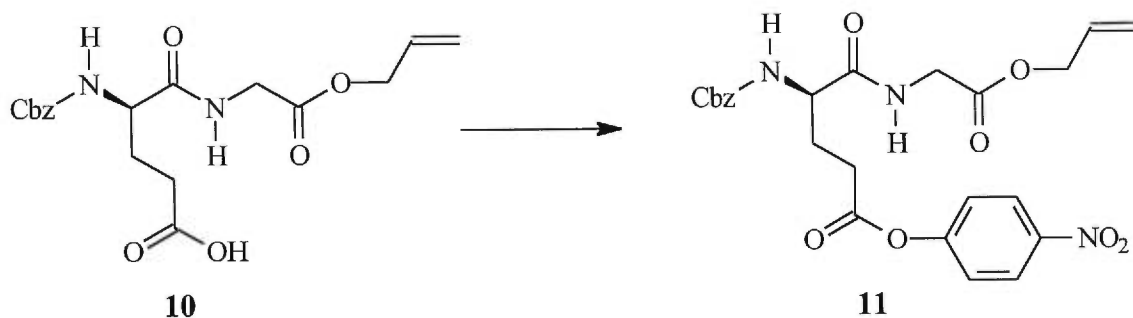
N-Cbz-*D*-glutamylglycine allyl ester (**10**)

The oxazolidinone derivative of *N*-Cbz-*D*-glutamic acid (**9**) (1.10 g, 3.73 mmol, 1 eq) was dissolved in 2 mL of ACN. Once dissolved, 2 mL of water was added to generate a 1:1 mixture of acetonitrile:water (solution A). In a separate flask, allyl glycine hydrochloride (3 g, 19.5 mmol, 5.2 eq) was added to 2 mL of water and triethylamine (2.7 mL, 19.5 mmol, 5.2 eq) was added slowly, causing the compound to completely dissolve (solution B). Solution B was transferred to solution A and reaction mixture was stirred for 24 hrs at ambient temperature under nitrogen. The solution was initially clear, but a white suspension was observed at the end of the reaction. The reaction was complete after 24 hrs by TLC analysis. The organic solvent was evaporated and 20 mL of 0.1 N HCl was added in order to precipitate the product, which was in turn extracted with EtOAc (4 \times 5 mL). The organic phase was dried over MgSO₄ and evaporated. The product was purified by flash column chromatography (15 \times 2 cm, elution with 10 % - 30 % EtOAc/1 % AcOH/hexanes) and 1.22 g of pure product was recuperated (65 % yield); mp = 98 °C.

¹H NMR: δ (CDCl₃) = 1.92-2.17 (m, 1 H); 2.09-2.17 (m, 1 H); 2.42-2.58 (m, 2 H); 3.98 (dd, 1 H, J = 18.0, 5.4); 4.11 (dd, 1H, J = 18.1, 5.2); 4.52 (td, 1 H, J = 8.0, 6.3); 4.61 (d, 2 H, J = 5.8); 5.09 (br s, 2 H); 5.25 (dd, 1 H, J = 10.4, 1.1); 5.32 (dd, 1 H, J = 17.1, 1.4); 5.88 (ddt, 1 H, J = 17.1, 5.6, 5.9); 5.96 (d, 1 H, J = 8.7); 7.32 (s, 5 H).

¹³C NMR (CDCl₃): δ = 28.0, 29.5, 41.1, 53.4, 66.0, 67.2, 118.9, 127.9, 128.1, 128.4, 131.2, 135.8, 156.5, 156.1, 169.4, 172.0.

N-Cbz-*D*-glutamyl(γ -*p*-nitrophenyl ester)glycine allyl ester (**11**)



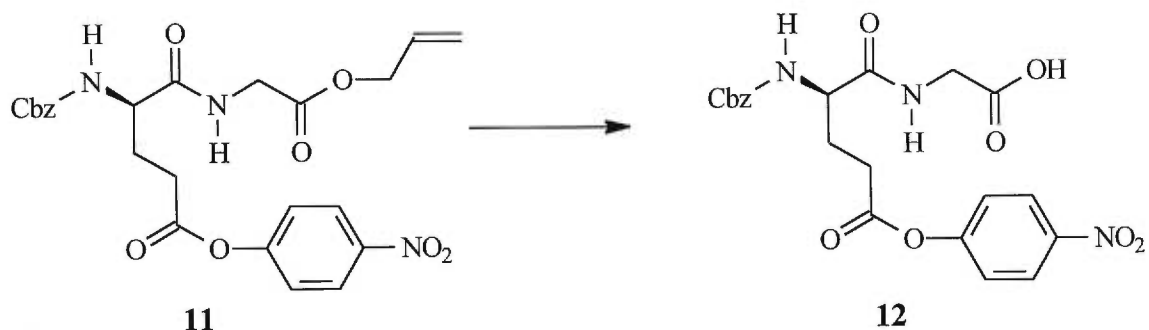
The same coupling method procedure as described in **Appendix B-3** (page 110) was followed; **10** (635 mg, 1.61 mmol, 1 eq), *p*-nitrophenol (260 mg, 1.69 mmol, 1.05 eq), EDC (575 mg, 1.93 mmol, 1.2 eq) and HOBt (210 mg, 1.61 mmol, 1 eq). The product was isolated by flash column chromatography (2 × 15 cm; eluted with 5 – 31 % EtOAc/hexanes), and the oily residue obtained upon evaporation was recrystallized from Et₂O and hexanes. The overall yield obtained was 659 mg (82 %) of a white powder.

mp = 116 – 117 °C

¹H NMR: δ (CDCl₃) = 2.03-2.12 (m, 1H); 2.27-2.35 (m, 1H); 2.70-2.87 (m, 2H); 4.02 (dd, J = 18.8, 3.9, 1H); 4.12 (dd, J = 18.2, 5.4, 1H); 4.43 (d, J = 5.6, 1H); 4.65 (d, J = 5.7, 2H); 5.12 (td, J = 12.2, 9.1, 2H); 5.27 (d, J = 10.4, 2H); 5.33 (d, J = 17, 2H); 5.64 (d, J = 7.6, 1H); 5.90 (m, 1H); 6.67 (s, 1H); 7.27 (m, 2H); 7.34 (s, 5H); 8.24 (d, J = 9.2, 2H).

¹³C NMR (CDCl₃): δ = 27.8, 30.1, 41.1, 53.5, 66.1, 67.2, 119.1, 122.4, 125.1, 128.0, 128.2, 128.5, 131.1, 135.8, 145.3, 155.1, 156.1, 169.1, 170.9, 171.0.

N-Cbz-*D*-glutamyl(γ -*p*-nitrophenyl ester)glycine (**11**)



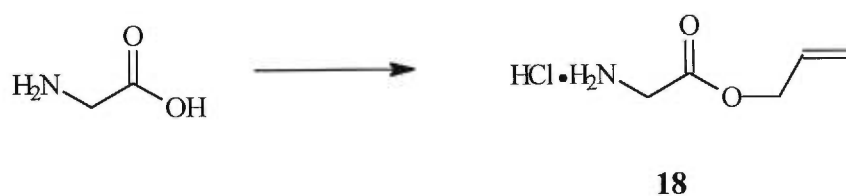
Allyl deprotection was conducted as described in **Appendix B-3** (page 111). The quantities used were as follows: 300 mg (0.600 mmol, 1 eq) **11**, 968 μ L (3.60 mmol, 6 eq) Bu_3SnH , and 4.2 mg (0.006 mmol, 1 mole %) palladium catalyst. The overall yield was 83 % (230 mg) and a white powder was obtained.

mp = 141-143 $^{\circ}\text{C}$ (lit. = 140 $^{\circ}\text{C}$)(8)

^1H NMR (CD_3OD): δ = 1.91-2.10 (m, 1H); 2.21-2.42 (m, 1H); 2.88-2.98 (m, 2H); 3.85-4.04 (m, 2H); 4.32-4.38 (m, 1H); 5.06-5.18 (m, 2H); 7.28-7.40 (m, 6H), 8.21 (d, J = 9.0, 2H); 8.47-8.55 (m, 1H).

^{13}C NMR (CD_3OD): δ = 27.3, 28.1, 53.7, 68.1, 82.5, 124.1, 125.9, 129.0, 129.2, 129.5, 135.9, 145.4, 156.1, 157.0, 168.1, 170.8, 170.9.

Synthesis of glycine allyl ester hydrochloride (18)



Glycine (3 g, 75 mmol, 1 eq), *p*-toluenesulfonic acid hydrate (8.36 g, 82.5 mmol, 1.1 eq), and a few flakes of benzophenone were added to a 1 L round bottom flask containing 350 mL benzene. Allyl alcohol (54 mL, 1.5 mol, 20 eq) was transferred into the reaction vessel via double-ended needle. The reaction flask was fitted with a Dean-Stark condenser, and reaction mixture was left refluxing for 24 hrs. The reaction is over when all the glycine has dissolved. After evaporation, the product was dissolved in 200 mL 0.1 N HCl and hexanes (2 × 30 mL). Solid Na₂CO₃ was added to the aqueous phase until a pH of 8 was attained. The solution was then saturated with NaCl and extracted with CH₂Cl₂ (4 × 50 mL). The pooled extracts were dried over NaSO₄, and evaporation yielded an oil. The product was dissolved in 50 mL CH₂Cl₂ and HCl gas was bubbled four times for ten minute intervals. Evaporation gave 3.1 g (65 %) of a pale yellow powder.

mp = 74 - 75°C

¹H NMR: δ (CDCl₃) = 3.98 (dd, 1 H, *J* = 18.0, 5.4); 4.11 (dd, 1H, *J* = 18.1, 5.2); 4.61 (d, 2 H, *J* = 5.8); 5.25 (dd, 1 H, *J* = 10.4, 1.1); 5.32 (dd, 1 H, *J* = 17.1, 1.4); 5.88 (ddt, 1 H, *J* = 17.1, 5.6, 5.9);

Appendix C: Kinetics

Materials, Methods & Results

Materials:

EDTA, MES buffer, Tris buffer, MOPS buffer, glycine methyl ester, 2-methoxyethylamine, 2,2,2-trifluoroethylamine, 2(Ethylthio)ethylamine, aminoacetonitrile, glycinamide, 4-nitrophenyl acetate, and 4-nitrophenol were all purchased from Aldrich. *N*-Acetyl-L-lysine methyl ester, propylamine and calcium chloride were obtained from Sigma. *N,N*-dimethylformamide was obtained from ACP. Deuterium oxide (99.9 % atom % D) was purchased from CDN Isotopes. Also, 2,4-dinitrophenyl acetate was purchased from Kodak (Eastman fine chemicals).

Methods:

C-1: GENERAL KINETIC PROCEDURES

All kinetics were conducted using semi-micro 1.5 ml disposable polystyrene cuvettes. TGase purified in our laboratory, was thawed from - 20 °C. A 1 mg/mL solution was prepared by adding distilled and deionized water. The enzyme solution was stable at 4 °C for several days without appreciable loss in activity. Enzyme concentration and activity was determined daily using the Lowry and hydroxamate assays, respectively. The Lowry standard curve was repeated daily, and fresh hydroxamate assay solution was prepared daily. All spectrophotometric data were collected using a Cary 100 Varian UV-visible spectrophotometer with a thermostatically controlled multicell changer maintained at 25 °C for all experiments. All primary data were obtained by monitoring the release of *p*-nitrophenolate at 400 nm. All zero order rate constants (V_{\max}) were corrected for the quantity of enzyme, the specific activity of enzyme, the molar extinction coefficient of *p*-nitrophenolate, enzymatic hydrolysis (for the transfer reaction), and background hydrolysis. To determine the k_{cat} parameter a molecular weight of TGase of 90 000 kDa (g/mol) (18)

was used with the assumption that the enzyme has 1 active site per molecule. This parameter, however, is not cited in this work and rather a V_{\max} parameter is commonly used for the purposes of comparison. We found it more useful to report data as V_{\max} which is representative of the mM of substrate catalysed per minute per mg of TGase (mM/min/mg), since no approximations are required as to the molecular weight of the enzyme. However, it should be noted that V_{\max} was standardized for specific activity. The highest SA reported in the literature prior to our purification results was 14.0, so we standardized V_{\max} to a factor of SA (our enzyme)/14.0. This takes into account variances in SA observed throughout various experiments.

Initial velocities were determined over a range of no more than 10 % disappearance of substrate analogue **5**, in adherence to steady-state kinetic conditions. The buffered solutions were verified daily for pH (using the Accumet Fisher Scientific pH-meter), and solution pH at the end of each kinetic run were measured in order to ensure that the pH varied by no more than 0.1 units. The pH meter was standardized daily with buffer solutions of pH 4.0, 7.0, and 10.0 purchased from Fisher Scientific. At least 8 concentrations of substrate (in duplicate) were used to generate the Michaelis-Menton saturation curves or the Lineweaver-Burke plots. For all kinetics, solutions of substrate analogue **5** and primary amine were prepared fresh daily.

C-2: REACTION PRODUCT EXTINCTION COEFFICIENTS

C-2.1 4-Nitrophenol

The molar extinction coefficients of *p*-nitrophenol (pK_a of 7.16 (45)), determined as a function of pH under experimental kinetic conditions, are listed in **Table VII** (page 126). The *p*-nitrophenolate (dissociated species of *p*-nitrophenol) is the UV-active species, and displays maximal absorbance at $\lambda_{\max} = 400$ nm. The undissociated form has λ_{\max} at 320 nm, and will therefore not interfere in readings of absorbance at 400 nm. To convert absorbance units into concentration units for *p*-nitrophenol liberation, a standard curve was generated at each of the following pH values: 5.5, 6.0, 6.5, 7.0, 7.5, 7.75, 8.0, 8.5 and 9.0. The buffers were select according to optimal range of buffering capacity and used at a final concentration 0.1 M: MES for pH's 5.5 - 6.5, 0.1

M MOPS for pH's 7.0 – 7.75, 0.1 M Tris for pH's 8.0 - 8.5, and 0.1 M CHES for pH 9.0. For the standard curves constructed at pH 5.5 - 6.5, 8 concentrations (in duplicate) of *p*-nitrophenolate were used in the 20 μM - 300 μM range. For all other pH values, the concentrations used were in the range of 10 μM - 120 μM . The *p*-nitrophenol was soluble in DMF, and the final conditions were 5 % DMF, 50 mM CaCl_2 , 50 μM EDTA and 0.1 M buffer prepared in 1 mL cuvettes. Absorbances were read at 400 nm and 25 $^\circ\text{C}$. The spectrophotometer was zeroed using sample solution without the *p*-nitrophenol, but including 5 % DMF. For the graphical representation of pH vs extinction coefficient for *p*-nitrophenolate see **Figure 14** (page 68).

Table VII: The results from the determination of the *p*-nitrophenol molar extinction coefficient (ϵ) as a function of the pH, at 400 nm.

pH	ϵ ($\text{M}^{-1} \text{cm}^{-1}$)
5.4	620
5.75	1050
6.0	1750
6.2	2375
6.5	4100
7.0	8040
7.5	13 700
8.0	18 050
8.5	18 950
9.0	21 200

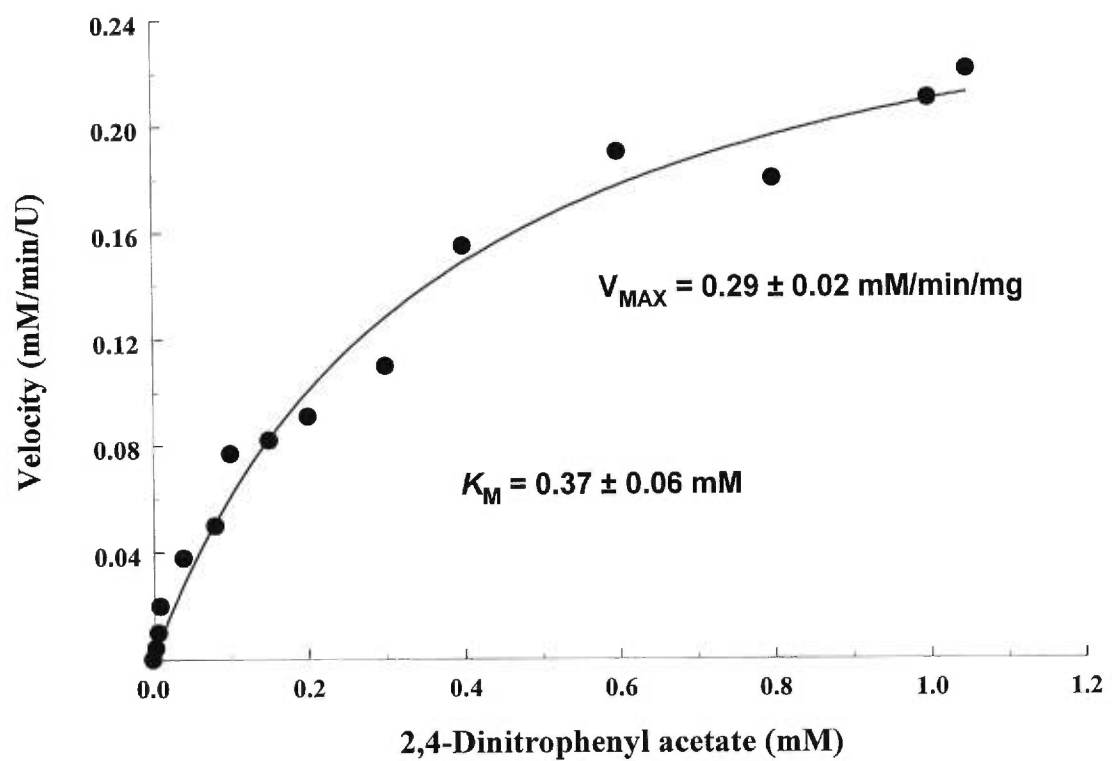
C-2.2 2,4-Dinitrophenol (2,4-DNP)

To determine the extinction coefficient of 2,4-DNP as a function of pH, a standard curve was generated at each of the following pH values: 5.5, 6.0, 6.5, 7.0, 7.5, 7.75, 8.0, 8.5 and 9.0 (prepared as described above). Concentrations ranged from 0.25 – 5.0 μM , and absorbances were read at 400 nm (its peak absorbance is also at this wavelength) (see **Table VIII** below). **Figure 27** (page 128) reveals that the extinction coefficient of 2,4-DNP does not change over the observed pH range. This is expected since its $\text{p}K_{\text{a}}$ is 4.06 (46). Therefore, an extinction coefficient of $12\,600\ \text{M}^{-1}\ \text{cm}^{-1}$ was used for all pH values in the range of 5.5 – 9.0.

Table VIII: Results for the determination of the extinction coefficients 2,4-dinitrophenol at various pH values, as observed at 400 nm.

pH	ϵ ($\text{M}^{-1}\ \text{cm}^{-1}$)
6.0	12 600
6.5	12 700
7.0	12 300
7.5	12 900
8.0	12 800
9.0	12 200
Avg = 12 600	

Figure 27: A graphical representation of the pH-dependence of the molar extinction coefficient of 2,4-dinitrophenolate, at pH 6.0 – 9.0 as measured at 400 nm.



C-3: TITRATION OF PRIMARY AMINES (p*K*_{NH+})

In order to determine the p*K*_a of the conjugate acid (p*K*_{NH+}) of each primary amine studied, 0.2 M solutions of primary ammonium chlorides were prepared in buffer containing 5 % DMF and an ionic strength (μ) adjusted to 0.25 M with KCl. The 0.25 M ionic strength of our kinetic medium as calculated using Equation 2 given below:

$$\mu = 1/2(m_1(Z_1)^2 + m_2(Z_2)^2 + m_3(Z_3)^2 + \dots) \quad (2)$$

m_1, m_2, m_3, \dots represent the molar concentration of the various ions in solution and Z_1, Z_2, Z_3, \dots are their respective charges.

The ammonium ion solutions were titrated with 0.1 N NaOH (in duplicate) to pH 13.5. Titrations were achieved using the Mettler Toledo DL53 autotitrator. For *N*-acetyl-L-lysine methyl ester, 2-methoxyethylamine, and propylamine, 1 mL pre-titration volumes of 0.1 N HCl were added in order to be able to properly observe the equivalence point. The primary alkyl ammonium p*K*_a values were calculated as the pH of the titration solution halfway to the measured equivalence point, and are reported in **Table V** (page 77).

C-4: STEADY-STATE KINETICS

C-4.1 The Catalyzed Hydrolysis Reaction

Steady-State kinetic assays for the TGase mediated hydrolysis reaction were performed in 0.1 M MOPS buffer (pH 7.0) that included 50 μ M EDTA, 50 mM CaCl₂ and 5 % DMF. At least 8 different concentrations of acyl-donor substrate, consisting of either the active ester substrate analogue **5** (0.001 – 0.8 mM), or 2,4-dinitrophenyl acetate (0.01 – 2.5 mM), or *p*-nitrophenyl acetate (0.05 – 4.0 mM), were used. Reactions were initiated by the addition of 15 μ L of purified TGase (1 mg/ml) and were followed as linear increases in absorbance at 400 nm over a maximum of 10 minutes. Enzyme stability over this time period was verified under these experimental conditions and displayed stability for at least one hour (results not shown). Slopes of

absorbance vs time were transformed into reaction rates by dividing by the appropriate extinction coefficient (*p*-nitrophenolate = 8040 M⁻¹cm⁻¹ and 2,4-DNP = 12 600 M⁻¹cm⁻¹). Blanks containing all components of the kinetic assay solution *except* enzyme were conducted in duplicate and used directly to correct the observed catalytic reaction rates. Initial velocities obtained at different acyl-donor concentrations were standardized (as previously described in **Appendix C-1**, page 124) and used to construct the hyperbolic Michaelis-Menton saturation curves (see **Figures 28, 29 and 30**, on pages 131-132). The kinetic parameters of V_{\max} and K_M were obtained through non-linear regression of these data according to Equation 3 using Axum 4.0 curve-fitting software.

$$v_o = \frac{V_{\max} [S]}{K_M + [S]} \quad (3)$$

Table IX: Kinetic parameters (V_{\max} , K_M and V_{\max}/K_M) obtained according to Equation 3 for the TGase catalyzed hydrolysis reaction involving various active ester substrate at 25 °C and pH 7.0 (0.1 M MOPS).

Active ester	p <i>K</i> _a (alcohol)	V_{\max} (mM/min/mg)	K_M (mM)	V_{\max}/K_M (min/mg)
<i>p</i> -nitrophenyl acetate	7.16 ^a	0.87	1.10	0.79
2,4-dinitrophenyl acetate	4.02 ^b	0.29	0.37	0.78
substrate analogue 5	7.16	0.20	0.02	6.70

^a ref (45), ^b ref (46)

Figure 28: The Michaelis-Menton saturation curve for the TGase catalyzed hydrolysis of *p*-nitrophenyl acetate as observed at pH 7.0 (0.1 M MOPS) and 25 °C, using Equation 3 to obtain V_{\max} and K_M .

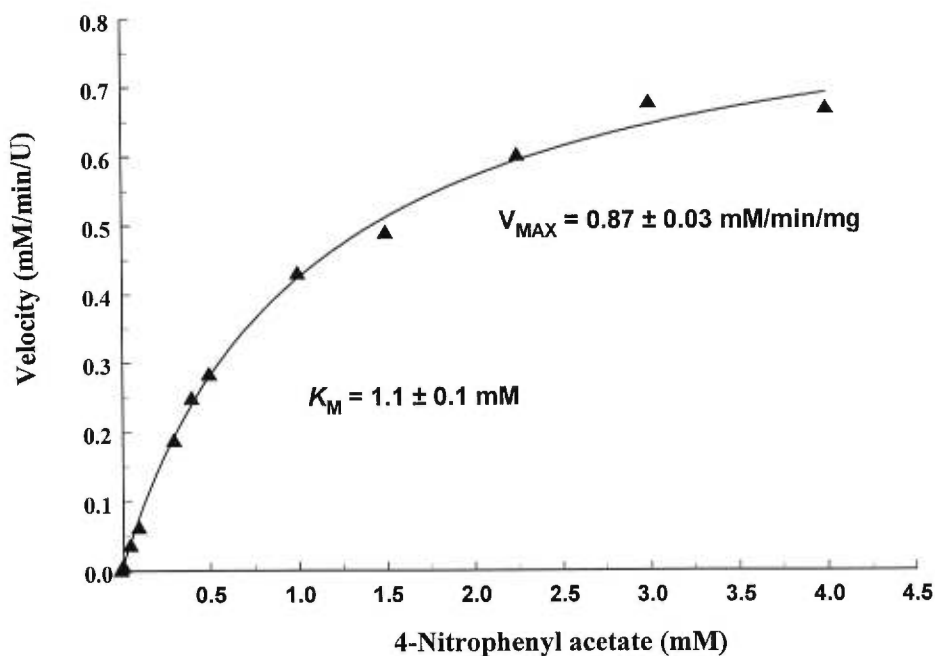


Figure 29: Saturation kinetics for the TGase catalyzed hydrolysis of 2,4-dinitrophenyl acetate as observed at pH 7.0 (0.1 M MOPS) and 25 °C, using Equation 3 to obtain V_{\max} and K_M .

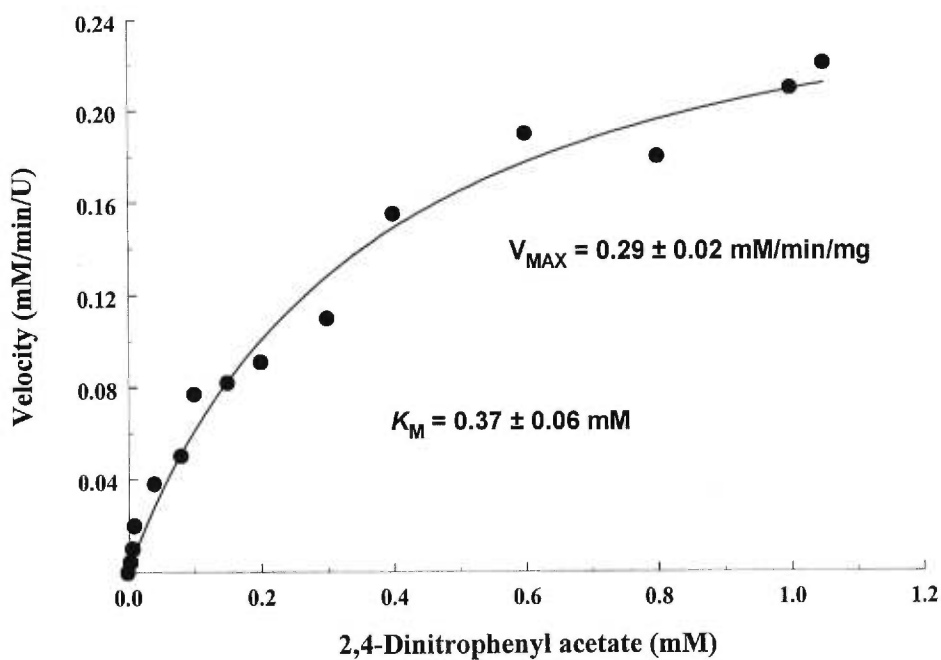
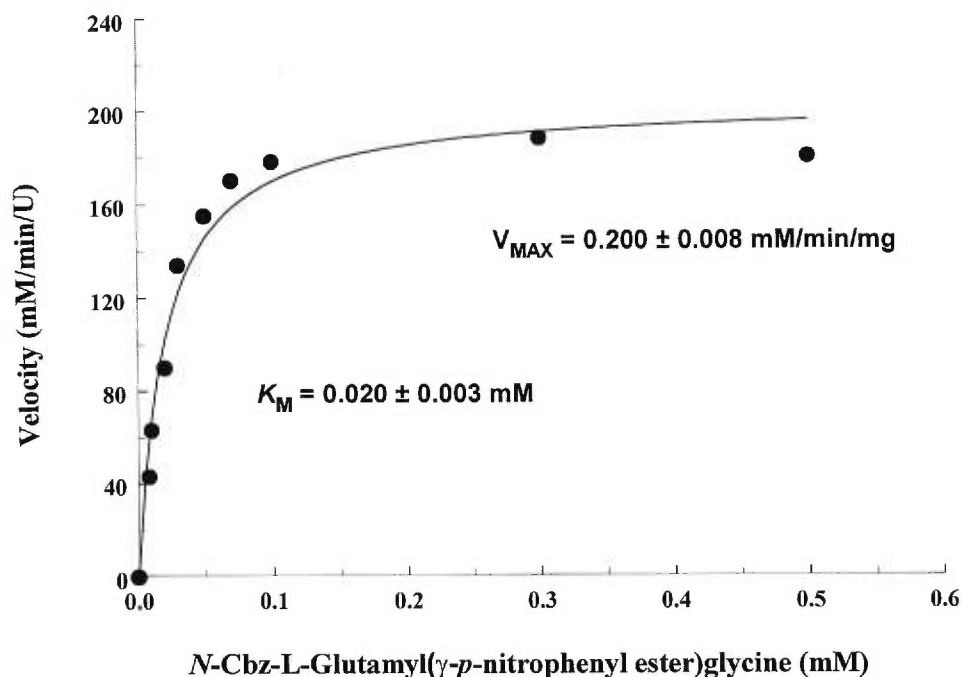


Figure 30: The Michaelis-Menton saturation curve for the TGase-catalyzed hydrolysis of substrate analogue **5** as observed at pH 7.0 (0.1 M MOPS) and 25 °C, using Equation 3 to obtain V_{\max} and K_M .



C-4.1.1 Background Hydrolysis of N-Cbz-L-glutamyl(γ-p-nitrophenylester)-glycine

The non-enzymatic hydrolysis of substrate analogue **5** was studied at pH values 6.0 – 8.5, in order to compare the pseudo-first order rate constant for hydroxide-ion catalyzed hydrolysis with the second order rate constant for the enzyme-catalyzed hydrolysis. The conditions used in determining the pseudo-first order rate constants are the same as described for hydrolysis kinetics above, with the exception of absence of TGase (see **Figure 31**, page 133, for graphical representation). The reaction was initiated by the addition of substrate **5**. At high pH values (7.5 – 8.5) the background hydrolysis is significant with as much as 68 % of the observed reaction. **Table X** (page 133) lists the observed enzyme-catalyzed and corresponding non-enzyme catalyzed hydrolysis rates in the presence of 0.1 mM substrate analogue **5** at the various pH values.

C-4.2 The Catalyzed Transamidation (Aminolysis) Reaction

In order to study the catalyzed aminolysis (transamidation) reaction, steady state kinetic assays were performed as described above using 0.1 mM *N*-Cbz-L-glutamyl(γ -*p*-nitrophenyl ester)glycine (substrate **5**) as acyl-donor substrate and at least 8 concentrations of a series of primary amines as acyl acceptor substrates ranging in pK_{NH^+} from 5.6 to 10.5. The concentrations employed for each primary amine were as follows: aminoacetonitrile (0.02 – 3.0 mM), 2,2,2-trifluoroethylamine (0.1 – 15 mM), glycine methyl ester (0.1 – 12 mM), glycinamide (0.2 – 18 mM), propylamine (1.0 – 80 mM), 2-methoxyethylamine (2 – 180 mM), 2-(Ethylthio)ethylamine (0.5 – 40 mM), *N*-acetyl-L-lysine methyl ester (1.0 – 40 mM). Reactions were initiated by the addition of substrate **5** and followed over a maximum of 5 minutes. Blanks contained all components of the kinetic assay solution except enzyme. Initial velocities, measured in duplicate for each amine concentration, were used to construct the Michaelis-Menton saturation curve. The maximal rates observed in the presence of primary amine acceptor substrates were always at least 30 % greater than the catalytic hydrolysis reaction ($V_{\text{max}}^{\text{hyd}}$). At very low amine concentrations, $V_{\text{max}}^{\text{hyd}}$ becomes relatively significant as water enters the active site to regenerate free enzyme. The apparent kinetic parameters for transamidation were therefore determined according to the slightly modified kinetic model given below as Equation 4.

$$v_0 = \frac{V_{\text{max}} [S]}{K_M + [S]} + V_{\text{max}}^{\text{hyd}} \quad (4)$$

The slope of the Brønsted-type plot (β_{nuc}) was obtained using the Equation 5 given below.

$$\log (V_{\text{max}}/K_M) = C + \beta_{\text{nuc}} pK_a \quad (5)$$

C-5: ISOTOPE EFFECT STUDIES

In order to measure the isotope effect (Kie) on the transamidation reaction rate, the same procedure as reported in **Appendix C-4.2** (page 134) for steady-state kinetic studies was applied, with the exception that all solutions used were prepared in D₂O. The pD was adjusted with 5 N NaOH according to the formula $pD = pH$ (meter reading) + 0.41 (63). pD fluctuations during any kinetic run did not exceed 0.1 units. Stability of the enzyme in D₂O was not a problem as verified by the hydroxamate enzyme activity assay (results not shown). The hydroxamate activity assay was conducted with solutions prepared in D₂O, in order to take into account catalytic activity of TGase as a consequence of the D₂O environment. The reactions were followed for at least 8 concentrations of *N*-acetyl-L-lysine methyl ester (1 – 10 mM), glycine methyl ester (0.1 – 12 mM) and aminoacetonitrile (0.01 – 2 mM). Results of the Kie experiments are summarized in **Table VI** (page 85).

C-6: pH-RATE PROFILE EXPERIMENTS

The pH-rate profiles of the TGase catalyzed hydrolysis of *N*-Cbz-L-glutamyl(γ -*p*-nitrophenyl ester)glycine (0.2 M) and its transamidation reaction with glycine methyl ester and aminoacetonitrile were prepared according to the same kinetic protocol described above, using 0.1 M buffer solutions to maintain reaction mixture pH values at 6.0, 6.5 (MES), 7.0, 7.5 (MOPS), 8.0 and 8.5 (Tris-HCl). In each case, pH values were measured before and after each kinetic run to verify that the pH variation was less than 0.1 pH units. The stability of TGase at the various pH levels studied was confirmed by incubating the enzyme at 25 °C in various buffers over a time period representative of a typical kinetic run (1 – 2 min) at that pH, followed by verification of its relative activity using the standard hydroxamate activity assay (involving incubation at 37 °C and pH 6.0, for 10 min). Results were compared to enzyme activity before incubation. Enzyme activity was found to be slightly affected by the pH of the environment with losses in the 5 – 15 % range, as shown in **Table XI** (page 135). Large experimental error was introduced at both extremities of pH. At low pH, very small slopes were observed since the concentration of the

p-nitrophenolate (dissociated form) is very small. At high pH, the background hydrolysis reaction of substrate **5** was as high as 75 % of the observed enzyme-catalyzed reaction. Both factors introduce very large experimental error for the observe the enzyme-catalyzed reaction at the extremities of pH values studied. Absorbances were measured using the Milton Roy Spectrophotometer.

Table XI: Results for the control experiments relating loss of TGase activity to pH environment effects.

pH	Incubation time (min)	Absorbance (525 nm)	Activity (%)
6.0	2	0.559	88
6.5	1	0.603	95
7.0	1	0.571	90
7.5	1	0.541	85
8.0	1	0.540	85
8.5	1	0.527	83
<i>standard</i>	<i>0</i>	<i>0.635</i>	<i>100</i>

Table XII: Kinetic results for the pH-rate experiment involving the TGase catalyzed *hydrolysis* of the active ester *N*-Cbz-*L*-glutamyl(γ -*p*-nitrophenyl ester)glycine at various pH values and 25 °C, where V_{\max} and K_M values were determined using Equation 3.

pH	K_M^a (mM)	$\log(K_M)$	V_{\max} (mM/min/mg)	$V_{\max(\text{corr})}^b$ (mM/min/mg)	$\log(V_{\max(\text{corr})})$	V_{\max}/K_M^c	$\log(V_{\max}/K_M)$
6.0	0.020	-1.70	0.14	0.16	-0.80	8.0	0.90
6.5	0.068	-1.17	0.21	0.22	-0.66	3.2	0.51
7.0	0.020	-1.70	0.20	0.22	-0.66	11.0	1.04
7.5	0.084	-1.07	0.36	0.42	-0.38	5.0	0.70
8.0	0.017	-1.77	0.27	0.32	-0.49	18.8	1.27
8.5	0.023	-1.63	0.27	0.33	-0.48	14.3	1.16

^{a, b, c} Experimental error of 10 % is associated with each of these values. ^b The velocity was corrected for loss of enzyme stability due to adverse conditions of pH (see **Table XI**, page 136).

Table XIII: Kinetic parameters (V_{\max} and K_M) obtained using Equation 4 for the TGase catalyzed *transamidation* reaction between 0.2 mM *N*-Cbz-*L*-glutamyl(γ -*p*-nitrophenyl)glycine and varying concentrations of glycine methyl ester at various pH values and 25 °C.

pH	K_M^a (mM)	$\log(K_M)$	V_{\max} (mM/min/mg)	$V_{\max(\text{corr})}^b$ (mM/min/mg)	$\log(V_{\max(\text{corr})})$	V_{\max}/K_M^c	$\log(V_{\max}/K_M)$
6.0	7.02	0.85	4.15	4.72	0.67	0.67	-0.17
6.5	7.02	0.85	4.15	4.37	0.64	0.62	-0.21
7.0	0.55	-0.25	3.80	4.22	0.63	7.67	0.88
7.5	0.20	-0.70	3.90	4.59	0.66	23.00	1.36
8.0	0.13	-0.89	3.90	4.59	0.66	35.00	1.54
8.5	0.12	-0.92	6.50	7.83	0.89	65.00	1.81

^{a, b, c} Experimental error of 10 % is associated with each of these values. ^b The velocity was corrected for loss of enzyme stability due to adverse conditions of pH (see **Table XI**, page 136).

Table XIV: Kinetic parameters (V_{\max} and K_M) obtained using Equation 4 for the TGase catalyzed *transamidation* reaction between 0.2 mM *N*-Cbz-L-glutamyl(γ -*p*-nitrophenyl ester)glycine and varying concentrations of aminoacetonitrile at various pH values and 25 °C.

pH	K_M^a (mM)	$\log(K_M)$	V_{\max} (mM/min/mg)	$V_{\max(\text{corr})}^b$ (mM/min/mg)	$\log(V_{\max(\text{corr})})$	V_{\max}/K_M^c	$\log(V_{\max}/K_M)$
6.0	0.22	-0.60	2.90	3.30	0.52	15	1.18
6.5	0.16	-0.80	6.40	6.74	0.83	42	1.62
7.0	0.08	-1.10	3.70	4.11	0.61	51	1.71
7.5	0.07	-1.15	3.90	4.59	0.66	65	1.81
8.0	0.06	-1.22	3.70	4.35	0.63	73	1.86
8.5	0.21	-0.68	7.7	9.3	0.97	44	1.64

^{a, b, c} Experimental error of 10 % is associated with each of these values. ^b The velocity was corrected for loss of enzyme stability due to adverse conditions of pH (see **Table XI**, page 136).

C-7: DATA ANALYSIS

The rate equations 6 and 7 listed in **Appendix D-4** (page 143) derived by Folk *et al* (28) for the TGase-catalyzed modified Ping Pong Bi Bi mechanism, were also tested as to their data fitting capabilities, in comparison with the simplified Michaelis-Menton rate equations (Equation 3 and 4, on pages 129 and 133, respectively). The former equations incorporate a larger number of kinetic parameters such as K_{ah} , K_{bt} , K_{ibb} , which must be estimated during the course of the non-linear regression of the data. These equations gave unreproducible values for these constants and were therefore not used in data analysis. Unduly influence by initial estimates of these parameters indicates that true convergence was not achieved, and suggested that under these conditions, variance of observed kinetic parameters as a function of substrate concentration did not justify more complex interpretation of the data.

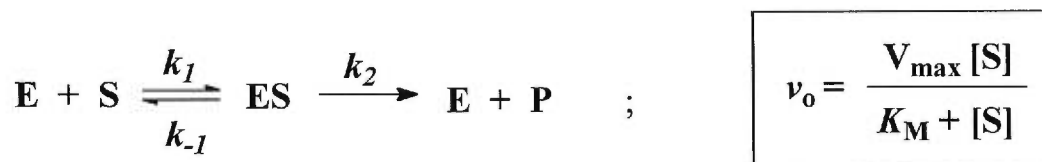
Appendix D:

Definitions and Equations

D-1: BRIGGS-HALDANE STEADY-STATE KINETICS

The velocity equation for Briggs-Haldane is identical to that of Michaelis-Menton, except the constant has a different meaning, due to the steady-state assumption. Here, K_M is a dynamic or pseudoequilibrium constant expressing the relationship between the actual steady-state concentrations rather than equilibrium concentrations (64).

Figure 32: Simple one substrate/one product mechanism and related rate expression.



where [S] = fixed
 v_o = initial velocity (no more than 5% of original [s] utilized)
 k_2 = rate constant for breakdown of ES complex to product
 K_M = dissociation constant (Michaelis constant) of the ES complex

$$K_M = \frac{k_{-1} + k_2}{k_1}$$

$$V_{\max} = k_2 [E]_{\text{tot}}$$

$$k_{\text{cat}} = \frac{V_{\max}}{[E]_{\text{tot}}}$$

D-2: THE MICHAELIS-MENTON KINETIC PARAMETERS

The only true value observed directly during kinetic analysis is the initial velocity at a given substrate concentration. The parameters V_{\max} and K_m must be estimated from initial velocities. below are definitions for each kinetic parameter.

k_{cat} = called the “turnover number”, because relates the number of substrate molecules converted to product per unit time. k_{cat} is in fact simply the rate limiting step in the mechanism.

K_M = is representative of the dissociation constant of ES, but represents apparent dynamic dissociation constant under steady-state conditions. When $[S] \gg K_M$, we have a 2nd order rate law.

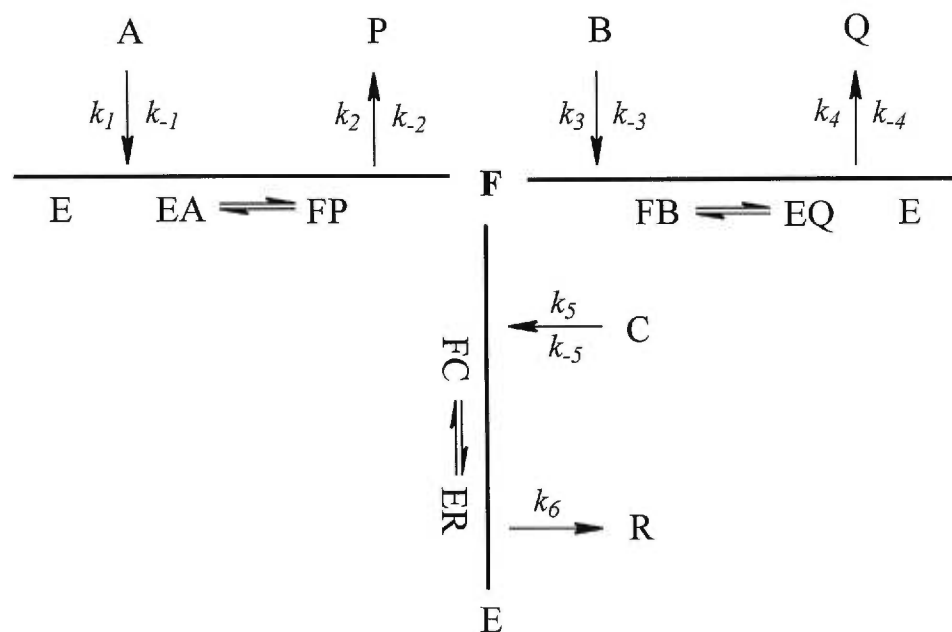
k_{cat}/K_M = the overall 2nd order rate constant for the conversion of substrate to product, and is the most useful kinetic parameter for assessing the effectiveness of enzymatic catalytic function. The larger the k_{cat}/K_m , the more efficient the reaction.

V_{\max} = maximum velocity of the enzyme catalyzed reaction. It is only a true value when the transglutaminase is saturated with both Ca^{2+} ion and substrate.

D-3: MODIFIED PING-PONG MECHANISM

A mechanism in which products are released between the addition of two substrates is called Ping Pong, and are common in group transfer reactions such as the acyl transfer conducted by the transglutaminases (64). Below is the schematic representation of events involved in the TGase-catalyzed modified Ping-Pong mechanism.

Figure 33: The transglutaminase modified ping-pong mechanism with the various rate constants.



where,

- E = free enzyme
- A = *N*-Cbz-L-Glu(γ -pnp)Gly
- EA, FB, FC = the enzyme-substrate complex (Michaelis-Menton complex)
- FP, EQ, ER = amino enzyme-product complex
- P = *p*-nitrophenol
- F = acyl-enzyme covalent intermediate
- B = primary amine
- Q = *N*-Cbz-L-Glu(γ -primary amine)Gly
- C = H₂O
- R = *N*-Cbz-L-GluGly

D-4: RATE EQUATION FOR THE MODIFIED PING PONG MECHANISM

From the generalized Michaelis-Menton equation, comes the adapted rate equation for the Ping-Pong mechanism of transglutaminases (21).

Equation for the **hydrolysis reaction**

$$v = \frac{V_a[A]}{K_{ah}(1 + [B]/K_{ibb}) + [A](1 + [B]/K_{bt})} \quad (6)$$

Equation for the **transfer reaction** following the release of the first product in the ping pong mechanism

$$v = \frac{V_a[A]}{K_{ah} + [A] \frac{(1 + ([B]/K_{bt}))}{(1 + ([B]/K_{ibb}))}} \quad (7)$$

$$K_{ah} = \frac{k_6(k_{-1} + k_2)}{k_1(k_2 + k_6)} \quad K_{bt} = \frac{(k_{-3} + k_4)(k_2 + k_6)}{k_3(k_2 + k_4)}$$

$$K_{ibb} = \frac{k_6(k_{-3} + k_4)}{k_1k_4} \quad V_a = \frac{k_6k_2 E_0}{k_2 + k_6}$$

where,

v = observed velocity

V_a = maximum velocity for hydrolysis

A is the first substrate and B is the second substrate

K_{bt} is Michaelis constants (K_M) for the transfer reaction of substrate B

K_{ah} is the complex dissociation constant for EA involving substrate A

E_0 = total enzyme concentration

Bibliography

1. Borth, W., Chang, V., Bishop, P. and Harpel, P. (1991) *J. Biol. Chem.* 268, 18149-18153.
2. Jensen, P. H., Sorensen, E. S., Petersen, T. E., Gliemann, J. and Rasmussen, L. K. (1995) *Biochem. J.* 310, 91-94.
3. Molberg, O., McAdam, S. N., Korner, R., Quarsten, H., Kristiansen, C., Madsen, L., Fugger, L., Scott, H., Noren, O., Roepstorff, P., Lundin, K. E. A., Sjostrom, H. and Sollid, L. M. (1998) *Nature medicine* 4, 713-717.
4. Groenen, P. J. T. A., Grootjans, J. J., Lubsen, N. H., Bloemendal, H. and de Jong, W. W. (1994) *J. Biol. Chem.* 269, 831-833.
5. Aeschlimann, D. and Paulsson, M. (1994) *Thrombosis and Haemostasis* 71, 402-415.
6. Wallis, E. S. and Lane, J. F. (1946) *Org. React.* 3, 267-306.
- 6a. Lebanc, A., Day, N., Ménard, A., Keillor, J.W. (1999) *Protein Expression and Purification*, 17, 89-95.
7. Gross, M., Whetzel, N. K. and Folk, J. E. (1975) *J. Biol. Chem.* 250, 4648-4655.
8. Chung, S. I., Shrager, R. I. and Folk, J. E. (1970) *J. Biol. Chem.* 245, 6424-6435.
9. Yee, V. C., Pedersen, L. C., LeTrong, I., Bishop, P. D. and Stenkamp, R. E. (1994) *Proc. Natl. Acad. Sci. U. S. A.* 91, 7296-7300.
10. Fersht, A. (1985) in *Enzyme Structure and Mechanism*, W.H. Freeman and Company, New York.
11. Lienhard, G. E. (1973) *Science* 180, 149-154.
12. Achyuthan, K. E., Slaughter, T. F., Santiago, M. A., Enghild, J. J. and Greenberg, C. S. (1993) *J. Biol. Chem.* 268, 21284-21292.
13. Kim, I.-G., Gorman, J. J., Park, S.-C., Chung, S.-I. and Steinert, P. M. (93 A.D.) *J. Biol. Chem.* 268, 12682-12690.

14. Kim, S.-Y., Kim, I.-G., Chung, S.-I. and Steinert, P. M. (1994) *J. Biol. Chem.* 269, 27979-27986.
15. Greenberg, C. S., Birckbichler, P. J. and Rice, R. H. (1991) *FASEB J.* 5, 3071-3077.
16. Cooper, A. J. L., Sheu, K. R., Burke, J. R., Onodera, O., Strittmatter, W. J., Roses, A. D. and Blass, J. P. (1997) *J. Neurochem.* 69, 431-434.
17. Abe, T., Chung, S. I., DiAugustine, R. P. and Folk, J. E. (1977) *Biochemistry* 16, 5495-5501.
18. Folk, J. E. and Chung, S. I. (1985) *Methods Enzymol.* 113, 358-375.
19. Folk, J. E. and Cole, P. W. (1966) *J. Biol. Chem.* 241, 5518-5525.
20. Folk, J. E. and Cole, P. W. (1966) *Biochim. Biophys. Acta* 122, 244-264.
21. Folk, J. E. (1969) *J. Biol. Chem.* 244, 3707-3713.
22. Folk, J. E. (1980) *Ann. Rev. Biochem.* 49, 517-531.
23. Keillor, J. W. and Brown, R. S. (1992) *J. Am. Chem. Soc.* 114, 7983-7989.
24. Street, J. P. and Brown, R. S. (1985) *J. Am. Chem. Soc.* 107, 6084-6089.
25. Lin, Y. and Welsh, W. J. (1996) *J. Mol. Graphics* 14, 62-72.
26. Micanovic, R., Procyk, R., Lin, W. and Matsueda, G. R. (1994) *J. Biol. Chem.* 269, 9190-9194.
27. Connellan, J. M., Chung, S. I., Whetzel, N. K., Bradley, L. M. and Folk, J. E. (1971) *J. Biol. Chem.* 246, 1093-1098.
28. Folk, J. E. and Chung, S. I. (1973) *Adv. Enzymol. Relat. Areas Mol. Biol.* 38, 109-191.
29. Croall, D. E. and DeMartino, G. N. (1986) *Cell Calcium* 7, 29-39.
30. Fernandez-Patron, C., Castellanos-Serra, L. and Rodriguez, P. (1992) *Biotechniques* 12, 564-573.
31. Gross, E. and Meienhofer, J. (1983) in *The peptides; analysis, synthesis, biology*, Academic Press, New York.

32. Huang, X., Luo, X., Roupioz, Y. and Keillor, J. W. (1997) *J. Org. Chem.* 62, 8821-8825.
33. Gagnon, P. and Keillor, J.W. (1999) in (unpublished observations) .
34. Bodansky, A.; Bodansky, M.; Chandramouli, N.; Kwei, J.Z.; Martinez, J.; Tolle, C. (1980) *J. Am. Chem. Soc.* 45, 72-76.
35. Green, T. W. and Wuts, P. G. M. (1991) in *Protective Groups in Organic Synthesis*, John Wiley & Sons, New York.
36. Bodansky, M. (1993) in *Principles of Peptide Synthesis*, Springer Laboratories, New York.
37. Gosselin, F. and Lubell, W. D. (1998) *J. Org. Chem.* 63(21), 7463-7471.
38. Windridge, G. and Jorgensen, E. C. (1971) *J. Am. Chem. Soc.* 93, 6318-6324.
39. Laspéras, M., Pascal, R., Taillades, J. and Commeyras, A. (1986) *New Journal of Chemistry* 10, 111-117.
40. Scholtz, J. M. and Bartlett, P. A. (1989) *Synthesis* 542-544.
41. Lee, K., Kim, J. H., Ko, K. K. and Kim, W. (1991) *Synthesis* 935-936.
42. Alberty, R. A. (1956) in *Methods in Enzymology and Related Subjects in Biochemistry* (Nord, F. F., Ed.)) pp 1-64, Interscience Publishers Inc., New York.
43. Chen, F. M. F. and Benoiton, L. N. (1992) *Int. J. Pept. Prot. Res.* 40, 13-18.
44. Folk, J. E., Cole, P. W. and Mullooly, J. P. (1968) *J. Biol. Chem.* 243, 418-427.
45. Martin, C. J., Golubow, J. and Axelrod, A. E. (1959) *Anal. Biochem.* 234, 294-298.
46. Satterthwait, A. C. and Jenks, W. P. (1974) *J. Am. Chem. Soc.* 96, 7018-7031.
- 46b. Holman, C.M.; Benisek, W.F. (1994) *Biochemistry*, 33, 2672-2681.
47. Folk, J. E., Cole, P. W. and Mullooly, J. P. (1967) *J. Biol. Chem.* 242, 4329-4333.
- 47b. Greenzaid, P.; Jencks, W.P. (1971) *Biochemistry*, 10, 1210-1221.
48. Duncan, G. D., Huber, C. and Welsh, W. J. (1992) *J. Am. Chem. Soc.* 114, 5784-5794.
49. Ege, S. (1994) in *Organic Chemistry*, pp 81-122, D.C. Heath and Company, Lexington, MA.

50. Gross, M., Whetzel, N. K. and Folk, J. E. (1977) *J. Biol. Chem.* 11, 3752-3759.
51. Isaacs, N. (1995) in *Physical Organic Chemistry*, Longman Scientific and Technical, Essex, England.
52. Carey, F. A. and Sundberg, J. (1990) in *Advanced Organic Chemistry: Part A: Structure and Mechanism*, Plenum Press, New York.
53. Zhao, Y. and Zhang, Z.-Y. (1996) *Biochemistry* 35, 11797-11804.
54. Adalsteinsson, H. and Bruice, T. C. (1998) *J. Am. Chem. Soc.* 120, 3440-3447.
55. Castro, E. A. and Ureta, C. (1989) *J. Org. Chem.* 54, 2153-2159.
56. Klinman, J. P. (1978) in *Adv. Enzymol. Rel. Areas Mol. Bio.* (Meister, A., Ed.) pp 415-494, Interscience Publishers Inc., New York.
57. Szawelski, R. J. and Wharton, C. W. (1981) *The biochemical society* 199, 681-692.
58. Cleland, W. W. (1977) in *Adv. Enzymol. Rel. Areas Mol. Bio.* (Meister, A., Ed.) pp 273-387, Interscience Publishers Inc., New York.
59. Allen, K. G. D., Stewart, J. A., Johnson, P. E. and Wettlaufer, D. G. (1978) *Eur. J. Biochem.* 87, 575-582.
60. Lowry, D. H., Rosebrough, N. J., Farr, A. L. and Randall, R. J. (1951) *J. Biol. Chem.* 193, 265-275.
61. Laemmli, U. K. (1970) *Nature* 227, 680-685.
62. Manesis, N. J. and Goodman, M. (1987) *J. Org. Chem* 52, 5331-5341.
63. Dale, M. P., Kopfler, W. P., Chait, I. and Byers, L. D. (1986) *Biochemistry* 25, 2522-2529.
64. Segel, I. H. (1993) in *Enzyme Kinetics: Behaviour and Analysis of Rapid Equilibrium and Steady-state Enzyme Systems*, John Wiley & Sons, Inc., New York.